Radioactive Fallout from Nuclear Weapons Tests

Proceedings of the Second Conference
Germantown, Maryland
November 3–6, 1964

Sponsored by the Fallout Studies Branch
Division of Biology and Medicine
U. S. Atomic Energy Commission

Alfred W. Klement, Jr.
Editor

November 1965

U.S. ATOMIC ENERGY COMMISSION / Division of Technical Information

SESSION I

Physical, Chemical, and Radiological Characteristics of Atmospheric Radioactivity and Fallout

Edward C. Freiling, Chairman

NUCLEAR-DEBRIS FORMATION

EDWARD C. FREILING, GLENN R. CROCKER,
and CHARLES E. ADAMS
U. S. Naval Radiological Defense Laboratory, San Francisco, California

ABSTRACT

This paper describes the present program, recent progress, and future plans of the U. S. Naval Radiological Defense Laboratory (NRDL) in the field of nuclear-debris formation.

Two fallout-formation prediction systems have been programmed for computer calculation. The predictions represent great advancements over systems that do not account for fractionation, but much room remains for improvement. The greatest needs appear to be for the definition of particle-size distribution, the accounting for agglomeration effects, and the development of a kinetic approach. Preliminary steps in the development of a kinetic approach are described.

A by-product of the prediction system is the calculation of unfractionated radiological properties. As an example of this work, decay rates, dose rates, and spectra are given for the most important case of ^{238}U fission produced by a thermonuclear neutron spectrum.

Some results of correlating radiochemical data from fractionated samples of air-burst debris are discussed, but numerical results are reserved for a following paper* to facilitate comparison with correlations from other burst types.

Preliminary laboratory investigations of fission-product interaction with various substrate materials are described. These show large negative deviations from Raoult's law, particularly when the interaction is between a basic fission product and acidic substrate or an acidic fission product and basic substrate.

---

*See paper by Glenn R. Crocker, Francis K. Kawahara, and Edward C. Freiling, this volume.

Finally, the directions that we expect future efforts to take are indicated. These include a sensitivity analysis of our prediction system, extended fractionation correlations, model refinements, model extensions to new conditions, the retrieval of information from old debris, and laboratory studies of fallout formation under irreversible conditions.

INTRODUCTION

We have been asked to describe in this paper the project on studies of nuclear-debris formation that we are carrying out at NRDL for the Fallout Studies Branch, U. S. Atomic Energy Commission (AEC). This project is entitled "The Formation, Distribution and Characteristics of Nuclear Debris." However, if we were to limit this paper strictly to this part of our nuclear-debris program, we would present a very incomplete picture of our efforts. We have therefore chosen to preface this paper with a few remarks on what we are trying to do and for whom we are doing it. Figure 1 is a schematic presentation of the Physical Chemistry Branch, NRDL, fallout studies program at the present and in the recent past. Other, related work at NRDL is shown only where necessary. The various boxes are coded to identify sponsorship. Next to the AEC, the Defense Atomic Support Agency (DASA) sponsors most of our work. The focal point, the ultimate goal, is prediction capability. This is indicated by the box labeled "Model of Formation and Properties of Nuclear Debris." As input this box requires basic data from nuclear and physical chemistry, in addition to empirical relations such as scaling functions and fractionation correlations. The scaling functions come from laboratory experiments and the fractionation correlations from the analysis of nuclear debris. In addition to NRDL, data come from various sources.

This paper reports primarily, but not exclusively, on research completed or nearly completed in the four following subprojects of our work for the AEC:

1. Prediction of fractionation effects
2. Prediction of radiological properties
3. Fractionation correlations
4. Laboratory studies

Also included in each section is an indication of the future direction we visualize these studies will take.

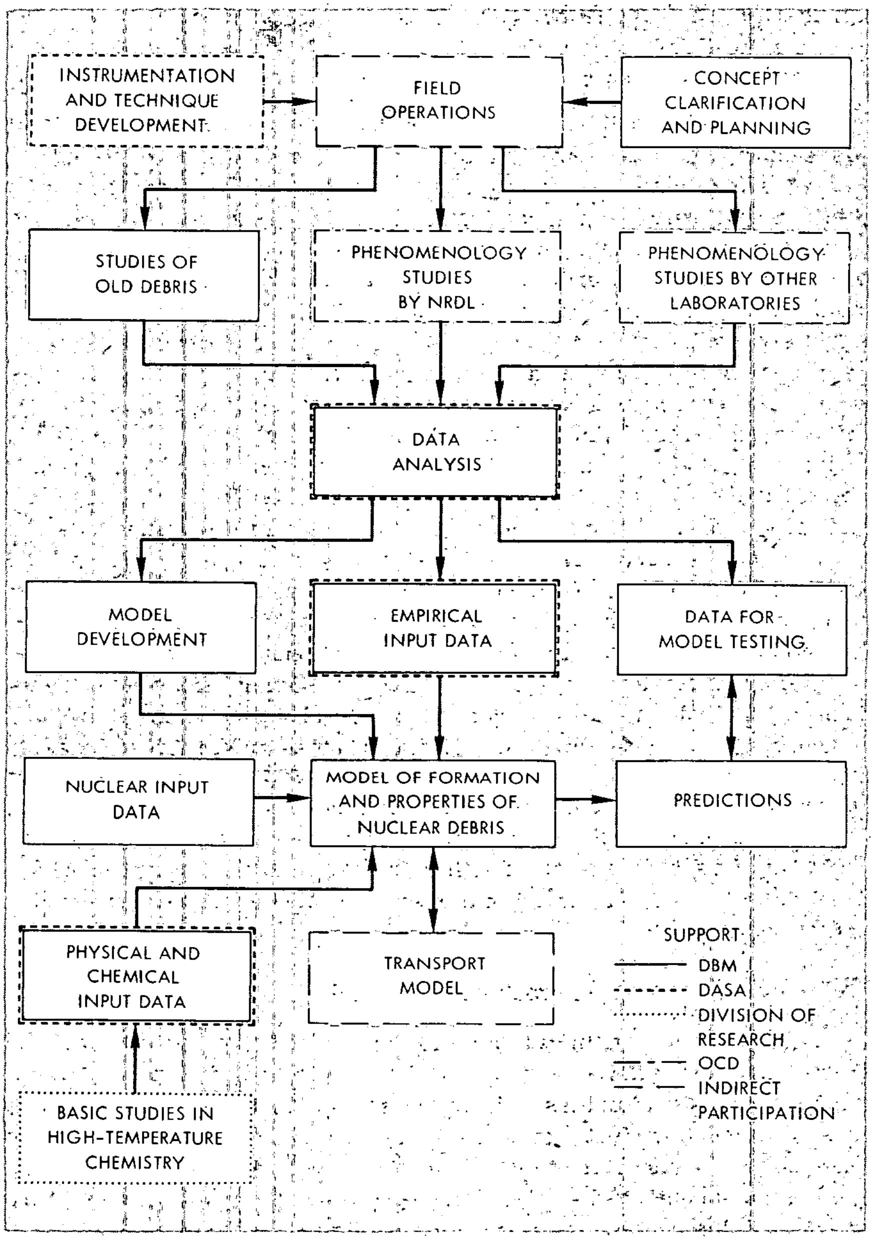

Fig. 1—Nuclear-debris study program.

PREDICTION OF FRACTIONATION EFFECTS

Clarification of Concepts

If the reader will permit a heterodox interpretation of the title of this subproject, it is appropriate to begin this discussion with the effect of fractionation on thought and communication — the semantic effect, if you will. With a realization of the existence and significance of fractionation, many terms previously used to describe and discuss fallout have become undefined and meaningless. Thus phrases like "bomb fraction," "fissions in the sample," and "kilotons per square mile" are no longer "OK terms." Moreover, as our understanding of fractionation has increased, deviation of fission-product abundances from those expected in instantaneous thermal-neutron fission of ^{235}U and of decay rates from the Way–Wigner $t^{-1.2}$ rule are no longer considered significant criteria or acceptable measures of fractionation effects. We have considered it an important part of our effort to suggest new definitions and, where possible, operational definitions for many of these terms. These are listed in the appendix to this paper. The essential features of some of these definitions are soundly grounded in the fundamental properties of the debris. Accidental features (e.g., the choice of standards for measuring fractionation) can be varied if sufficient justification appears for doing so. Other terms and definitions are merely matters of convenience, and these are appropriately indicated in the appendix. The adoption of these or similar definitions will be of great assistance, not only in promoting clear thinking and improving the signal-to-noise ratio when fractionation is discussed but also in planning analyses of those properties of nuclear debris affected by this phenomenon. Further background and justification for these definitions can be found in our set of reports with the series title "Fractionation."[1–4]

First Phase of Predicting Fractionation Effects

Early in the program we came to the conclusion that the prediction of fractionation effects could best be carried out in two concurrent phases.[5] The first of these phases consisted of rapidly assembling a prediction system that would give answers to urgent questions in as reasonable a manner as time allowed. The second phase consisted of a more fundamental long-range approach. The effects of interest are gross radiological effects (exposure-dose rate, exposure dose, decay rate, gamma spectra); radiochemical-composition effects (radionuclide partition between local and worldwide fallout, radionuclide ratios in particles of different size, type, and location, and relative biological availability); effects related to mass deposit (specific activity, mass–dose ratio); and various combinations of these (e.g., ^{131}I–dose ratio).

The first phase of this subprogram is virtually complete. We have available two models for prediction (a thermodynamic model and a radial-power-distribution model) and a means of modifying each semiempirically. The information flow in the system is shown schematically in Fig. 2.

Thermodynamic Equilibrium Model The thermodynamic equilibrium model developed by C. F. Miller has already been adequately described in detail in several publications[5–7] and applied with some success to the case of reactor excursions by C. E. Miller, Jr.[8] Essentially it consists of distributing the available radionuclides in the nuclear cloud among the particles present according to the predicted equilibrium distribution. The model takes 1400°C as the temperature below which particles are impenetrable to condensing nuclides. Unfortunately, adequate thermodynamic input data are not available to properly use and test the model in several critical cases (e.g., mass chains 89, 132, and 140 and their adjacent chains).

Radial-power-distribution Model The radial-power-distribution model[3] is an amplification of suggestions by R. D. Cadle, R. C. Tompkins, and P. W. Krey, namely, that refractorily behaving nuclides distribute themselves among particles according to the available volume whereas volatilely behaving nuclides distribute themselves according to the available surface. By assuming that a collection of spherical particles exists and that all mass chains are distributed according to some power of the radius, one finds that the model predicts logarithmic correlations of radionuclide ratios for monodisperse samples. This is a happy result because radionuclide ratios observed in fractionated nuclear debris can be correlated logarithmically, at least as well as they can linearly, and the correlation parameters then become useful for model predictions. If one further assumes a particle distribution such that the mass is distributed lognormally with particle diameter with modal diameter x_v and variance σ^2, one finds that all mass chains are distributed among the particles with variance σ^2 and modal diameters given by $x_v \exp [(b_i - 1)\sigma^2]$. Here b_i is a slope correlation parameter. This permits a great simplification in the calculations and makes hand calculation feasible, whereas, in the case of the thermodynamic equilibrium model, a computer is required. Although the thermodynamic equilibrium model is a more fundamental approach, the assumptions, simplifications, and approximations involved in its use, together with the state of the available input data, make the two approaches, at least for the present, of competitive reliability. The radial-power model has a great advantage in being presently applicable to air-, tower-, and surface-burst predictions.

The semiempirical aspect of the radial-power-distribution model consists of the way it utilizes empirical correlation parameters (ob-

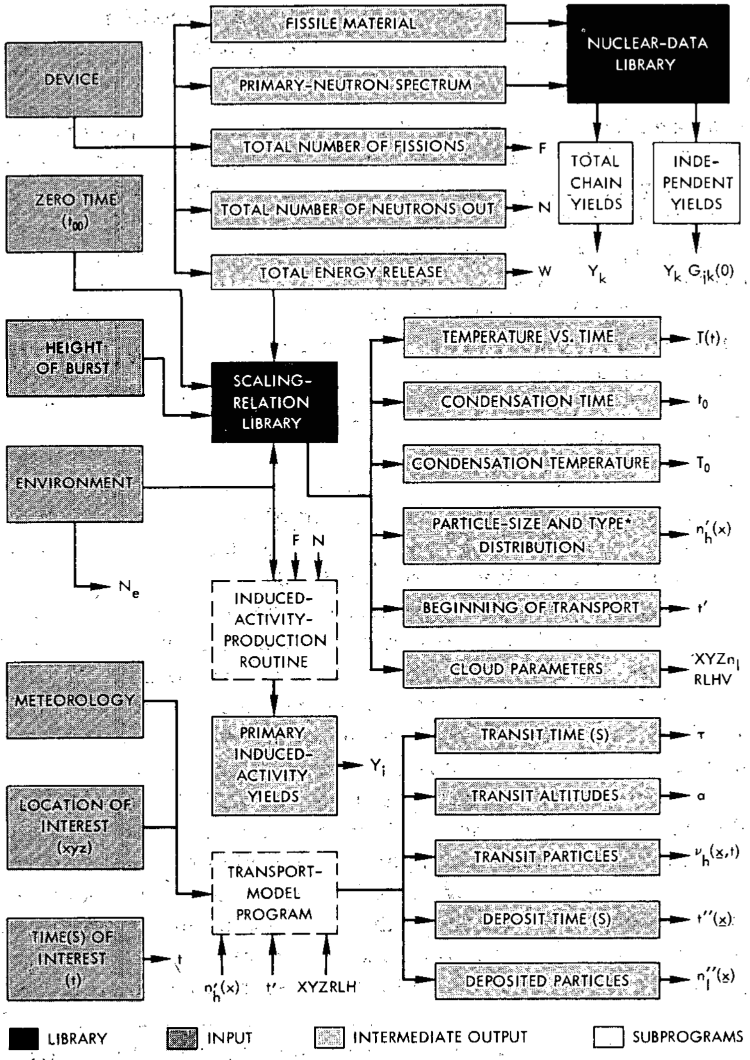

*Inactive, Spherical, or Irregular

Fig. 2—Information flow in the present system for predicting fractionation effects.

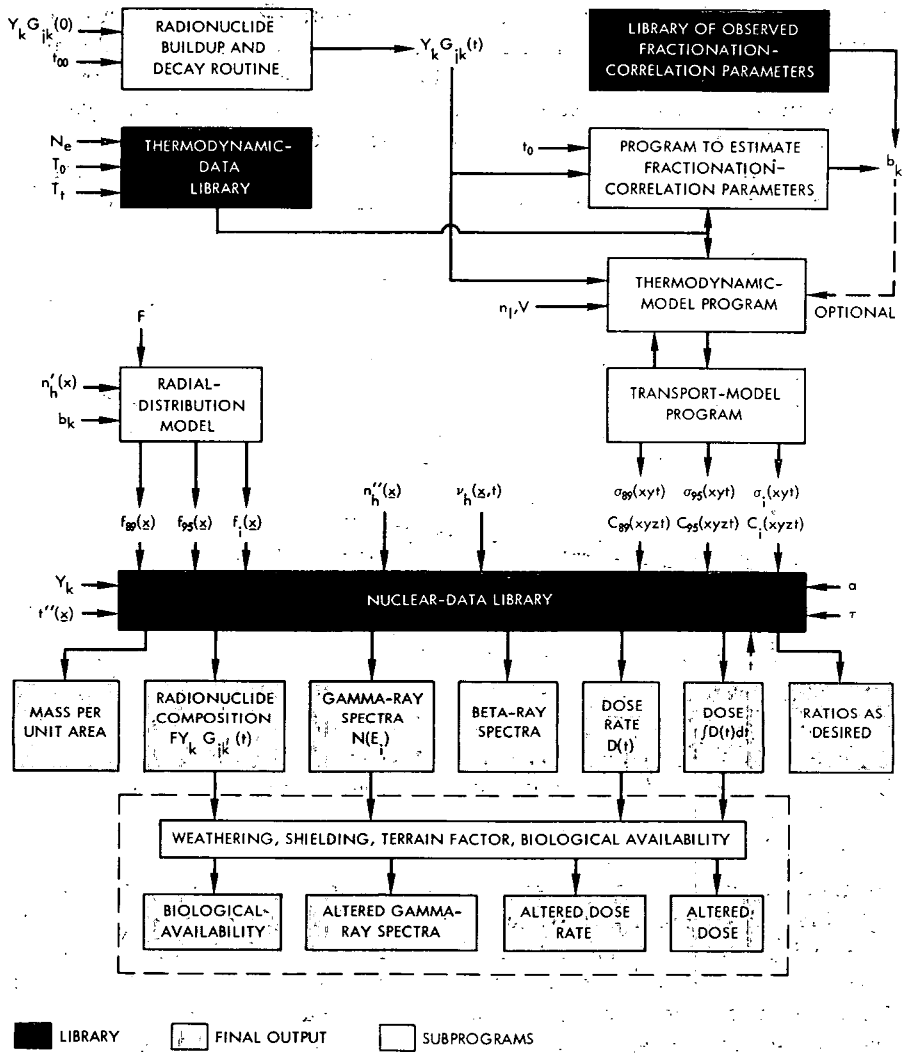
$Y_k G_{jk}(0)$
t_{00}
RADIONUCLIDE BUILDUP AND DECAY ROUTINE
$Y_k G_{jk}(t)$
LIBRARY OF OBSERVED FRACTIONATION-CORRELATION PARAMETERS
N_e
T_0
T_f
THERMODYNAMIC-DATA LIBRARY
t_0
PROGRAM TO ESTIMATE FRACTIONATION-CORRELATION PARAMETERS
b_k
THERMODYNAMIC-MODEL PROGRAM
n_l, V
OPTIONAL
F
$n_h'(x)$
b_k
RADIAL-DISTRIBUTION MODEL
TRANSPORT-MODEL PROGRAM
$f_{89}(\underline{x})$
$f_{95}(\underline{x})$
$f_i(\underline{x})$
$n_h''(\underline{x})$
$\nu_h(\underline{x}, t)$
$\sigma_{89}(xyt)$
$\sigma_{95}(xyt)$
$\sigma_i(xyt)$
$C_{89}(xyzt)$
$C_{95}(xyzt)$
$C_i(xyzt)$
Y_k
$t''(\underline{x})$
NUCLEAR-DATA LIBRARY
a
τ
t
MASS PER UNIT AREA
RADIONUCLIDE COMPOSITION $FY_k G_{jk}(t)$
GAMMA-RAY SPECTRA $N(E_i)$
BETA-RAY SPECTRA
DOSE RATE D(t)
DOSE $\int D(t)dt$
RATIOS AS DESIRED
WEATHERING, SHIELDING, TERRAIN FACTOR, BIOLOGICAL AVAILABILITY
BIOLOGICAL AVAILABILITY
ALTERED GAMMA-RAY SPECTRA
ALTERED DOSE RATE
ALTERED DOSE
LIBRARY
FINAL OUTPUT
SUBPROGRAMS

tained from the radiochemical analysis of fractionated fallout samples) to predict fractionation effects.[4] When so used, with a lognormal particle-size distribution, mass-balance requirements are automatically fulfilled for each mass chain. The assumptions of spherical particles and radial power distribution guarantee logarithmic correlations for monodisperse samples, and mass-balance fulfillment can be expected for any overall particle-size distribution.

The thermodynamic equilibrium model can be utilized in a semiempirical manner by using it as originally described to calculate the degree of fractionation for each sample and then attaching to that sample the effect empirically expected for that degree of fractionation. It has not yet been demonstrated, however, that mass-balance requirements will then be fulfilled. The seriousness of this defect would be less for dose-rate estimates than for radionuclide partition and may not be serious in either case, compared to the magnitude of other uncertainties.

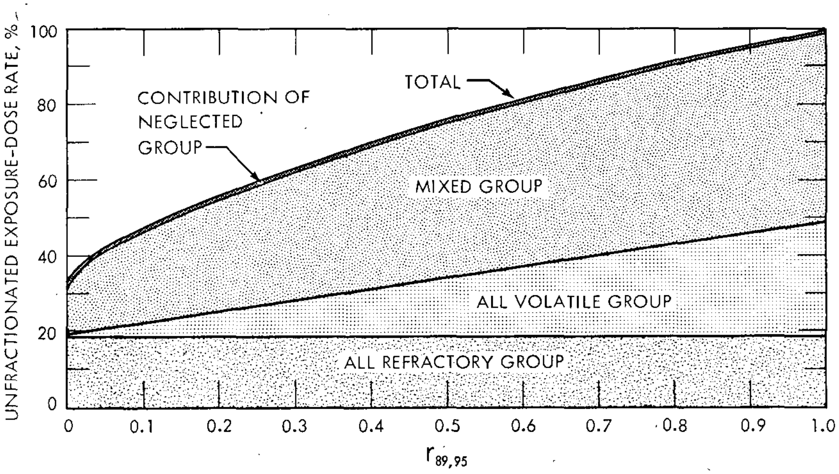

Fig. 3—Semiempirical model prediction of the effect of fractionation on the 1.12-hr dose rate for a burst in which solidification occurs in 6 sec.

Figure 3 shows the percentage of unfractionated exposure-dose rate expected for different degrees of fractionation at 1.12 hr from a burst in which solidification occurred in 6 sec. According to Miller's estimates[7] this would correspond to a yield of 25 kt. The prediction indicates a maximum depletion of a factor of 5 in the dose rate from local fallout. We have data from the 1962 test series in Nevada which indicate that depletion may be much greater in actual situations. The observations require further substantiation and verification, however.

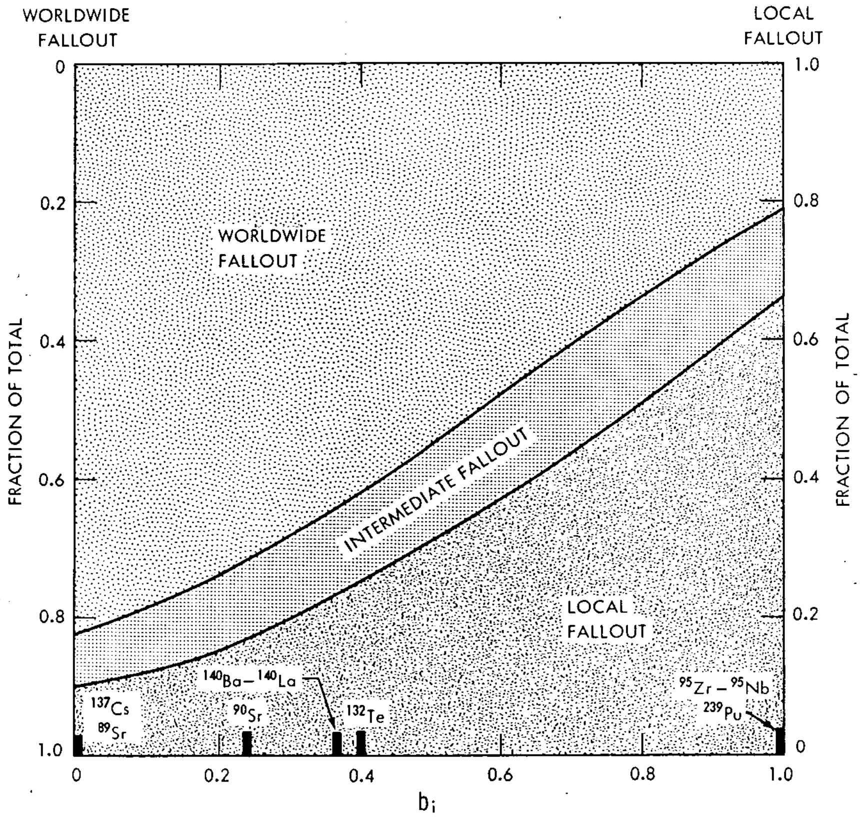

Fig. 4—Semiempirical model prediction of radionuclide partition in a land-surface burst.

In the case of volatile-chain enrichment under extreme conditions (base surge from an underwater burst or gas venting from a subsurface burst), the ratio of dose rate to the unfractionated dose rate calculated from the mass-95 chain may greatly exceed a factor of 10.

Another point of interest predicted by our model is that debris may adhere more closely to the Way–Wigner $t^{-1.2}$ decay rule if it is fractionated than if it is unfractionated; this is supported by unpublished observations on fallout from weapons tests.

Finally, the model has been used to predict the partition of various mass chains among local fallout (particles of 50 μ or greater in diameter), intermediate fallout (particles between 25 and 50 μ in diameter), and worldwide fallout (particles less than 25 μ in diameter). The predictions are shown in Fig. 4 and are compared in Table 1 with partitions inferred from fallout analysis.[9,10] The data from the high-yield coral-surface burst are of poor reliability and show only qualitative agreement. The data from the low-yield silicate-surface burst agree much better. The agreement is somewhat fortuitous, however, because the

Table 1 — COMPARISON OF RADIONUCLIDE PARTITIONS PREDICTED BY THE SEMIEMPIRICAL METHOD WITH OTHERS INFERRED FROM ANALYSIS OF NUCLEAR DEBRIS

	Predicted fractions			Fractions in 24-hr cloud of a high-yield, coral-surface burst	Fractions in a low-yield, silicate-surface burst		
Radionuclide	Local	Intermediate*	Worldwide		Local	Intermediate†	Worldwide
^{137}Cs	0.1	0.1	0.8	0.36 ± 0.36	0.00	0.22	0.78
^{89}Sr	0.1	0.1	0.8		0.02	0.24	0.74
^{90}Sr	0.15	0.1	0.75	0.11 ± 0.11	0.07	0.24	0.69
$^{140}Ba-^{140}La$	0.25	0.1	0.65		0.20	0.26	0.54
^{132}Te	0.25	0.1	0.65		0.18	0.26	0.56
$^{95}Zr-^{95}Nb$	0.65	0.1	0.25		0.72	0.19	0.09
^{99}Mo (coral)	0.65	0.1	0.25	0.02 ± 0.02	0.72	0.19	0.09

*Intermediate fraction taken as 25 to 50 μ in diameter.
†Intermediate fraction taken as 18 to about 90 μ in diameter.

particle-size distribution in the latter case differed considerably from that used in the model.

In summary, the present state of the art puts us in the position of the meteorologist who has to predict the weather even though he can't. We make the most reasonable attempt our knowledge permits and cross our fingers.

Second Phase of Predicting Fractionation Effects

We will now discuss the second, long-term phase of predicting fractionation effects, the phase concerned with piecewise refinement of weak links in the calculational chain. Figure 5 shows the fallout-formation processes that have to be taken into account in a fundamental approach. Our thinking on this is still the same as when we presented this diagram at the last conference.[5] Perhaps the weakest links are the definition of particle size and the absence of accounting for agglomeration effects, and next in importance is the transition from an equilibrium (thermodynamic) to a nonequilibrium (kinetic) approach. However, the definitive work being done by Russell on the first problem[10] and the need to properly plan our high-temperature experimental work has led us to attack the last problem first. Our efforts in this direction form the subject of this section of the report. One should not jump to the conclusion that the thermodynamic equilibrium treatment is inapplicable or that, even if it were, thermodynamic data are no longer required. As will be seen, each approach has its place in the overall development.

The plan of developing a kinetic model has been, first, to decide on a mechanism; second, to assemble useful, available theoretical and experimental results; and, third, to integrate these and fill in the missing steps to obtain the complete treatment. We are now in stage two. We are obviously not concerned so much at this point with developing a new theory of fallout formation as with the application of established theory.

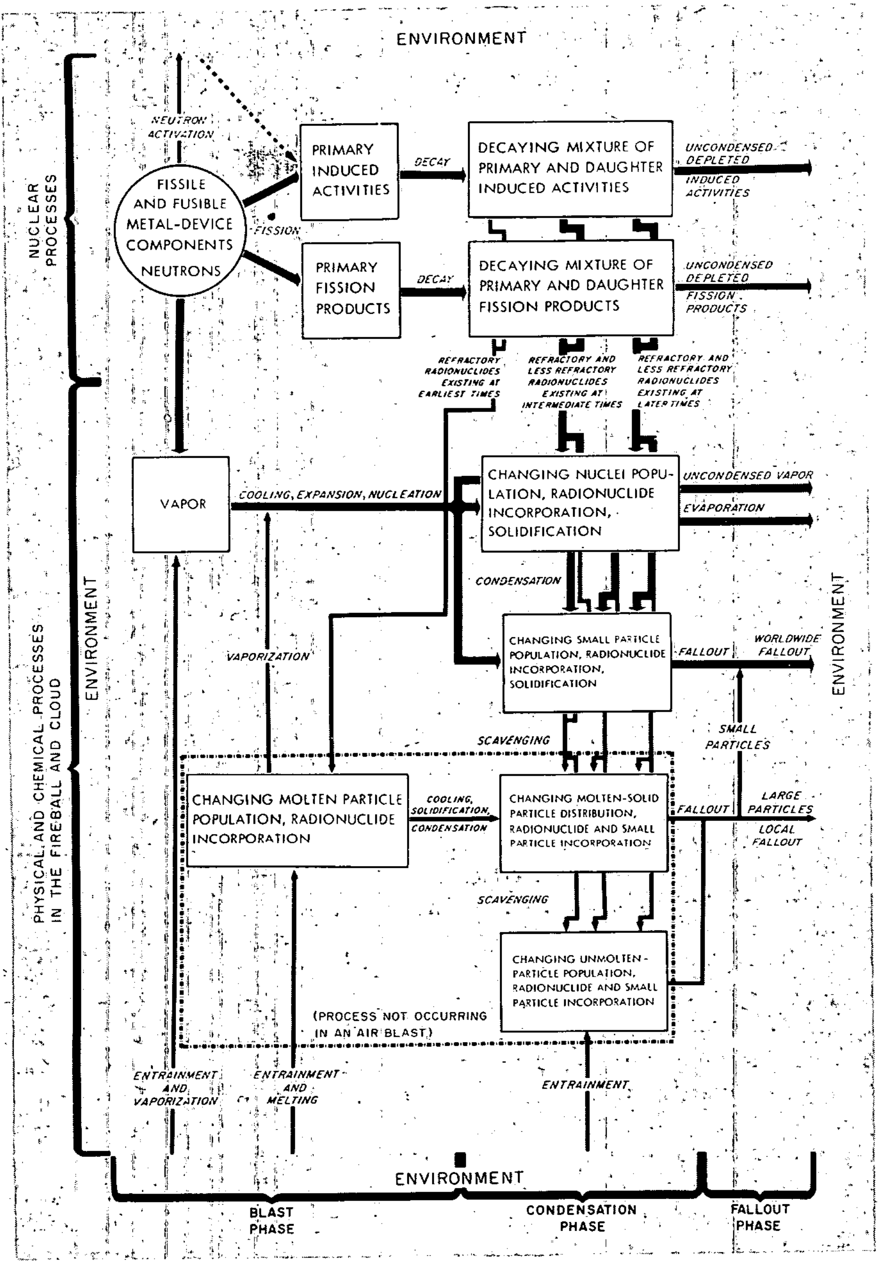

Fig. 5—Fallout-formation processes in air and surface bursts.

Mechanism With the help of Fig. 6, the mechanism can be described in the simple case from the viewpoint of a condensable molecule in the vapor phase. To be condensed, the molecule must first diffuse through the gas to the surface of a particle. Upon striking the surface the molecule can either rebound into the vapor or cling to the surface. After clinging to the surface awhile, the molecule may reevaporate or diffuse into the bulk of the particle. If it reevaporates, it can easily be deflected back to the surface by the first collision with another vapor molecule. Inside the particle the molecule may diffuse back to the surface. In the actual case these processes will be occurring while the temperature is dropping. Simultaneous condensation of macroscopic quantities of evaporated carrier can occur at early stages. Particles can collide and stick. Various chemical reactions and changes of species can occur at different steps of the way. Radioactive transformations will proceed concurrently. Evaporation of volatile daughters of condensed nuclides may be important, and radiation effects may be considerable. A rigorous treatment would obviously be highly complex. However, we can visualize certain simplifications under various conditions.

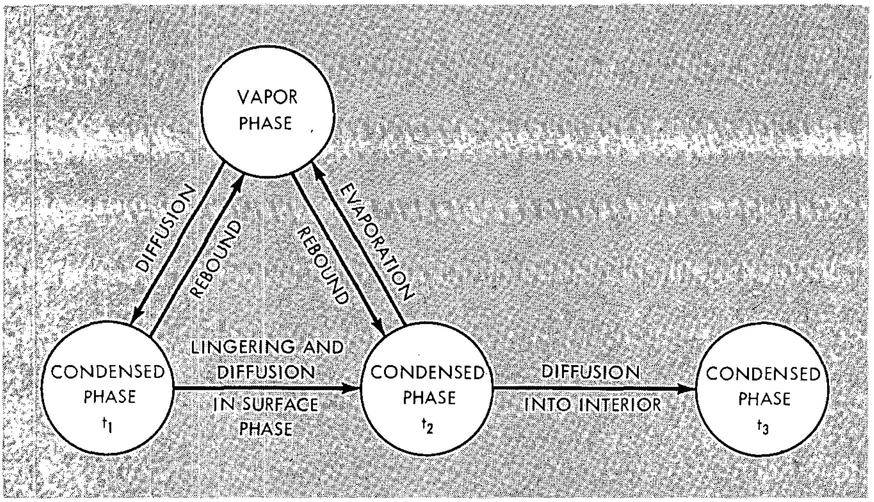

Fig. 6—Mechanism for kinetic approach to radionuclide incorporation by fallout particles.

Equilibrium Approximation One such simplification is the thermodynamic approach already described.[4,5] This will apply when the times for condensation and diffusion are short in comparison to the rates of radioactive decay and temperature decrease. This approximation will be favored by small particles and rapidly diffusing molecules. Einstein's equation

$$t = \frac{\xi^2}{2D_{12}}$$

provides a helpful rule of thumb in this regard. This equation relates the time t required for the mean-square displacement $\overline{\xi^2}$ to the coefficient of interdiffusion D_{12}. To estimate the time required to approach a significant degree of equilibrium, we can calculate the time required for ξ to equal one-tenth of a particle diameter. The degree achieved in this time will be appreciable as shown in the section entitled "Particle Diffusion." Thus, for D_{12} equal to 5×10^{-7} cm²/sec, a 100-μ-diameter particle would be well on the way to equilibrium in about a second. Interdiffusion coefficients for fission products in fused silicates are scarce. Figure 7 shows some cases that have been measured, together with some for elements that reasonably approximate fission products. Thus the curves for Rb^+ and Cs^+ in $Na_2O \cdot CaO \cdot 4SiO_2$ would probably be similar to, but below, that for Na^+, with Cs^+ being lowest. Similar relations would be expected among Sr^{2+}, Ba^{2+}, and Ca^{2+}.

To determine the validity of the thermodynamic equilibrium treatment under different conditions, one must compare the diffusion times with the cooling rate. The cooling rate is easily calculated by combining Hillendahl's equations,[15]

$$T(^\circ K) = 7000\ W(kt)^{-0.07} \left(\frac{t}{t_{fmax}}\right)^{-0.34}$$

and

$$t_{fmax}(sec) = 0.037\ W(kt)^{0.49}$$

to eliminate t_{fmax} (the time of the final maximum) and differentiating the result. The cooling rate, in terms of either time or temperature, is then given by

$$\begin{aligned} \frac{-dT}{dt} &= 776W^{0.10}\ t^{-1.34} \\ &= 30W^{-0.29} \left(\frac{T}{1000}\right)^{3.94} \\ &\cong 3 \times 10^{-11}\ W^{-0.3}\ T^4 \end{aligned}$$

The last equation was used to prepare Fig. 8, which shows cooling rate as a function of temperature for a wide range of total yields. We can now see what would happen during the 1-sec equilibration time referred

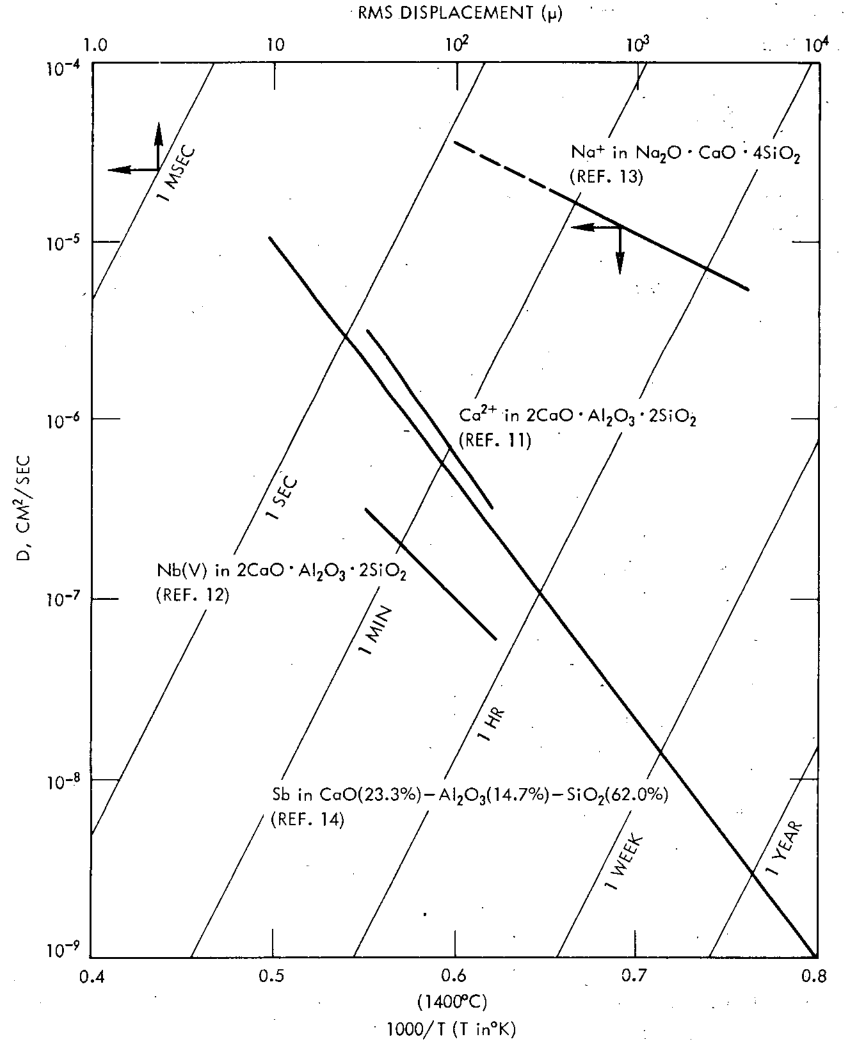

Fig. 7—Some experimental values of diffusion coefficients in molten silicates compared with the values necessary to achieve various root-mean-square displacements in given times.[11–14]

to previously under various conditions. At a temperature of 1400°C, a fireball from a 10-kt device would cool about 100°C in a second, and equilibration would never catch up to the falling temperature. For a 10-Mt burst (which is more in the high-yield range for which the treatment was originally designed), the temperature would fall only about 10°C, and the approximation is much more realistic, if still not entirely satisfactory. It should not be surprising, then, if the accuracy of

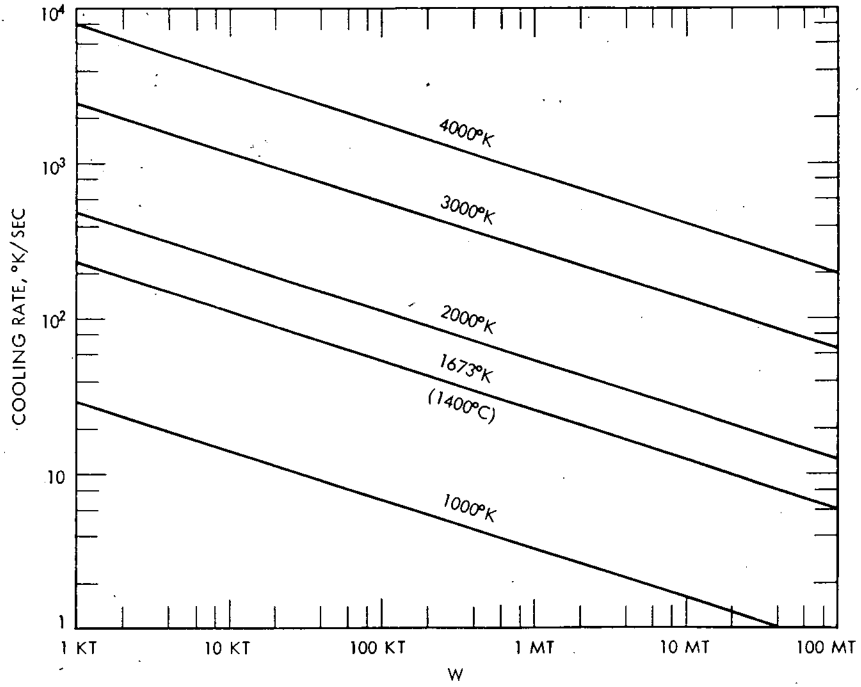

Fig. 8—Cooling rates as a function of temperature and total weapon yield.

predictions made with the thermodynamic equilibrium model is sensitive to yield.*

Examination of the previous figures clarifies the nature of another approximation used by the present system. The equilibrium treatment considers fallout formation to occur in two distinct stages. According to this approach, the particles during the first stage form an assembly of liquid drops, and condensing radionuclides distribute themselves among the particles in proportion to their volumes. At 1400°C the particles solidify, and further condensation results in surface distributions.

The diffusion data in Fig. 7 show no breaks, either in the neighborhood of 1400°C or anywhere else, for any of the silicates studied.

---

*Unfortunately, Hillendahl's equations are based on data which do not extend below 2000 degrees. Below 2000 degrees radiation becomes less important as a means of cooling than other processes, especially the engulfment of cold air. The cooling rates estimated here are therefore merely lower limits. Storebö[21] has attempted to accountfor the engulfment of cold air in air bursts. His cooling equations lead to cooling rates of the order of 10^3 degrees per second at 1400°C.

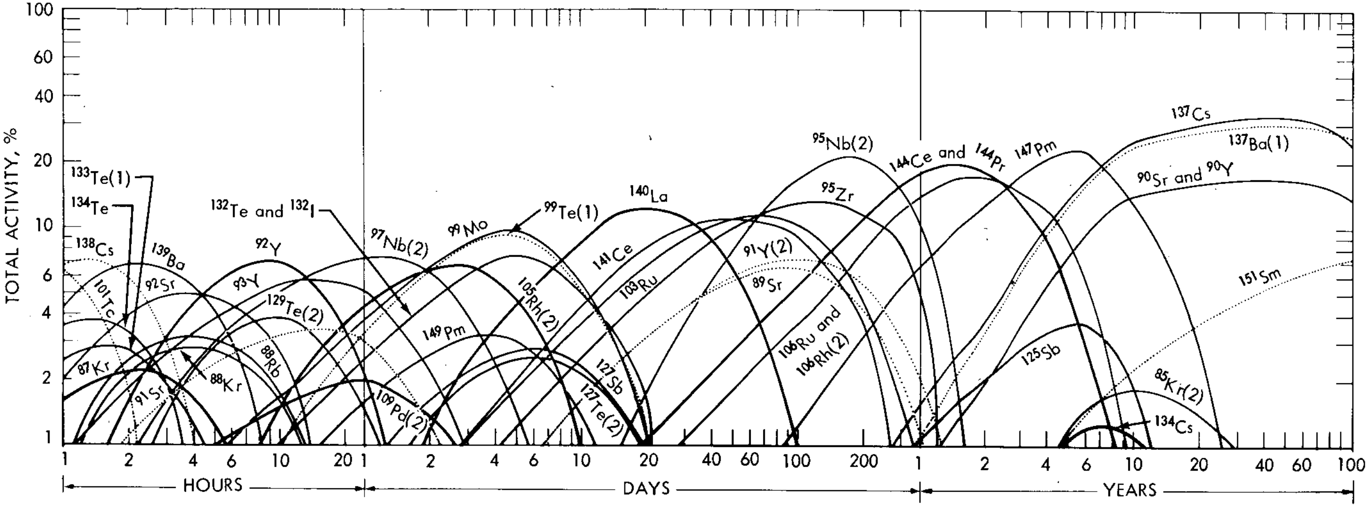

Fig. 11—Relative disintegration rates as a function of time for individual fission products in the case of ^{238}U fission produced by a thermonuclear neutron spectrum.

TCF 55

Conf 765

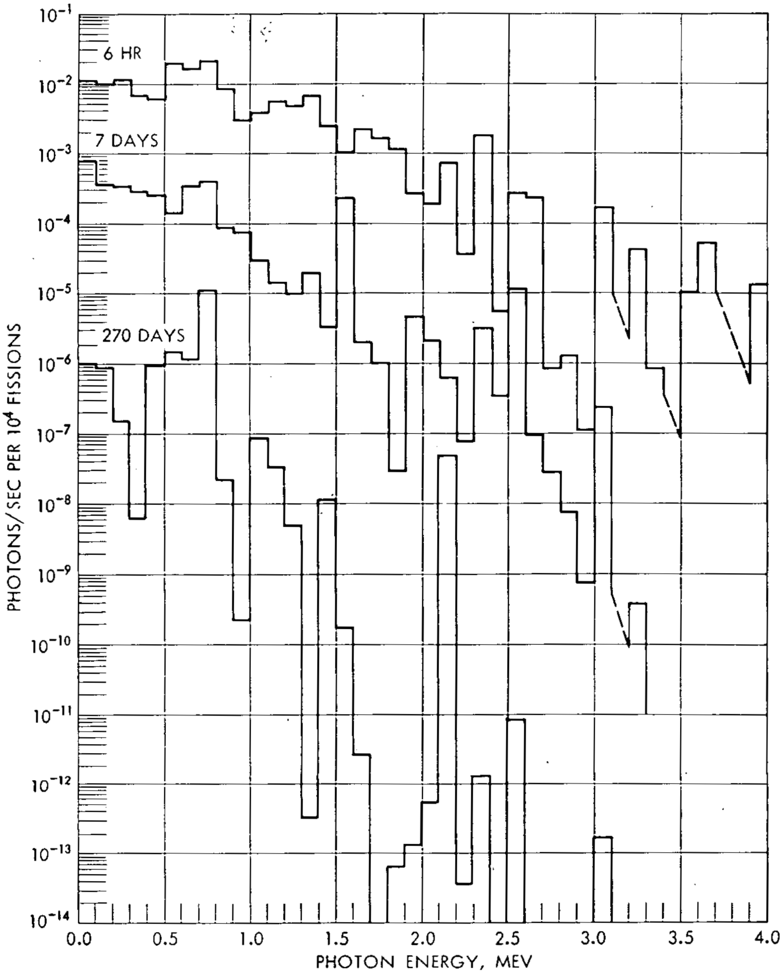

Fig. 12—Gamma-photon spectra from fission products at various times after ^{238}U fission produced by a thermonuclear neutron spectrum.

The relative contributions of the important gamma-emitting nuclides to the total dose-rate have been plotted vs. time in Fig. 14. It is interesting to note that from a few days onward much of the dose rate at any given time can be accounted for in terms of two or three nuclides and that volatilely behaving mass chains contribute prominently to the dose rate. The dose-rate contributions given here pertain, of course, to unfractionated debris. Since many of the hard emitters (e.g., cesium and iodine isotopes) are subject to fractionation, the relative dose-rate contributions will be greatly modified in the case of fractionated debris.

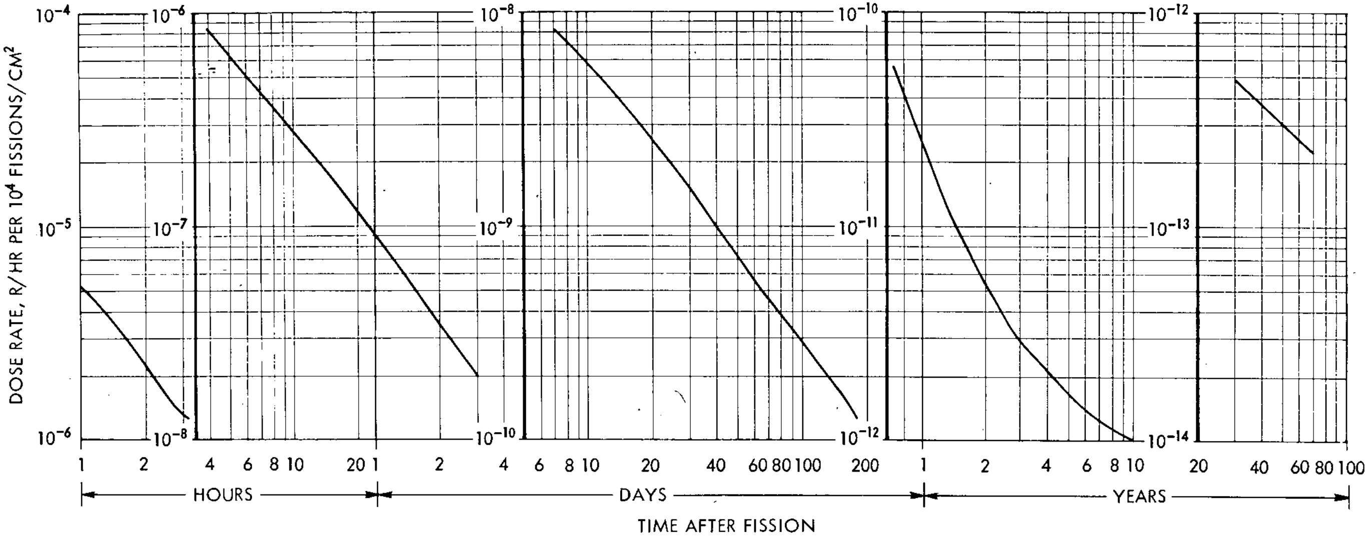

Fig. 13—Gross exposure-dose-rate decay for products of ^{238}U fission produced by a thermonuclear neutron spectrum.

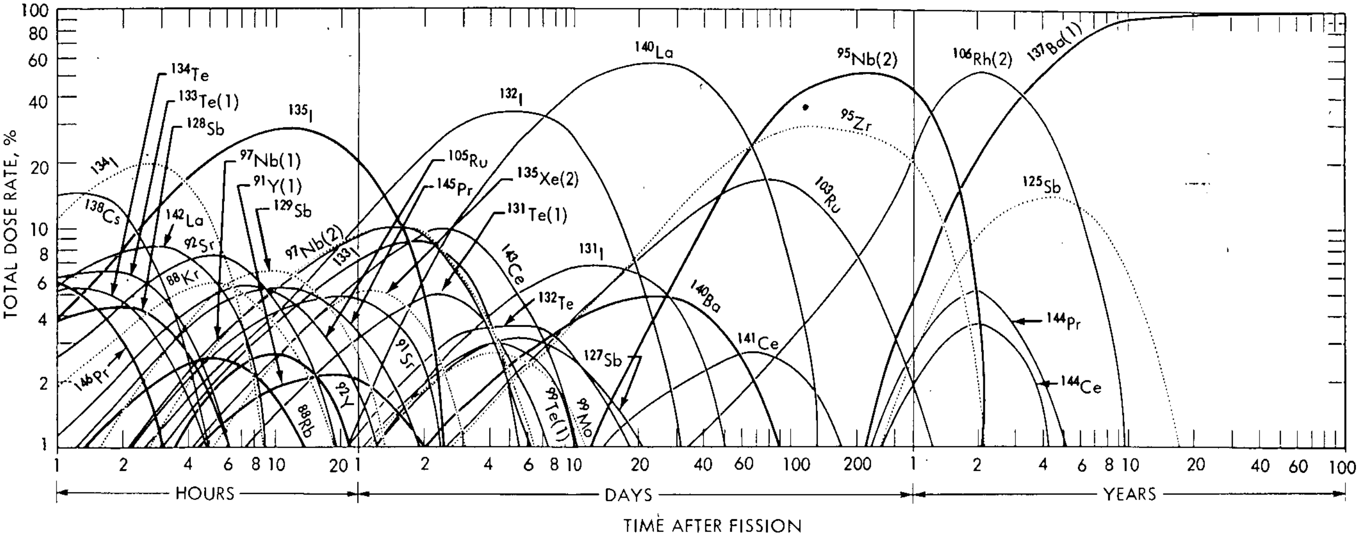

Fig. 14—Relative contributions to the exposure-dose rate as a function of time for individual fission products in the case of ^{238}U fission produced by a thermonuclear neutron spectrum.

ACKNOWLEDGMENTS

We are most grateful to Col. Irving J. Russell of the Air Force Weapons Laboratories and Dr. John Norman of General Atomic Division, General Dynamics Corporation, for permission to present their data prior to publication.

APPENDIX

TERMS AND DEFINITIONS

RADIONUCLIDE FRACTIONATION Any alteration of radionuclide composition occurring between the time of detonation and the time of radiochemical analysis which causes the debris sample to be nonrepresentative of the detonation products taken as a whole.

FRACTIONATED Two substances, either radionuclides or inert material, are fractionated with respect to each other in a sample of debris if they are not present in their representative ratio. The term is meaningless when applied to a single substance.

*POTENTIAL FRACTIONATION The existence of different compositions in various portions of a sample of debris when these portions are subject to separation by subsequent natural processes, e.g., the existence of particles of different size with different compositions in the same portion of a nuclear cloud or of a slurry in which different nuclides are distributed between liquid and solid phases in different proportions.

*NATURAL FRACTIONATION Fractionation produced by the processes occurring subsequent to detonation.

*PRIMARY FRACTIONATION IN AIR, TOWER, AND SURFACE BURSTS Actual fractionation produced by meteorological, gravitational, and centrifugal separation of potentially fractionated particles in a cloud.

*SECONDARY FRACTIONATION IN AIR, TOWER, AND SURFACE BURSTS Fractionation produced by interaction of the debris with radioactively inert environment (e.g., leaching with water or preferential small particle adsorption on surfaces).

*ARTIFACTITIOUS FRACTIONATION Fractionation resulting from human intervention (e.g., biased sampling, incomplete decontamination of collector surfaces, and faulty analytical techniques).

FRACTION OF CONSITITUENT OR EXTENSIVE PROPERTY IN A SAMPLE The ratio of the quantity of said constituent or property to the total amount produced by the device and measured at the same time when necessary (replaces the "bomb-fraction" concept).

---

*Asterisks indicate convenient, but not essential, terms.

EQUIVALENT FISSIONS The number of equivalent fissions present in a sample as determined by analysis for any constituent is the product of the total number of fissions produced by the device and the fraction of the total amount of constituent present (replaces the "fissions in the sample" concept).

FRACTIONATION COEFFICIENT OF TWO CONSTITUENTS IN A SAMPLE The ratio of their fractions or equivalent fissions.

*THE FRACTIONATION RATIO The ratio of fractions or equivalent fissions of ^{89}Sr to ^{95}Zr.

*DEGREE OF FRACTIONATION The Briggsian logarithm of the fractionation ratio.

*TERACALORIE 10^{12} calories (the kiloton equivalent of energy).

*TERACALORIE EQUIVALENT OF A NUCLIDE The ratio of quantity of nuclide produced in a detonation to the energy release in teracalories by fission.

TERACALORIE EQUIVALENT PER SQUARE MILE A unit of contamination surface density (replaces the "kilotons per square mile" concept).

REFERENCES

1. E. C. Freiling, *Fractionation. I. High Yield Surface Burst Correlations,* Report USNRDL-TR-385, U. S. Naval Radiological Defense Laboratory, Oct. 29, 1959; and *Science, 133:* 1991 (1961).
2. E. C. Freiling and S. C. Rainey, *Fractionation. II. On Defining the Surface Density of Contamination,* Report USNRDL-TR-631, U. S. Naval Radiological Defense Laboratory, Mar. 13, 1963.
3. E. C. Freiling, *Fractionation. III. Estimation of Degree of Fractionation and Radionuclide Partition for Nuclear Debris,* Report USNRDL-TR-680, U. S. Naval Radiological Defense Laboratory, Sept. 12, 1963; and *Science, 139:* 1058 (1963).
4. E. C. Freiling, M. A. Kay, and J. V. Sanderson, *Fractionation. IV. Illustrative Calculations of the Effect of Radionuclide Fractionation on Exposure Dose Rate from Local Fallout,* Report USNRDL-TR-715, U. S. Naval Radiological Defense Laboratory, Jan. 6, 1964.
5. E. C. Freiling, Fractionation in Surface Bursts, in *Radioactive Fallout from Nuclear Weapons Tests,* A. W. Klement, Jr. (Ed.), USAEC Report TID-7632, pp. 25-46, Feb. 1962.
6. C. F. Miller, *A Theory of Formation of Fallout from Land-surface Nuclear Detonations and Decay of the Fission Products,* Report USNRDL-TR-425, U. S. Naval Radiological Defense Laboratory, May 27, 1960.
7. C. F. Miller, *Fallout and Radiological Countermeasures,* Stanford Research Institute, Menlo Park, Calif., January 1963.
8. C. E. Miller, Jr., W. E. Browning, Jr., B. F. Roberts, and R. P. Shields, *Theory of Fission Product Fractionation in Reactor Fuel Experiments, Reactor Accidents and Weapons Fallout,* paper presented at the 148th National Meeting of the American Chemical Society, Chicago, Ill., Aug. 30 to Sept. 4, 1964.
9. S. L. Whitcher, L. R. Bunney, R. R. Soule, and R. da Roza, *Fallout Measurements by Aircraft and Rocket Sampling,* Operation Hardtack Report, WT-1625, U. S. Naval Radiological Defense Laboratory, Sept. 29, 1961. (Classified)

10. I. J. Russell, *A Radiochemical and Physical Investigation of a Low-yield Surface Burst,* Defense Atomic Support Agency, Project Officers Report, in preparation.
11. T. B. King and P. J. Koros, Diffusion in Liquid Silicates, in *Kinetics of High-Temperature Processes,* W. D. Kingery (Ed.), pp. 80-85, published jointly by Technology Press of Massachusetts Institute of Technology and John Wiley & Sons, Inc., New York, 1959.
12. V. I. Musikhin and O. A. Esin, Diffusion Coefficients in Molten Slags, in *Physical Chemistry of Molten Salts and Slags, Proceedings of the All-Union Conference, Nov. 22 to 25, 1960,* USAEC Report AEC-tr-5948, pp. 481-491.
13. V. I. Malkin and V. M. Mogutnov, Measurement of Coefficients of Autodiffusion of Sodium Ion in Three-component Silicate Melts, in *Physical Chemistry of Molten Salts and Slags, Proceedings of the All-Union Conference, Nov. 22-25, 1960,* USAEC Report AEC-tr-5948, pp. 492-501.
14. J. H. Norman, personal communication, 1964.
15. R. W. Hillendahl, *Characteristics of the Thermal Radiation from Nuclear Detonations,* Report USNRDL-TR-383, U. S. Naval Radiological Defense Laboratory, June 30, 1959. (Classified)
16. O. Knacke and I. N. Stranski, The Mechanism of Evaporation, in *Progress in Metal Physics,* Vol. 6, B. Chalmers and R. King (Eds.), p. 181, Pergamon Press, London, 1956.
17. N. Fuchs, Über die Verdampfungsgeschwindigkeit kleiner Tröpfchen in einer Gasatmosphäre, *Phys. Z. Sowjet, 6:* 224 (1934).
18. L. Lassen, G. Rau, and H. Weicksel, The Deposition of Radioactive Atoms on Monodisperse and Polydisperse Aerosols, *Z. Physik, 160:* 504-519 (1960); *161:* 339-345 (1961); and *163:* 363-376 (1961); see also USAEC Report UR-tr-647, University of Rochester, June 8, 1964.
19. H. S. Carslaw and J. C. Jaeger, *Conduction of Heat in Solids,* Clarendon Press, Oxford, 1959.
20. H. Scholze, H. Mulfinger, and H. Franz, Measurement of the Physical and Chemical Solubility of Gases in Glass Melts (He and H_2O), in *Advances in Glass Technology,* p.230, Plenum Press, New York, 1962.
21. P. B. Storebö, *On Particle Formation in Nuclear Bomb Debris,* Report F-446, Norwegian Defense Research Establishment, May 12, 1964.
22. L. E. Weaver, P. O. Strom, and P. A. Killeen, *Estimated Total Chain and Independent Fission Yield for Several Neutron-Induced Fission Processes,* Report USNRDL-TR-633, U. S. Naval Radiological Defense Laboratory, Mar. 5, 1963.
23. G. R. Crocker, *Estimates of Fission Product Yields of a Thermonuclear Explosion,* Report USNRDL-TR-642, U. S. Naval Radiological Defense Laboratory, Apr. 4, 1963.
24. C. D. Coryell, M. Kaplan, and R. D. Fink, Search for Correlations of Most Probable Nuclear Charge Z_p of Primary Fission Fragments with Composition and Excitation Energy, *Can. J. Chem., 39:* 646 (1961).
25. I. F. Croall and H. H. Willis, The Yields of the Isomers of Se-81 and Se-83 in the Thermal Neutron Fission of Pu-239, *J. Inorg. Nucl. Chem., 25:* 1213 (1963).
26. Massachusetts Institute of Technology, *Laboratory for Nuclear Science Progress Report,* USAEC Report NYO-10063, May 1, 1963.
27. R. C. Bolles and N. E. Ballou, *Calculated Activities and Abundances of U^{235} Fission Products,* Report USNRDL-456, U. S. Naval Radiological Defense Laboratory, Aug. 30, 1956.
28. G. R. Crocker and M. A. Connors, *Gamma Emission Data for the Calculation of Exposure-Dose Rates from Nuclear Debris,* Report USNRL-R&L-143, U. S. Naval Radiological Defense Laboratory, May 12, 1964.
29. L. D. Gates, Jr. and C. Eisenhauer, *Spectral Distribution of Gamma Rays Propagated in Air,* Report AFSWP-502A, Armed Forces Special Weapons Project, 1954.

30. D. A. Holme and K. Stewart, *The Gamma Dose-Rate above an Infinite Plane Source,* Report AWRE-E-6/63, United Kingdom Atomic Energy Authority, May 1963.
31. C. F. Miller, *Response Curves for USNRDL 4-pi Ionization Chamber,* Report USNRDL-TR-155, U. S. Naval Radiological Defense Laboratory, May 17, 1957.
32. R. Björnerstedt, Health Hazards from Fission Products and Fallout. II. Gamma Radiation from Nuclear Weapons Fallout, *Ark. Fysik, 16:* 293 (1959).
33. O. Glemser and H. G. Wendlandt, Gaseous Hydroxides, in *Advances in Inorganic Chemistry and Radiochemistry, Vol. 5,* H. J. Emeleus and A. G. Sharpe (Eds.), Academic Press Inc., New York, 1963.
34. C. E. Lapple, *Fallout Control,* Report SRIA-3, Stanford Research Institute, Aug. 1, 1958.

SMALL BOY SHOT FALLOUT RESEARCH PROGRAM

CARL F. MILLER and JAMES D. SARTOR
Stanford Research Institute, Menlo Park, California

ABSTRACT

In this paper the general outline of a field test program is presented along with the application of the outline to the design of the experimental program for the Small Boy shot. Also, a preliminary analysis and correlation of the data obtained on two of the projects is presented in a discussion and an evaluation of the intensity–activity ratio and the intensity–area integral per unit fission yield (i.e., the ratio of roentgens per hour at 1 hr per kiloton per square mile) for the fallout from the Small Boy shot.

INTRODUCTION

Over the past decade many significant advances in development and field testing of nuclear explosives have been made. In the field testing of nuclear weapons, explosion products, called fallout, received increasing attention as the testing proceeded. One of the major reasons for the increased attention to fallout was that, during this same period of time, better understanding and recognition of the radiological hazards to biological species from exposures to nuclear radiation were accomplished. In addition, studies of the application of nuclear explosives in possible future warfare showed that exposure of human beings and other living species to the nuclear radiations associated with fallout could result in many fatalities.

Field experimental programs designed to obtain information on fallout became increasingly complex as time progressed. The evolvement of experimental procedures in the field tended to reflect, at the time, both the understanding of the radiological hazards and the

γ

technical parameters that influenced the character and magnitude of the hazards.

The fallout study program for the Small Boy shot, as part of the last series of aboveground field tests of nuclear weapons, was cooperatively organized and sponsored by the Office of Civil Defense (OCD), the Department of Defense (DOD), and the Atomic Energy Commission (AEC). The projects sponsored by OCD were under the operational control of the Defense Atomic Support Agency (DASA); those sponsored by AEC were under the operational control of their Civil Effects Test Organization (CETO).

WEAPON-TEST-FALLOUT STUDY PROGRAM

A general outline of the information and data requirements and the program objectives was prepared prior to the establishment of the experimental projects for the Small Boy shot field test. This outline was reviewed by various representatives of OCD, DASA, and AEC.

The outline, reflecting operational data requirements by the three agencies, included an overall design of field experimental programs for improving the data base on fallout. The data needs were divided into the following four subprograms or study areas:

1. Fallout formation
2. Distribution of fallout
3. Definition of radiological exposure environments
4. Alteration of exposure environments by radiological countermeasures

For each of the four study areas, a general list of the parameters for direct or indirect experimental evaluation was prepared. These are given in Tables 1 to 4. The first three study areas were organized to provide input data for fallout-model development and radiological-hazard evaluations needed by all three agencies. The fourth study area was designed somewhat more specifically for providing information for use in the evaluation of radiological-safety programs for AEC and in the design and evaluation of radiological-defense systems for OCD.

The main overall objective of the weapon-test-fallout study was to make experimental determinations and to obtain and report experimental data needed for describing and defining the parameters in each of the four study areas. The objective for the field-test program was limited to the taking and reporting of experimental data because each agency sponsored other research tasks for the correlation and evaluation of the observed data and because inclusion of data analysis in field-test reports previously had usually resulted in extended delays in report publication.

Table 1— FALLOUT-FORMATION PARAMETERS

- Initial condition variables
  - Composition of the device
  - Composition and physical properties of the environmental materials at shot point
- Geometric parameters
  - Dimensions and location of the visible fireball and cloud as a function of time after detonation
  - Dimensions of the apparent crater and crater lip
  - Spatial distribution of radioactivity in the fireball and cloud volume as a function of time after detonation
  - Spatial geometry of toroidal circulation of the rising fireball and cloud
- Energy balance parameters
  - Air overpressures and ground-shock energies
  - Radiant energy emitted as a function of time after detonation
  - Temperature of fireball gas as a function of time after detonation
  - Material composition of fireball and influx, mixing, and ejection of gases and particles as a function of particle size and time after detonation
  - Energetics (dynamics) of particle circulations in and about the rising fireball and cloud
- Related resultant parameters
  - Chemical composition of fallout particles
  - Radiochemical composition of particles as a function of particle diameter, including specific activity of the particles
  - Radioactivity and mass-distribution functions
  - Solubility of radioelements as a function of particle size
  - Shape, structure, and density of fallout particles and internal distributions of crystalline and glass phases and of the radioelements within the fallout particles

Table 2— FALLOUT-DISTRIBUTION PARAMETERS

- Initial-condition variables
  - Spatial distribution of radioactivity and mass of particles at the time of cloud stabilization and at the times when particles start free-gravity fall
- Particle-fall-rate parameters
  - Density distribution of fallout particles as a function of particle diameter, shape, and number or mass
  - Atmospheric conditions (air density, viscosity, temperature, pressure, relative humidity, etc.) as a function of altitude over the fallout area
  - Particle shape and drag factors
  - Agglomeration effects (including incorporation of solid particles in raindrops)
- Meteorological parameters
  - Wind speeds and direction as a function of altitude and time over the whole fallout area
  - Vertical air motions
  - Effect of terrain features and diurnal heating and cooling on the air-flow patterns
- Deposition dynamics
  - Time of arrival of fallout particles at given locations on the ground or in the air as a function of particle size
  - Duration of fallout deposition at given locations in the fallout area

(Table 2 continues on page 47)

Rate of accumulation of particles in terms of radioactivity and mass at given locations in the fallout area
Effect of rainfall on deposition rates and air concentration of particles

Area distribution of the fallout particles
  Standard intensity contours (usual fallout pattern expressed in roentgens per hour at 1 hr at 3 ft above an open contaminated area)
  Intensity–activity ratios (in roentgens per hour at 1 hr per kiloton per square mile at various locations in the fallout area
  Intensity–area integral and fraction of the device in the fallout area
  Fraction of the total radioactivity and mass of particles deposited on the earth's surface as a function of time after detonation
  Surface-density contours (mass of particles deposited per unit area)
  Gross fractionation numbers for the fallout deposited at given locations in the fallout area as a function of particle diameter

Table 3 — RADIOLOGICAL-EXPOSURE-ENVIRONMENT PARAMETERS

Initial contamination of surfaces
  Surface wind speeds and directions and relative humidity
  Effect of large- and small-scale surface roughness features of terrain on the airflow over the surface
  Shape, size, general orientation, *and character of the surface*
  Impaction and retention efficiency of particles and surfaces as a function of the above parameters, particle diameter, and surface density of the deposit
  Initial contamination factors for plants, animals, and humans
  Inhalation of fallout particles during fallout deposition by animals and humans as a function of particle diameter, wind speed, and related factors

Natural redistribution of deposited fallout particles and radiation sources
  Transfer of soluble radionuclides from the fallout particles to surfaces by dew *and rain as a function of time, particle size,* and amount of dew and/or rain
  Effect of erosion by wind and rain of the deposited fallout particles from and onto surfaces on the ionization rate and particle surface density as a function of particle diameter, type of surface, wind speed, amount of rainfall, time period over which erosion occurs, and general terrain features
  Movement of soluble radionuclides and particles in and over soils due to rainfall as a function of particle diameter, gross deposit surface density, soil type, number of rain showers, and amount of rainfall
  Movement of soluble radionuclides and particles in streams and rivers as a function of particle size, deposit surface density, water flow rates, and other stream or river characteristics
  Variation of retention efficiencies and contamination factors on meteorological parameters (wind, rainfall, relative humidity, etc.)
  Inhalation of redistributed (wind-blown) particles
  Movement of particles by people and vehicular traffic

External gamma-radiation-exposure parameters
  Variation of air ionization rates with time *after detonation at given locations* in the fallout region (reference geometry: 3 ft above an open contaminated area)
  Gross ionization-rate decay of the radioactivity carried by particles as a function of particle diameter
  Attenuation of gamma rays by terrain-roughness features
  Variation of the air ionization rate with altitude over given locations in the fallout area

(Table 3 continues on page 48)

Table 3—(Continued)

- Response factors for radiation detecting instruments
- Area radiation-contribution factors for discontinuous source geometries and variable source intensities
- Skyshine-contribution factors as a function of surface roughness and source geometry

Contact radiation exposures
- Beta dose and dose rates in air over contaminated surfaces as a function of distance from the surface
- Absorbed beta dose to the tissue of contaminated plants, animals, and humans
- Dependence of absorbed contact beta doses on meteorological factors, exposure times, and environmental factors (all biological species, including insects)

Internal radiation-exposure parameters
- Biological availability of individual radionuclides as a function of particle size
- Foliar absorption of radionuclides by edible plants or plant parts as a function of particle diameter
- Uptake rate of radionuclides by edible plants grown on tilled and untilled soils as a function of particle diameter or location, plant growth rates, soil type, and climatic variables
- Ingestion and assimilation rates of radionuclides by tissues of animals and radionuclide concentrations in animal tissues and food products from animals fed with contaminated plant parts and water obtained from different locations in the fallout area
- Absorbed doses to plants, animals, and humans from ingestion of radionuclides (all intake paths)

Table 4—ALTERATION OF EXPOSURE ENVIRONMENTS BY RADIOLOGICAL COUNTERMEASURES

Attenuation of gamma-ray intensities
- Shelter protection factors as a function of wall materials and thickness, radiation-source geometry, and compartment size, shape, and location in building
- Attenuation by barriers as a function of barrier height and thickness and other geometric parameters, such as the distance from barrier or the dimensions of area enclosed by the barrier
- Attenuation by burial of the fallout particles by covering them with soil or by plowing (i.e., mixing the fallout with soil to various depths) land areas

Decontamination
- Effectiveness of the removal of fallout particles from contaminated surfaces as a function of the method and its procedural parameters, particle diameter of the fallout, surface density of the fallout, weathering, type of surface, and effort applied
- Disposal of fallout particles removed by decontamination
- Exposure dose to decontamination crews during decontamination operations as a function of the type of area that is cleaned, the operation schedule, and the methods of decontamination
- Effectiveness of water purification methods in the removal of soluble radionuclides and fallout particles from exposed water sources
- Effectiveness of food processing and treatment methods in the removal of soluble radionuclides from contaminated food products (i.e., milk decontamination, removal of particles from grains in threshing and milling, desorption of radionuclides from vegetables into water, etc.)

(Table 4 continues on page 49)

Exposure control methods
  Reduction in exposure doses by scheduling of exposures for operations
  Reduction in exposure doses by adjustment of living routines as a function of time after detonation and radiation intensity
  Reduction in absorbed doses to animals and humans by storage and allocation of contaminated foodstuffs
  Ingress of fallout particles into shelter spaces through openings and ventilation systems and effect on the exposure dose or on the shelter protection factor
  Verification of shielding provided by specially designed shelter-entryway configurations
  Proof tests of operational radiological-defense systems and overall effectiveness evaluations

The individual project titles, as parts of the field-test fallout program for the Small Boy shot, are listed in Table 5. The projects, with a few exceptions, were very successful in meeting their individual objectives. This general success was due, first, to the detailed development of the project experimental designs on the part of the project leaders and the efforts of all the project personnel in carrying out the work and, second, to the favorable winds that carried the fallout over the established station array. It should be noted that projects involving the design and testing of sampling equipment for possible use in future programs were included in the program.

Table 5 — PROJECT PARTICIPATION IN SMALL BOY SHOT FALLOUT PROGRAM

1. Thermal measurements and fireball photography
2. Meteorological measurements
3. Radiological survey of the fallout area
4. Aerial survey of the fallout area
5. Fallout collection and gross sample analysis (onsite and offsite)
6. Field ionization-rate measurements
7. Long-range fallout collection and radiochemical analysis
8. Physiochemical and radiochemical analysis of fallout samples
9. Terrain shielding measurements and field spectra (onsite and offsite)
10. Contamination of plants
11. Ingestion of radionuclides in fallout by native animals
12. Assimilation of radionuclides in fallout by humans
13. Contamination of milk (unscheduled)
14. Proof-test of a prototype rocket-mounted collector
15. Test of a prototype fallout sampler
16. Comparison of aerial-survey instruments

THEORY OF THE INTENSITY-ACTIVITY RATIO AND THE INTENSITY-AREA INTEGRAL

Known relations between the observed radiation rates and the radioactivity carried by fallout particles spread over real (open) terrain are required to evaluate radioactive-material balances and the relative worldwide disposition of all the radionuclides produced in a nuclear detonation. The ratio of the roentgens per hour at 1 hr to kilotons per square mile, where the kilotons are taken as being a measure of the radioactivity carried by the fallout particles, is used in the integration of fallout-pattern contours to estimate the fraction of the device accounted for in the pattern. Other more detailed uses of the ratio include the effects of terrain roughness and radionuclide fractionation on gamma-radiation intensities. Some mathematical fallout models utilize this ratio in estimating standard intensities (i.e., the roentgens per hour at 1 hr values at 3 ft above a uniformly contaminated plane) in computing fallout patterns.

It is generally known that the intensity–activity ratio can be defined for the intensity as observed at a given location or, as an average, for a whole fallout area, where it is sometimes called the intensity–area integral per unit fission yield. It is convenient in data analyses to express the surface density of the radioactivity in fissions per square foot rather than in kilotons per square mile. Both representations of the surface density of radioactivity are independent of time after detonation. Since the relation between the number of fissions and the energy released in fission is about the same for most common fissile materials, namely, $(1.45 \pm 0.03) \times 10^{23}$ fissions per kiloton of fission yield, the two representations of the surface density of radioactivity are related by

$$A_f = 5.20 \times 10^{15} A_w \tag{1}$$

where A_f is in fissions per square foot and A_w is in kilotons per square mile.

The intensity–activity ratio for a given location in a fallout region is defined by

$$K_0 = \frac{I_s}{A_f} \tag{2}$$

where I_s is an observed or a measured value of the (standard) intensity in roentgens per hour at 1 hr at 3 ft above an extended open flat area uniformly covered with fallout particles carrying the appropriate amount of radionuclides to result in the surface density, A_f, in fissions per square foot or the equivalent surface density, A_w, in kilotons per square mile, as given by Eq. 1. The standard intensity, I_s, is usually determined from a measurement of the roentgens per hour at the location after all the fallout has been deposited and a decay correction of the observed intensity to the standard time of 1 hr after detonation has been made.

The value of K_0 has been computed for uniform depositions of unfractionated fission products on ideal smooth planes. However, the calculated values of K_0 from observed values of I_s over real terrain for a given value of A_f or A_w are lower than those computed for the ideal plane because of attenuation of the gamma-ray intensity by both small- and large-scale roughness of real terrain, nonidealized responses of radiac instruments used in measuring the intensity, and decreased contributions from the more volatile fission-product radionuclides whose relative concentrations in the fallout are decreased (i.e., the radioactive composition is altered or fractionated). The values of I_s, relative to those for the fission products, are increased by the production of induced radionuclides (usually through neutron capture) in both weapon components and nearby environmental materials. The representation of K_0, including consideration of the four factors discussed in this paragraph, is given by

$$K_0 = Dq(r_{fp}k_{fp} + r_i k_i) \tag{3}$$

where D = instrument response factor for the assumed detector–radiation source geometry

q = terrain attenuation factor

k_{fp} = computed value of I_s/A_f for 3 ft above an ideal plane uniformly contaminated with unfractionated fission products

r_{fp} = gross fractionation number and is equal to the ratio of I_s for the fractionated mixture of radionuclides to the I_s for the unfractionated mixture

k_i = computed value of the I_s/A_f contributions from induced radionuclides for the same detector–source geometry as for k_{fp}

r_i = gross fractionation number for the induced radionuclides and is related to k_i in the same way that r_{fp} is related to k_{fp}

If it is accepted that the radionuclide composition varies with the size of the fallout particles, the major factors in Eq. 3 that are dependent on particle diameter are r_{fp} and r_i. In more precise treatments, D and q also depend on the radionuclide composition because both of these parameters are functions of gamma-ray energy, which, in turn, depends on the relative abundance of the radionuclides in the fallout.

The value of the intensity–area integral for a fallout pattern usually is determined by integration of the standard intensity contours from the highest intensity to a selected low-valued contour. The fractions of the radionuclides deposited outside the lowest contour are not included in the pattern summations. Also, the quantities that are buried in the crater and crater lip would not be included in the pattern summations. The intensity–area integral is defined mathematically by

$$J_R = \int_R I_s \, da \tag{4}$$

$$= \int_R K_0 A_f \, da \tag{5}$$

where da is the incremental area, dx dy, and R is the region within the lowest I_s contour included in the integral. If $\overline{K}_0$ is designated as the weighted average value of the K_0's and C as the ratio of intensity area for the region R to the integral for the region enclosed by the contour of I_s equal to zero, then J_R can be represented by

$$J_R = C\overline{K}_0 BW \tag{6}$$

where W is the total weapon yield and B is the fraction of the total yield due to fission. If the $\overline{K}_0$ value for the unfractionated mixture of radionuclides produced in the detonation is designated as K_0^0 ($r_{fp} = 1$, $r_i = 1$), then the fraction of the device deposited in the region, R, is given by

$$F_D = \frac{J_R/BW}{K_0^0} \tag{7}$$

or

$$F_D = \frac{C\overline{K}_0}{K_0^0} \tag{8}$$

If $\overline{K}_0$ is written in the form of Eq. 3, then Eq. 8 becomes

$$F_D \approx \frac{C[\overline{r}_{fp}k_{fp} + \overline{r}_i k_i]}{[k_{fp} + k_i]} \tag{9}$$

In Eq. 9 the two bracketed terms refer to the intensities over an ideal smooth plane on the assumption that the product $D\overline{q}$ for $\overline{K}_0$ is equal to Dq for K_0^0.

The values of $C\overline{K}_0$ and F_D for a fallout pattern can be estimated from the intensity–area integral and the values of k_{fp}, k_i, D, and $\overline{q}$ or q. The value of C can be estimated if $\overline{K}_0$ is evaluated separately, and K_0 can be evaluated if the variation of K_0 with particle size and the fraction of the total radioactivity carried by particles of different sizes are known. With these two types of data, K_0 is calculated from

$$\overline{K}_0 = \sum_j f_j K_{0j} \tag{10}$$

where f_j is the fraction of the total activity carried by particles with a range in diameter designated by j and K_{0j} is the value of K_0 for the same particle-size groups. However, for a determination of the variation of K_0 with particle size, the variation of r_{fp} and r_i with particle size must be known, and approximate values of q or Dq must be determined.

The average value of r_{fp} (and of r_i) for the intensity summation can be calculated in the same way as $\overline{K}_0$ so that

$$\overline{r}_{fp} = \sum_j f_j r_j \tag{11}$$

where r_j is the r_{fp} value for the *jth* particle group.

TREATMENT OF THE DATA

Preliminary analyses and correlations of the radiochemical data and gross-sample-activity, sieved-sample-activity, decay-rate, and intensity measurements in the field on the fallout from the Small Boy shot have been made, leading to the evaluation of preceding parameters. Certain simplifying assumptions are made for portions of the analyses to facilitate the treatment of the data and the presentation of the computational results.

First, it is assumed that, in Eq. 3, the values of $r_i k_i$ are small compared with the values of r_{fp}, and K_0 is represented only by

$$K_0 = Dqr_{fp}k_{fp} \tag{12}$$

The values of K_0 were determined according to Eq. 2, in which the I_s value of each fallout-collecting station was derived from correlations between data from gamma intensity time recorders (GITR's) and activity measurements on the collected samples.[1,2] The values of A_f were derived from radiochemical analyses of the collected fallout samples, and the fission yield equivalent for each sample was based on the amount of ^{95}Zr found in each sample.[3]

The values of r_{fp} were determined by taking the ratio of the ion current per fission of a gross fallout sample, as measured in a calibrated 4π ion chamber[4] to the computed ion current per fission for an unfractionated fission-product mixture.[5] In the field project,[1] the radioactive content of all collected gross samples and all sieved fractions of gross samples was measured either with the ion chamber or with a calibrated gamma scintillation counter. The activity of many samples was measured with both instruments. The measured ion currents in milliamperes and the photon pulse rates in counts per minute for each sample were decay-corrected to 100 hr after detonation.

If the measured ion current per ^{95}Zr fission at 100 hr from the ion chamber is designated as i(100) and the calculated ion current per fission for the unfractionated fission product at 100 hr after fission is designated as $i_0(100)$, then the gross fractionation number for the measured sample at 100 hr is

$$r_{fp}(100) = \frac{i(100)}{i_0(100)} \tag{13}$$

The definition of the r_{fp} by ratios of the ion currents from the ion chamber implies the assumption that i/i_0 is equal to I_s/I_s^0, where I_s^0 is the roentgens per hour for an unfractionated fission-product mixture. This assumption is fairly valid for most measurements on fission-product mixtures.[5] For correlation purposes, a fractionation number, r'_{fp}, is defined for the calibrated gamma-scintillation-counter measurements as

$$r'_{fp}(100) = \frac{i'(100)}{i'_0(100)} \tag{14}$$

where $i'(100)$ is the observed counting rate per ^{95}Zr fission at 100 hr after detonation for a sample of fallout and $i'_0(100)$ is the calculated counting rate per fission for the unfractionated fission-product mixture.

The r_{fp} of Eq. 12 is for the i ratios at 1 hr after detonation rather than at 100 hr. For evaluation of r_{fp} the i(100) values were decay-corrected to 1 hr after detonation (or after fission). The assumed decay-correction factors for i and i′ are represented by

$$i(1) = 250\ i(100) \tag{15}$$

and

$$i'(1) = 200\ i'(100) \tag{16}$$

The only available computed values of i_0 and i'_0 for the 4π ion chamber and the calibrated gamma scintillation counter, respectively, are those[5,6] for the products from thermal-neutron fission of ^{235}U. For this mixture $i_0(100)$ is 2.48×10^{-20} ma/fission and $i'_0(100)$ is 2.10×10^{-9} counts/min per fission. The two respective calculated decay-correction factors from 100 to 1 hr after fission are represented by

$$i_0(1) = 435\ i_0(100) \tag{17}$$

and

$$i_0'(1) = 246\ i_0'(100) \tag{18}$$

Thus

$$r_{fp} = 0.575 \frac{i(100)}{i_0(100)} \tag{19}$$

and

$$r'_{fp} = 0.813 \frac{i(100)}{i_0(100)} \tag{20}$$

Actually the decay factors for i and i′ should vary with r_{fp} or with the particle size of the fallout. Thus, for samples in which the degree of fractionation (^{235}U products) is small, the decay factor from 100 to 1 hr should approach 435. In this preliminary analysis, the previously assumed decay factors (Eqs. 15 to 18) were used for all samples; neither observed nor specially computed decay factors for all fallout samples were available for application in Eq. 19. The assumption that all samples had the same decay factor could result in an error of a factor of 2 in the r_{fp} value for some of the fallout samples.

The variation of i(100), $r_{fp}(100)$, and r_{fp} with particle size was investigated by using ion-chamber and radiochemical-analysis data[3] on sieved fractions of collected fallout samples. Two sets of the ion-chamber measurements were reported. In addition to the field measurements, which were corrected to absolute ion-current values, an uncorrected second set of measurements was reported by the radiochemical-analysis project.[3] These data were corrected to 100 hr after fission by using $(t/100)^{1.07}$ for computing the decay factors. The decay-corrected data were then correlated with the field measurements to obtain a correction factor for conversion of the data to absolute units. This was done by computing the ratio of the two measurements (corrected to 100 hr) on each sample. The median value of this correction factor was calculated to be 0.788, which is close to the value of 0.78 obtained in the past with a radium standard.[7] After application of this second correction factor to the second set of measurements, the geometric mean value of i(100) was calculated from the two sets of the ion-chamber measurements and the reported[3] fission-yield content of each sample. The i(100) values thus obtained are given in Table 6 and are plotted in Fig. 1 as a function of the midrange particle diameter, $\bar{d}$, for each sieve fraction. Subsieve analyses indicated the

Table 6—ION CURRENT PER FISSION FOR SIEVED FRACTIONS OF FALLOUT SAMPLES

[i(100) (10^{-20} ma at 100 hr per fission)]

Station	Midrange particle diameter, μ							
	22	66	132	264	530	1060	2120	>4000
100	3.88	3.30	0.950	1.02	0.676	0.844	1.32	
101	3.74	1.48	1.14	0.855	0.680		0.791	1.48
201	4.50	2.07	1.02	0.668	0.967	0.751	0.846	15.9*
203	0.271*	1.70	1.72	0.678	0.997	0.662	1.60	
305	3.96	1.78	1.10	1.04	0.983	0.784	0.741	1.08
403	3.90	2.34	0.782	1.02	0.693	1.04	4.62*	3.24*
505	4.42	2.39	0.669	1.00	0.768	16.8*	8.44*	4.28*
507	0.821*	1.37		1.01	0.656	0.726	19.7*	
603	3.52	1.72	0.610	0.462	0.682	35.9*	0.880	
707	5.49	1.86	1.06	1.00	0.615	10.3*		
813	3.56	0.942	1.25	0.810	3.90*	1.53	1.52	
Mean	4.06	1.82	0.989	0.848	0.759	0.871	1.05	1.26
Smoothed curve	4.06	1.82	1.10	0.78	0.76	0.87	1.05	1.26
$r_{fp}(100)$	1.64	0.734	0.444	0.315	0.306	0.351	0.424	0.508
r_{fp}	0.942	0.422	0.255	0.181	0.176	0.202	0.244	0.292

*Values not used in calculating mean values.

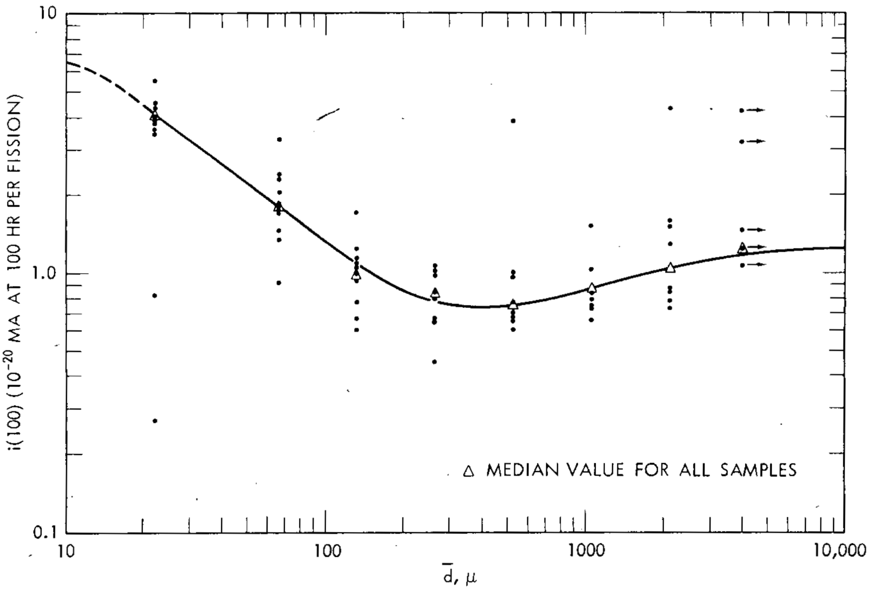

Fig. 1—Variation of i(100) with particle diameter.

presence of particles with diameters as small as 1 to 3 μ in all samples;[2] therefore the midrange diameter of the 0- to 44-μ fraction was taken as 22 μ.

The mean values of i(100) were computed for each particle-size fraction on the assumption that the average radionuclide composition carried by particles of a given size is the same everywhere and is independent of where the particles land. After correlation the two sets of ion-chamber data were generally in very good agreement; therefore most of the spread in the i(100) values for each particle size is due mainly to spread in the radiochemical results. The spread in the values is largest for the smallest and largest particle diameters where the analytical sample sizes were smallest. In the midrange of the curve, the minimum-to-maximum spread in i(100) is a factor of about 3.

The major significance of the data is in the variation of i(100) and therefore of $r_{fp}(100)$ and r_{fp} with particle size. From the average particle diameter of 22 μ up to an average particle diameter of about 400 μ, i(100) decreases by a factor of about 5.5. At 400 μ diameter, a minimum in the curve exists. A similar variation with particle size in the gross solubility of the radionuclides is observed.[3]

The K_0 values for the collecting-station locations in the fallout area from the Small Boy shot were calculated with adjusted and averaged A_f values; correlations of the variation in i′(100) and i(100) with the median particle size of the fallout particles at each station were used to make the adjustments in A_f. Initial correlations of i′(100) indicated a consistent difference in value depending on the time at which the samples were allocated for chemical analysis; the median value of the correlation factor for this difference was calculated to be 1.56. Since evidence for locating the cause of this difference is presently not available and since the calibrated gamma-scintillation-counter measurements were a highly unlikely source of error, the reported A_f values[3] for the samples with the higher values of i′(100) were increased by a factor of 1.25, and the A_f values for the remainder of the samples were decreased by a factor of 1.25. If the same type of correlation, including comparisons with the observed I_s values,[1] are applied to a third set of samples collected at offsite locations, the reported A_f values[2] are found to be more or less consistently high by a factor of 10.

The data for the fallout samples leading to the calculation of K_0 for each location are summarized in Table 7. Included are the activity median particle size, d_{50}; the ion-chamber measurements on the gross samples, I_1, I_2, and I; the values of $i_1(100)$, $i_2(100)$, and i′(100), as calculated from the initially adjusted values of A_f (given as A_1); the smoothed-curve values of i(100) and i′(100), as taken from the curves in Figs. 2 and 3; the recomputed values of A_f, where A_2 is $I_1/\bar{i}(100)$, A_3 is $I_2/\bar{i}(100)$, and A_4 is $I'/i'(100)$; the average value of A_f; I_s; and K_0.

57

Table 7—SUMMARY OF CALCULATIONS* OF A_f AND K_0 FOR THE SMALL BOY SHOT FALLOUT

Station–sample No.	d_{50}, μ	$I_1(100)$, ma/ft^2	$I_2(100)$, ma/ft^2	$I'(100)$, counts/min per sq ft	$i_1(100)$, 10^{-20} ma / fission	$i_2(100)$, 10^{-20} ma / fission	$i'(100)$, 10^{-9} counts/min / fission	$\bar{i}(100)$, 10^{-20} ma / fission	$\bar{i}'(100)$, 10^{-9} counts/min / fission
100–1	640	212×10^{-8}	220×10^{-8}	2.22×10^5	0.763	0.791	0.802	0.836	0.785
100–2	640	220×10^{-8}	220×10^{-8}	2.37×10^5	1.048	1.048	1.130	0.836	0.785
101–1	1100		174×10^{-7}	1.30×10^6		1.193	0.890	0.880	0.893
101–6	1100		174×10^{-7}	1.29×10^6		0.650	0.482	0.880	0.893
103–9		131×10^{-11}			0.0570†			(1.0)	(0.93)
200–9	130	122×10^{-9}	143×10^{-9}	1.16×10^4	1.100	1.288	1.046	1.13	0.985
201–7	750		831×10^{-8}	7.95×10^5		0.950	0.908	0.842	0.835
201–10	750	113×10^{-7}	831×10^{-8}	7.92×10^5	0.876	0.645	0.614	0.842	0.835
202–9		827×10^{-12}			0.484			(0.843)	(0.84)
203–16	780	246×10^{-8}	258×10^{-8}		0.779	0.816		0.844	0.840
203–21	780	266×10^{-8}	258×10^{-8}	2.65×10^5	0.873	0.846	0.870	0.844	0.840
204–9		300×10^{-12}			0.848			(0.85)	(0.85)
207–9		451×10^{-12}			0.780			(0.90)	(0.91)
209–9		488×10^{-12}			0.175†			(0.95)	(0.92)
300–9		259×10^{-10}		2.53×10^3	1.006		0.984	(0.85)	(0.74)
303–9	530	746×10^{-8}	673×10^{-8}	8.34×10^5	10.10†	9.12†	11.28†	0.830	0.758
305–2	660		460×10^{-8}	3.34×10^5		0.788	0.572	0.837	0.800
305–4	660	452×10^{-8}	460×10^{-8}		0.820	0.834		0.837	0.800
305–9	660	456×10^{-8}	460×10^{-8}	5.31×10	0.818	0.825	0.954	0.837	0.800
309–16		167×10^{-11}			4.75†			(0.85)	(0.85)
311–9		341×10^{-12}			0.573			(0.90)	(0.91)
400–9		469×10^{-10}		3.41×10^3	0.635		0.462	(0.84)	0.74
401–9	380	473×10^{-8}	456×10^{-8}	5.48×10^5	0.663	0.639	0.768	0.852	0.744
403–2	340		629×10^{-8}	3.45×10^5		0.955	0.524	0.856	0.750
403–3	340		629×10^{-8}	5.43×10^5		1.182	1.022	0.856	0.750
403–4	340	697×10^{-8}	629×10^{-8}		0.817	0.737		0.856	0.750
405–9	310	192×10^{-8}	214×10^{-8}	1.23×10^5	0.725	0.808	0.465	0.868	0.760
407–9	310	158×10^{-10}	159×10^{-10}	1.20×10^3	0.963	0.969	0.731	0.868	0.760
413–9		596×10^{-12}			0.390†			(0.95)	(0.84)
501–9	250	406×10^{-10}	893×10^{-10}	4.70×10^3	0.708	1.556	0.820	0.896	0.792
502–9		379×10^{-12}			0.907			(0.88)	(0.78)
503–9	310	182×10^{-8}	182×10^{-8}	1.59×10^5	0.847	0.847	0.740	0.868	0.760
505–1	260		334×10^{-8}	2.99×10^5		0.994	0.890	0.890	0.780
505–6	260	345×10^{-8}	334×10^{-8}	3.42×10^5	0.876	0.849	0.869	0.890	0.780
507–4	180	890×10^{-9}	124×10^{-8}	1.53×10^5	0.940	1.310	1.616	0.990	0.870
507–5	180	128×10^{-8}	124×10^{-8}	1.53×10^5	1.202	1.164	1.437	0.990	0.870
509–9		286×10^{-9}	650×10^{-9}	2.98×10^4	1.173	2.665†	1.222	(1.0)	(0.88)
513–9		296×10^{-12}			0.304†			(1.1)	(0.95)
601–9		104×10^{-9}	188×10^{-9}	1.07×10^4	0.971	1.758	1.000	(1.1)	(0.95)
603–1	150	169×10^{-8}	173×10^{-8}	2.04×10^5	0.478†	0.489†	0.577	1.06	0.930
603–4	150		173×10^{-8}	2.01×10^5		0.112†	0.130†	1.06	0.930
605–9	160	177×10^{-8}	144×10^{-8}	1.64×10^5	1.106	0.900	1.025	1.03	0.905
607–9		128×10^{-9}		1.16×10^4	0.800		0.725	(1.0)	(0.88)
700–9		145×10^{-11}			0.900			(1.4)	(1.2)
701–9		176×10^{-11}			0.682			(1.3)	(1.1)
703–9		171×10^{-9}		1.75×10^4	0.768		0.785	(1.2)	(1.0)
704–9		131×10^{-11}			1.928			(1.1)	(0.95)
707–3	145	683×10^{-9}	767×10^{-9}	6.23×10^4	0.905	1.016	0.826	1.07	0.942
707–6	145		767×10^{-9}	7.44×10^4		1.056	1.023	1.07	0.942
813–10	90	914×10^{-10}	813×10^{-10}	9.61×10^3	1.057	0.910	1.112	1.42	1.17
814–4	88	850×10^{-10}	886×10^{-10}	7.88×10^3	0.265†	0.276†	0.246†	1.43	1.18
815–10	37		133×10^{-9}	8.86×10^3		3.03	2.02	2.73	1.94
816–16	40	961×10^{-10}	108×10^{-9}	8.65×10^3	2.29	2.57	2.06	2.57	1.85
18–9	(77)			9.28×10^3			1.232	1.58	1.27
18–10	(79)			9.60×10^3			1.207	1.55	1.25
18–11	(79)			1.11×10^4			1.115	1.55	1.25
18–12	(79)			1.43×10^4			1.560	1.55	1.25
27–1	(64)			2.91×10^3			38.75†	1.82	1.39
27–2	(64)			2.43×10^3			1.273	1.82	1.39
27–3	64.5			2.44×10^3			1.220	1.80	1.38
27–4	(64)			7.79×10^2			0.815	1.82	1.39
35–17	(43)			4.41×10^2			1.522	2.43	1.77
35–18	(43)			7.13×10^2			1.873	2.43	1.77
35–19	(42)			1.05×10^3			2.55	2.48	1.79
35–20	38			1.10×10^3			1.280	2.70	1.90
56–11	(23)			7.69×10^2			3.37	3.90	2.67
56–12	(21)			7.88×10^2			3.97	4.20	2.87
56–14	(20)			3.47×10^2			1.753	4.36	2.97

*Values in parentheses are estimated. †Values not used in the analyses.

Notes: (1) I_1 is the ion-chamber measurements by the radiochemical project corrected to 100 hr and to absolute units by a factor of 0.788.

Table 7—(Continued)

A_1, fission/sq ft	A_2, fission/sq ft	A_3, fission/sq ft	A_4, fission/sq ft	$\bar{A}_f$, fission/sq ft	I_s, r/hr at 1 hr	K_0, 10^{-13} r/hr at 1 hr / fission/sq ft	K_0, r/hr at 1 hr / kt/sq mile
2.78×10^{14}	2.54×10^{14}	2.63×10^{14}	2.83×10^{14}	2.70×10^{14}	26.0	0.963	501
2.10×10^{14}	2.63×10^{14}	2.63×10^{14}	3.02×10^{14}	2.60×10^{14}	26.0	1.00	520
1.46×10^{15}		1.98×10^{15}	1.46×10^{15}	1.63×10^{15}	206	1.26	657
2.68×10^{15}		1.98×10^{15}	1.44×10^{15}	2.03×10^{15}	206	1.01	528
2.30×10^{12}	1.31×10^{11}			1.31×10^{11}	0.015	1.14	595
1.11×10^{13}	1.08×10^{13}	1.26×10^{13}	1.18×10^{13}	1.16×10^{13}	1.69	1.46	758
8.76×10^{14}		9.88×10^{14}	9.52×10^{14}	9.39×10^{14}	98.4	1.05	545
1.29×10^{15}	1.34×10^{15}	9.88×10^{14}	9.48×10^{14}	1.14×10^{15}	98.4	0.862	449
1.71×10^{11}	9.81×10^{10}			9.81×10^{10}	0.010	1.02	530
3.16×10^{14}	2.92×10^{14}	3.06×10^{14}		3.05×10^{14}	30.5	1.00	520
3.05×10^{14}	3.15×10^{14}	3.06×10^{14}	3.15×10^{14}	3.10×10^{14}	30.5	0.985	512
3.54×10^{10}	3.53×10^{10}			3.54×10^{10}	0.0035	0.990	515
5.79×10^{10}	5.01×10^{10}			5.01×10^{10}	0.0052	1.04	540
2.79×10^{11}	5.13×10^{10}			5.13×10^{10}	0.0057	1.11	578
2.57×10^{12}	3.05×10^{12}		3.42×10^{12}	3.01×10^{12}	0.30	0.998	519
7.39×10^{13}	8.99×10^{14}	8.11×10^{14}	1.10×10^{15}	8.55×10^{14}	79.7	0.932	485
5.84×10^{14}		5.50×10^{14}	4.18×10^{14}	5.17×10^{14}	54.4	1.05	547
5.52×10^{14}	5.41×10^{14}	5.50×10^{14}		5.46×10^{14}	54.4	0.995	518
5.58×10^{14}	5.45×10^{14}	5.50×10^{14}	6.64×10^{14}	5.79×10^{14}	54.4	0.940	489
3.52×10^{10}	1.96×10^{11}			1.96×10^{11}	0.020	1.02	531
5.95×10^{10}	3.79×10^{10}			3.79×10^{10}	0.0040	1.06	549
7.39×10^{12}	5.58×10^{12}		4.61×10^{12}	5.09×10^{12}	0.54	1.06	551
7.14×10^{14}	5.55×10^{14}	5.35×10^{14}	7.37×10^{14}	6.35×10^{14}	53.9	0.848	441
6.59×10^{14}		7.35×10^{14}	4.60×10^{14}	6.18×10^{14}	74.5	1.20	627
5.32×10^{14}		7.35×10^{14}	7.24×10^{14}	6.64×10^{14}	74.5	1.12	584
8.54×10^{14}	8.14×10^{14}	7.35×10^{14}		8.01×10^{14}	74.5	0.930	483
2.65×10^{14}	2.22×10^{14}	2.47×10^{14}	1.62×10^{14}	2.24×10^{14}	25.4	1.13	590
1.64×10^{12}	1.82×10^{12}	1.83×10^{12}	1.58×10^{12}	1.72×10^{12}	0.18	1.05	545
1.53×10^{11}	6.18×10^{10}			6.18×10^{10}	0.0070	1.13	589
5.74×10^{12}	4.53×10^{12}	9.96×10^{12}	5.93×10^{12}	5.40×10^{12}	0.57	1.06	549
4.18×10^{10}	4.31×10^{10}			4.24×10^{10}	0.0044	1.04	540
2.15×10^{14}	2.10×10^{14}	2.10×10^{14}	2.09×10^{14}	2.11×10^{14}	21.5	1.02	530
3.36×10^{14}		3.76×10^{14}	3.83×10^{14}	3.65×10^{14}	39.6	1.08	565
3.94×10^{14}	3.88×10^{14}	3.76×10^{14}	4.38×10^{14}	3.86×10^{14}	39.6	1.03	533
9.48×10^{13}	8.99×10^{13}	1.25×10^{14}	1.76×10^{14}	1.22×10^{14}	14.7	1.20	626
1.065×10^{14}	1.29×10^{14}	1.25×10^{14}	1.76×10^{14}	1.34×10^{14}	14.7	1.10	570
2.44×10^{13}	2.86×10^{13}	6.50×10^{13}	3.39×10^{13}	2.90×10^{14}	3.4	1.17	610
9.74×10^{10}	2.69×10^{10}			2.69×10^{10}	0.0034	1.26	657
1.07×10^{13}	9.46×10^{12}	1.71×10^{13}	1.13×10^{13}	1.05×10^{13}	1.4	1.33	693
3.54×10^{14}	1.60×10^{14}	1.63×10^{14}	2.19×10^{14}	1.81×10^{14}	20.4	1.13	586
1.55×10^{15}		1.63×10^{14}	2.16×10^{14}	1.90×10^{14}	20.4	1.07	559
1.60×10^{14}	1.72×10^{14}	1.40×10^{14}	1.81×10^{14}	1.63×10^{14}	17.0	1.04	542
1.60×10^{13}	1.28×10^{13}		1.32×10^{13}	1.41×10^{13}	1.5	1.06	553
1.61×10^{11}	1.04×10^{11}			1.32×10^{11}	0.017	1.29	670
2.58×10^{11}	1.35×10^{11}			1.96×10^{11}	0.020	1.02	530
2.23×10^{13}	1.42×10^{13}		1.75×10^{13}	1.82×10^{13}	2.0	1.10	571
6.80×10^{10}	1.19×10^{11}			1.19×10^{11}	0.015	1.26	655
7.55×10^{13}	6.38×10^{13}	7.17×10^{13}	6.61×10^{13}	6.93×10^{13}	9.08	1.31	682
7.28×10^{13}		7.17×10^{13}	7.90×10^{13}	7.45×10^{13}	9.08	1.22	634
8.65×10^{12}	6.44×10^{12}	5.72×10^{12}	8.21×10^{12}	7.25×10^{12}	1.58	2.18	1133
3.21×10^{13}	5.95×10^{12}	6.20×10^{12}	6.68×10^{12}	6.28×10^{12}	1.32	2.10	1094
4.39×10^{12}		4.87×10^{12}	4.57×10^{12}	4.61×10^{12}	1.18	2.56	1330
4.20×10^{12}	3.74×10^{12}	4.20×10^{12}	4.68×10^{12}	4.20×10^{12}	1.17	2.79	1450
7.54×10^{12}			7.56×10^{12}	7.55×10^{12}	1.17	1.55	805
7.95×10^{12}			7.42×10^{12}	7.42×10^{12}	1.18	1.59	830
9.96×10^{12}			8.88×10^{12}	8.88×10^{12}	1.32	1.49	775
9.17×10^{12}			1.14×10^{13}	1.14×10^{13}	1.58	1.39	725
7.52×10^{10}			2.09×10^{12}	2.09×10^{12}	0.28	1.34	697
1.91×10^{12}			1.75×10^{12}	1.75×10^{12}	0.47	2.68	1395
2.00×10^{12}			1.77×10^{12}	1.77×10^{12}	0.27	1.52	793
9.68×10^{11}			5.60×10^{11}	5.60×10^{11}	0.15	2.68	1390
2.90×10^{11}			2.49×10^{11}	2.49×10^{11}	0.12	4.82	2510
3.81×10^{11}			4.03×10^{11}	4.03×10^{11}	0.18	4.47	2320
4.12×10^{11}			5.87×10^{11}	5.87×10^{11}	0.27	4.60	2390
8.60×10^{11}			5.82×10^{11}	5.82×10^{11}	0.26	4.47	2320
2.28×10^{11}			2.88×10^{11}	2.88×10^{11}	0.074	2.57	1335
1.98×10^{11}			2.75×10^{11}	2.75×10^{11}	0.16	5.72	3020
1.98×10^{11}			1.17×10^{11}	1.58×10^{11}	0.087	5.50	2860

Notes: (2) I_2 is the ion-chamber measurements by the field project (average for each station). (3) I' is the calibrated gamma-scintillation-counter measurements by the field project. (4) $\bar{i}$ and $\bar{i}'$ are values read from the curves in Figs. 2 and 3, respectively.

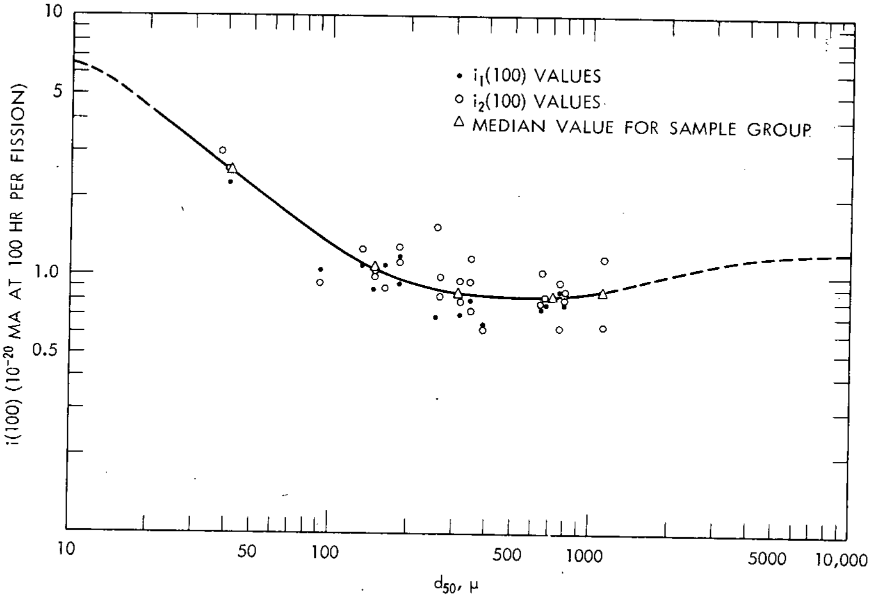

Fig. 2—Variation of i(100) with d_{50} for gross fallout samples.

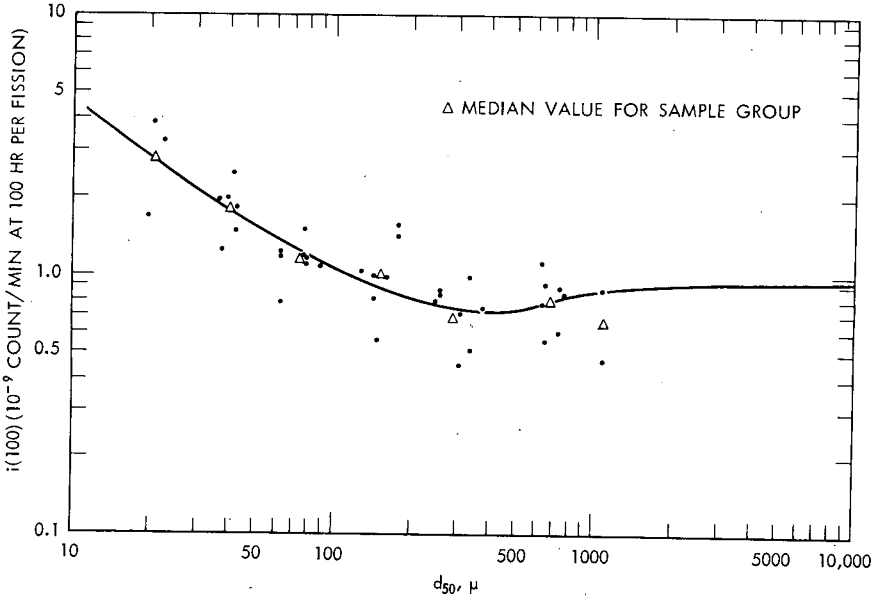

Fig. 3—Variation of i′(100) with d_{50} for gross fallout samples.

The computed values of K_0 are plotted as a function of d_{50} in Fig. 4. It may be noted that the curves of i(100), i′(100), and K_0 given as a function of d_{50} in Figs. 2, 3, and 4 are very similar to the curve for i(100) plotted as a function of $\bar{d}$ in Fig. 1.

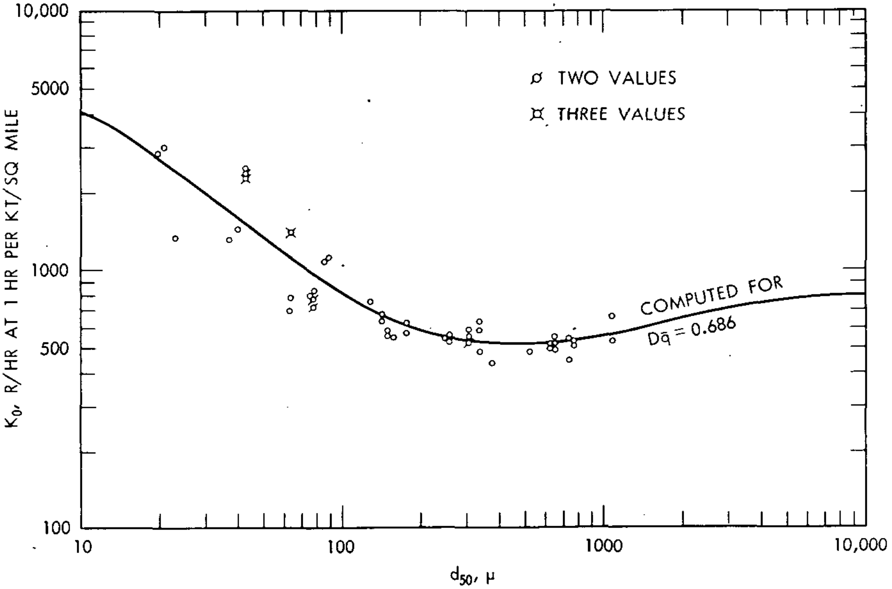

Fig. 4—Variation of K_0 with d_{50} for fallout-collecting stations.

The high values of K_0 for the stations in the 35- and 56-numbered series (Table 7) suggest that the I_s values are overestimated by correction of the monitoring data[1] to 1 hr with the $t^{-1.2}$ function. The adjustment of the two apparently different sets of reported A_f values[2] to a midvalue rather than correction of one of the two sets of data to be consistent with the other may have resulted in K_0 values that are either low or high by 25%. Further investigation of the reported data[3] together with theoretical analyses may suggest what corrections are appropriate.

The Dq terms of Eq. 12 can be evaluated using an appropriate value of k_{fp}. The selection of a value here is limited to the k_{fp} value for the fission products from the thermal-neutron fission of ^{235}U because the i(100) and r_{fp}- values, as deduced from the ion-chamber measurements, are based on the response of the ion-chamber to the ^{235}U products. The calculated value[8] of k_{fp} is 3950 r/hr at 1 hr per kiloton per square mile. The Dq of Eq. 12 is given by

$$Dq = \frac{K_0}{3950\, r_{fp}} \tag{21}$$

The values of $r_{fp}(100)$, $r'_{fp}(100)$, r_{fp}, r'_{fp}, K_0, and Dq for each station are summarized in Table 8. The value of K_0 in Table 8 for stations having more than one estimated value of K_0 in Table 7 is a median value. The terrain about the stations generally increased in roughness[1] proceeding from station 100 to station 707; however, this general increase in roughness is not reflected in a corresponding general decrease in Dq values for these stations. At the stations of the 800 series, the terrain was fairly smooth and flat at stations 813 and 814 and somewhat rougher at stations 815 and 816. The terrain features at the remainder of the stations were varied. At the stations in series 100 through 800, the GITR's were calibrated to have a response factor, D, near unity; thus for these stations the computed value of Dq is practically equal to q. For the other stations the response factor for the instruments and monitor has not been reported, but it is assumed to be about 0.7. Therefore, where the computed value of Dq is in excess of 0.7, either the I_s value is too large or the A_f value is too small (i.e., the r_{fp} value is too small).

Table 8—SUMMARY OF CALCULATED r_{fp}, r'_{fp}, K_0, AND Dq VALUES* FOR THE SMALL BOY SHOT FALLOUT-COLLECTING STATIONS

Station and sample No.	$r_{fp}(100)$	$r'_{fp}(100)$	r_{fp}	r'_{fp}	K_0, $\frac{\text{r/hr at 1 hr}}{\text{kt/sq mile}}$	Dq
100	0.338	0.369	0.194	0.304	511	0.667
101	0.355	0.425	0.204	0.346	589	0.731
103	(0.403)	(0.443)	(0.232)	(0.361)	595	0.650
200	0.456	0.469	0.262	0.382	758	0.724
201	0.340	0.398	0.195	0.324	494	0.642
202	(0.340)	(0.400)	(0.196)	(0.326)	530	0.685
203	0.341	0.400	0.196	0.326	515	0.666
204	(0.343)	(0.405)	(0.197)	(0.330)	515	0.663
207	(0.363)	(0.433)	(0.209)	(0.353)	540	0.678
209	(0.383)	(0.438)	(0.220)	(0.357)	578	0.665
300	(0.343)	(0.352)	(0.197)	(0.287)	519	0.691
303	0.335	0.361	0.192	0.294	485	0.640
305	0.338	0.381	0.195	0.310	518	0.673
309	(0.343)	(0.405)	(0.197)	(0.330)	531	0.684
311	(0.363)	(0.433)	(0.209)	(0.353)	549	0.665
400	(0.339)	(0.352)	(0.195)	(0.287)	551	0.717
401	0.344	0.354	0.198	0.289	441	0.564
403	0.346	0.357	0.199	0.291	561	0.715
405	0.350	0.362	0.202	0.295	590	0.741
407	0.350	0.362	0.202	0.295	545	0.684
409	(0.383)	(0.400)	(0.220)	(0.326)	589	0.678
501	0.362	0.378	0.208	0.308	549	0.669
502	(0.355)	(0.372)	(0.204)	(0.303)	540	0.671
503	0.350	0.362	0.202	0.295	530	0.665

(Table 8 continues on page 63)

Table 8—(Continued)

Station and sample No.	$r_{fp}(100)$	$r'_{fp}(100)$	r_{fp}	r'_{fp}	K_0, $\frac{\text{r/hr at 1 hr}}{\text{kt/sq mile}}$	Dq
505	0.359	0.372	0.206	0.303	549	0.674
507	0.399	0.415	0.230	0.338	598	0.659
509	(0.403)	(0.419)	(0.232)	(0.342)	610	0.666
513	(0.444)	(0.452)	(0.255)	(0.369)	657	0.654
601	(0.444)	(0.452)	(0.255)	(0.369)	693	0.688
603	0.428	0.443	0.246	0.361	572	0.590
605	0.415	0.431	0.239	0.351	542	0.575
607	(0.403)	(0.419)	(0.232)	(0.342)	553	0.605
700	(0.565)	(0.571)	(0.325)	(0.466)	670	0.523
701	(0.524)	(0.524)	(0.302)	(0.427)	530	0.445
703	(0.484)	(0.476)	(0.278)	(0.388)	571	0.522
704	(0.444)	(0.462)	(0.255)	(0.369)	655	0.644
707	0.431	0.449	0.248	0.366	658	0.673
813	0.573	0.557	0.330	0.454	1,133	0.870
814	0.576	0.562	0.332	0.458	1,094	0.836
815	1.100	0.924	0.633	0.753	1,330	0.533
816	1.037	0.880	0.596	0.718	1,450	0.617
18-9	0.638	0.605	0.367	0.482	805	0.556
18-10	0.625	0.595	0.360	0.485	830	0.585
18-11	0.625	0.595	0.360	0.484	775	0.546
18-12	0.625	0.595	0.360	0.485	725	0.511
27-1	0.735	0.662	0.422	0.540	697	0.418
27-2	0.735	0.662	0.422	0.540	1,395	0.838
27-3	0.726	0.657	0.418	0.535	793	0.482
27-4	0.735	0.662	0.422	0.540	1,390	0.835
35-17	0.980	0.843	0.564	0.687	2,510	1.128
35-18	0.980	0.843	0.564	0.687	2,320	1.043
35-19	1.000	0.852	0.575	0.695	2,390	1.053
35-20	1.090	0.905	0.626	0.737	2,320	0.939
56-11	1.573	1.272	0.905	1.037	1,335	0.374
56-12	1.695	1.367	0.975	1.113	3,020	0.785
56-14	1.760	1.414	1.012	1.152	2,860	0.717

*Values in parentheses are derived from estimated d_{50} values for the station.

The mean value of Dq for all the stations in the 100 to 700 series, for which d_{50} is given, is 0.686 ± 0.025. With this value of Dq, Eq. 12 becomes

$$K_0 = 2710\ r_{fp} \qquad (22)$$

Thus K_0^0 for all the indicated stations is 2710 (i.e., K_0 with $r_{fp} = 1$).

The f_j values for the Small Boy shot fallout pattern were computed by constructing fallout patterns for a given range in particle size and evaluating the intensity-area integral for each pattern. The fraction of

I_s at each station contributed by each particle-size group was calculated from activity measurements on sieved fractions of the fallout samples. The constructed fallout patterns for several of the particle-size ranges and for the total fallout pattern are shown in Figs. 5 to 8. The activity–size distribution derived from this analysis is shown in Fig. 9. The median particle diameter for the distribution is 210 μ. The derived distribution is not lognormal.

The f_j values from which the distribution was determined are summarized in Table 9; also given in the table are the $f_j r_j$ and $f_j K_{0j}$ values leading to the estimates of $\bar{r}_{fp}$ and $\bar{K}_0$ for the whole fallout pattern. The sum of the intensity–area integrals, J_R, of the fallout patterns for the different particle groups is 580 r/hr at 1 hr per square mile; the value of J_R for the pattern of the gross I_s contours is 640 r/hr at 1 hr per square mile, about 11% larger. The yield of the Small Boy shot has not been reported, except that the yield was small.[9] With the use of the intensity–area integral for the I_s contours and the yield, the value of J_R/BW for the pattern thus could be estimated. With a $\bar{K}_0$ value of 1070 r/hr at 1 hr per kiloton per square mile, the value of C could be estimated; and the fraction of device, F_D, accounted for within the constructed fallout pattern of Fig. 8 could similarly be estimated.

The fallout patterns constructed for the various particle-size fractions do not include contributions from the regions of high I_s values near ground zero nor from the large area of low-level fallout that was deposited in northern Utah. These contributions are not included in the analysis because fallout samples for determining the distribution of radioactivity among the fallout particles deposited in these regions were not available for analysis. For the total fallout pattern, including the contributions to I_s from these areas, a J_R value of 1460 r/hr per square mile is obtained; this value is a factor of about 2.3 larger than that calculated for the fallout pattern constructed from the I_s values at the stations for which particle-size data are available.

The fraction of the device, F_D, accounted for within the larger fallout pattern, would therefore be 2.3 times that for the smaller pattern mentioned earlier. The ratio of the contributions to the intensity–area integral for the high-intensity region to the low-intensity region, as determined from integrals, is about 3 to 1. If an average r_j value of 0.29 is assumed for the fallout in the high-intensity region and an average r_j value of 1.5 for the low-intensity region, a value of $\bar{K}_0$ can be estimated for the larger pattern from the data of Table 9. Allocation of appropriate fractions of the intensity–area integral to the three areas gives a weighted average value for $\bar{K}_0$ of 1400 r/hr at 1 hr per kiloton per square mile; the corresponding

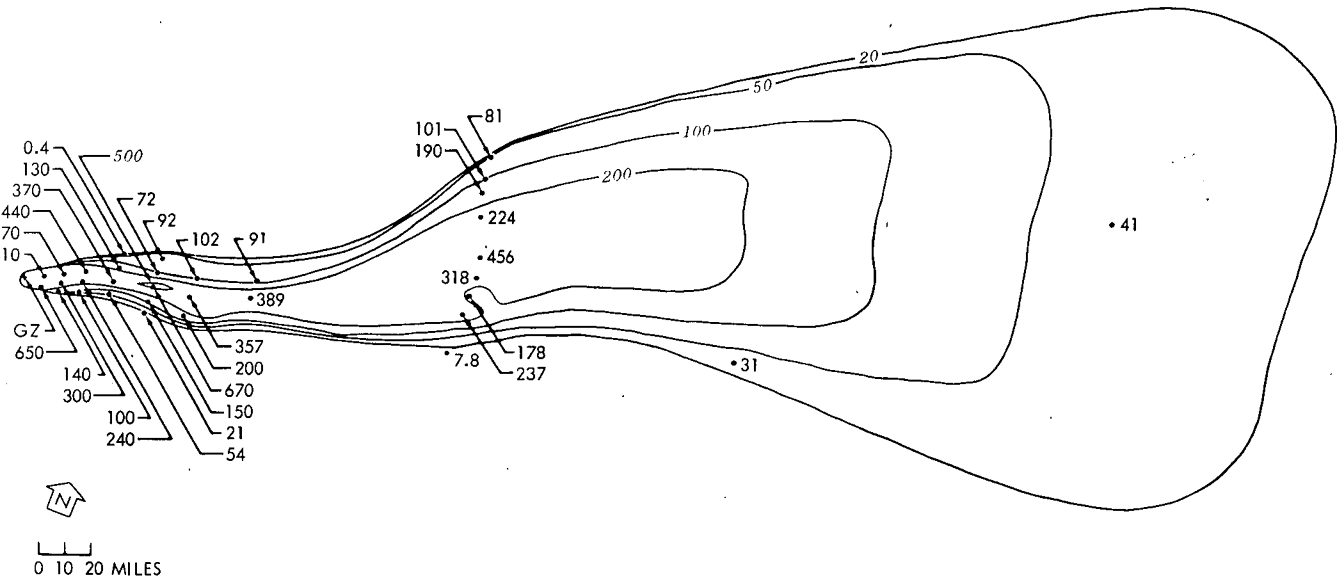

Fig. 5—Isointensity contours for 20- to 50-μ particle diameters in milliroentgens per hour at 1 hr.

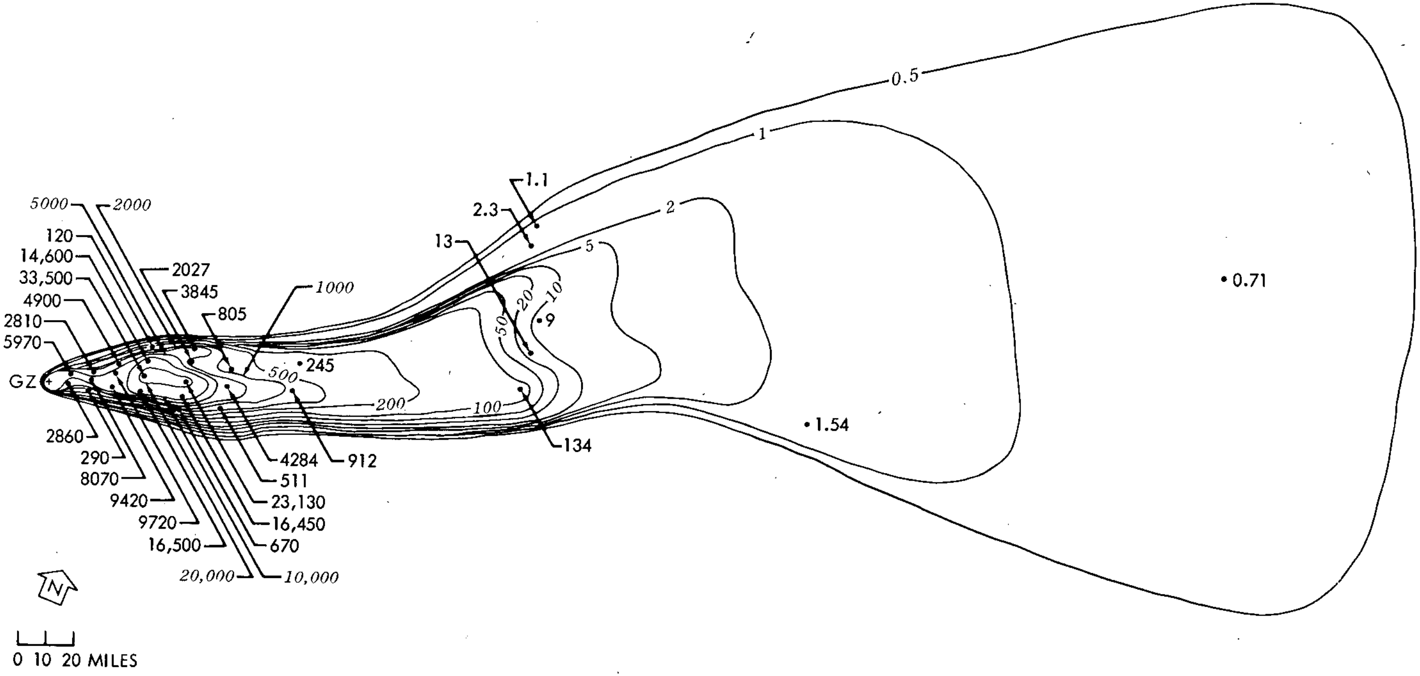

Fig. 6—Isointensity contours for 200- to 350-μ particle diameters in milliroentgens per hour at 1 hr.

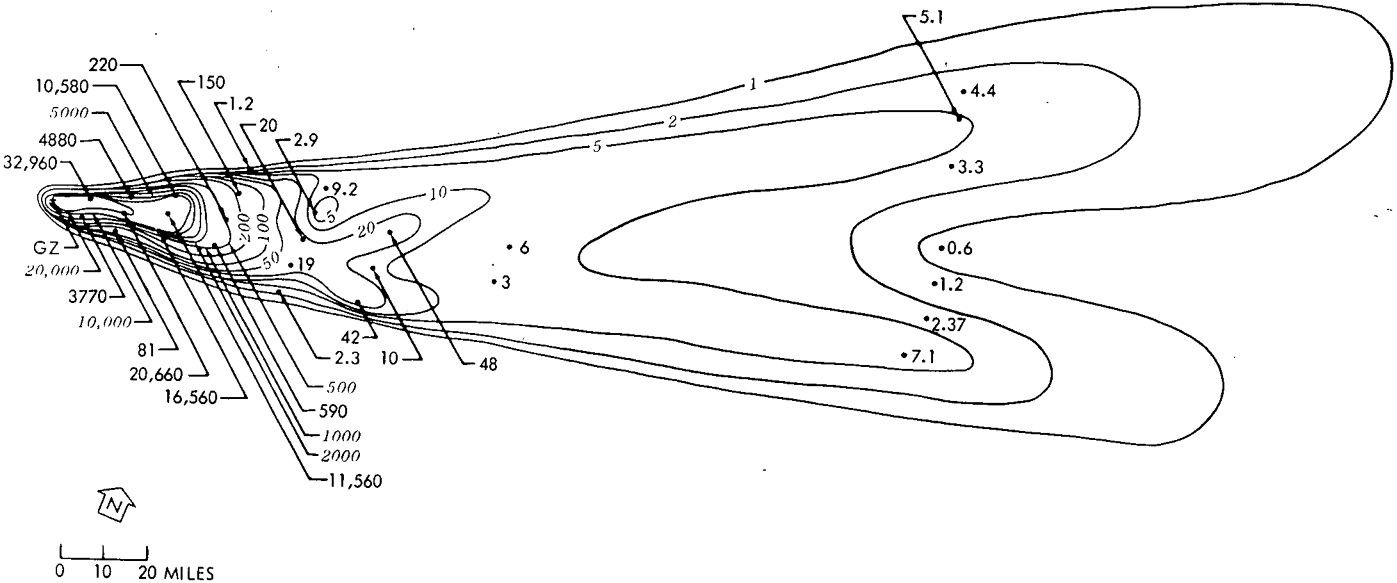

Fig. 7—Isointensity contours for 750- to 1000-μ particle diameters in milliroentgens per hour at 1 hr.

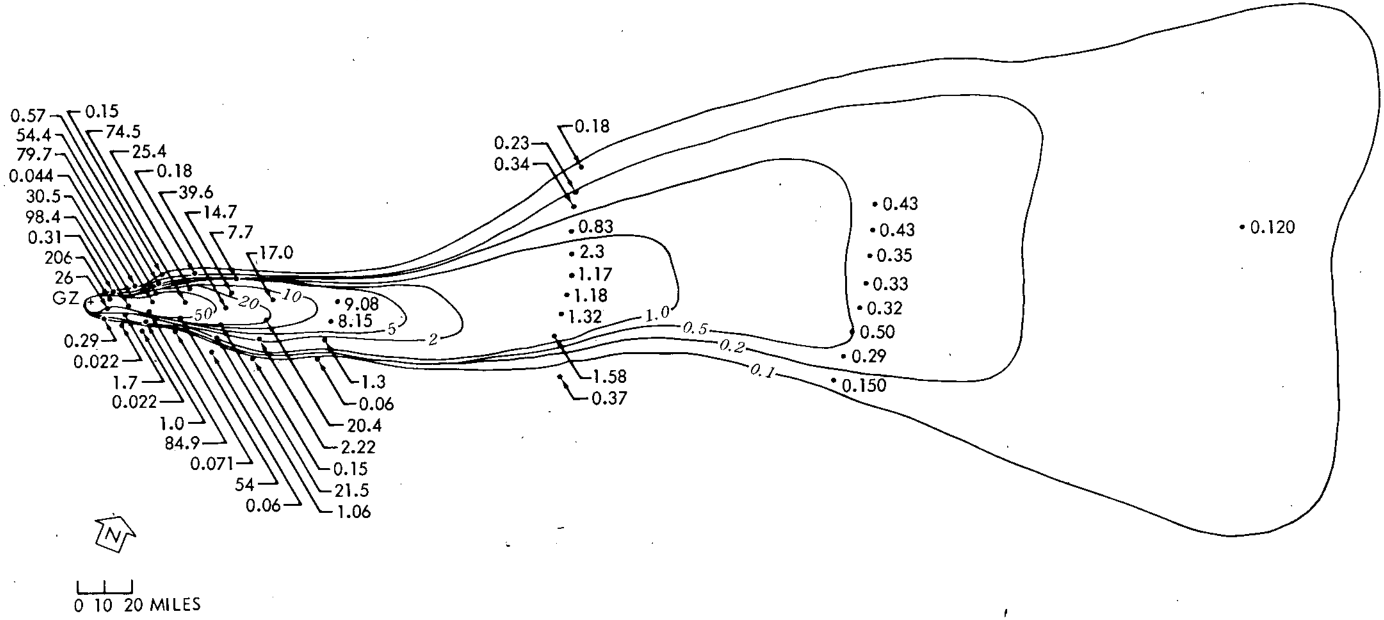

Fig. 8—Total fallout isointensity contours in roentgens per hour at 1 hr.

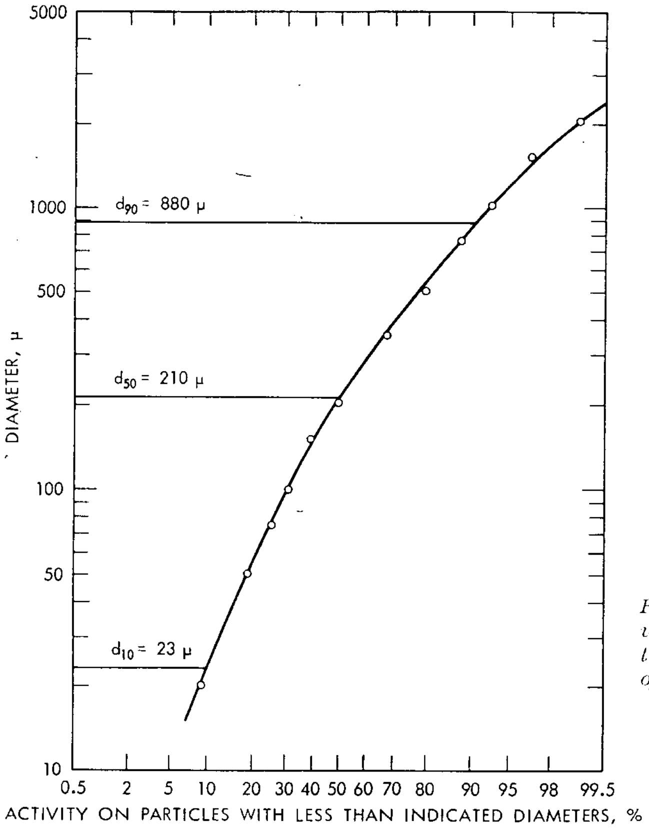

Fig. 9—Gross size vs. activity–area integrals for particles of different sizes.

Table 9—SUMMARY OF THE f_j VALUES FOR THE SMALL BOY SHOT FALLOUT AND THE CALCULATIONS FOR $\bar{r}_{fp}$ AND $\overline{K}_0$

Δd, μ	$\bar{d}$, μ	r_j	K_{0j}, r/hr at 1 hr / kt/sq mile	f_j	$f_j r_j$	$f_j K_{0j}$, r/hr at 1 hr / kt/sq mile
0 to 20	10	1.51	4090	0.091	0.137	372
20 to 50	35	0.665	1800	0.093	0.062	167
50 to 75	62.5	0.429	1160	0.075	0.032	87
75 to 100	87.5	0.334	905	0.049	0.016	44
100 to 150	125	0.269	729	0.076	0.020	55
150 to 200	175	0.232	629	0.108	0.025	68
200 to 350	275	0.204	553	0.182	0.037	101
350 to 500	425	0.195	529	0.122	0.024	64
500 to 750	625	0.194	526	0.082	0.016	43
750 to 1000	875	0.198	537	0.053	0.011	28
1000 to 1500	1250	0.210	570	0.040	0.008	23
1500 to 2000	1750	0.230	623	0.021	0.005	13
>2000		0.292	791	0.0095	0.003	7
				Sum	0.396	1072

Notes: (1) $r_{fp} = \Sigma f_j r_j = 0.396$. (2) $\overline{K}_0 = \Sigma f_j K_{0j} = 1072$ r/hr at 1 hr per kiloton per square mile.

value of C for the larger fallout pattern could then be calculated if the yield were known.

A commonly used value of K_0^0 in Eq. 7 for estimating the fraction of a device in the fallout pattern, especially when experimental values of $D\bar{q}$ are not directly available, is 2000 r/hr at 1 hr per kiloton per square mile. If this value is used with the J_R value, 1460 r/hr at 1 hr per square mile, for the Small Boy fallout pattern, the estimated value of F_D could be compared to that obtained through use of the radiochemical analysis of the fallout material and the methods outlined in this report.

COMMENTS AND CONCLUSIONS

The computed r_{fp} values appear to be somewhat low, especially for the median particle diameters between about 200 and 800 μ. Further examination of the radiochemical data with respect to the fractionation of individual nuclides and to the fission yield of ^{95}Zr, as a measure of the number of fissions, could provide further information on the r_{fp} values. The major factors in determining the r_{fp} values, if the data from ion-chamber measurements are accepted as being by far the most accurate, are the fission content of the samples and the decay factors from 100 to 1 hr after detonation for the ion-chamber data. The absolute value of i_0 for the unfractionated mixture of radionuclides from thermal-neutron fission of ^{235}U rather than for fission by fission neutrons would result in a relatively small error in the r_{fp} estimates. It should be expected that the decay factors for the samples would approach those for i_0 as the $r_{fp}(100)$ values approach unity, indicating a relatively unfractionated mixture of radionuclides.

The Dq values derived from the data are consistent with other previously derived values of q for the Nevada Test Site terrain.[8] These values generally would not be influenced by possible future changes in the r_{fp} values since any change in r_{fp} would result in an equivalent change in the values of the K_0.

The example analysis of some of the Small Boy shot data applicable to evaluation of the intensity–activity ratio shows that the ratio is not a constant for a given fallout pattern but varies over the pattern depending on the particle sizes in the deposited fallout. However, when gross activity–size distribution data are evaluated, an average value of the ratio can be derived for the fallout pattern. On the other hand, the average value of the intensity–activity ratio is not required for estimating the fraction of the device within a fallout pattern. A value for this ratio for the fallout deposited uniformly over an ideal plane, an average terrain attenuation factor, and an instrument response factor, however, are needed for estimating the fraction of device in the pattern.

Further detailed analyses of the available data are needed to verify or adjust the values of several of the parameters, as described in this preliminary analysis of the reported data, for more accurate evaluations of the intensity–activity ratios and the fraction of device accounted for within the fallout pattern.

REFERENCES

1. P. D. LaRiviere, Hong Lee, and K. H. Larson, Ionization Rate Measurements, Project 2.11, Operation Sun Beam Report POR-2217, April 1964. (Classified)
2. P. D. LaRiviere, J. D. Sartor, W. B. Lane, and K. H. Larson, Fallout Collection and Gross Sample Analysis, Project 2.9, Operation Sun Beam Report POR-2215, October 1964. (Classified).
3. E. C. Freiling, L. R. Bunney, and F. K. Kawahara, Physiochemical and Radiochemical Analysis, Project 2.10, Operation Sun Beam Report POR-2216, October 1964. (Classified)
4. C. F. Miller, Response Curves for USNRDL 4-pi Ionization Chamber, Report USNRDL-TR-155, U. S. Naval Radiological Defense Laboratory, May 1957.
5. C. F. Miller and P. Loeb, Ionization Rate and Photon Pulse Decay of Fission Products from the Slow-Neutron Fission of U-235, Report USNRDL-TR-247, U. S. Naval Radiological Defense Laboratory, August 1958.
6. P. D. LaRiviere, Response of a Low-Geometry Scintillation Counter to Fission and Other Products, Report USNRDL-TR-303, U. S. Naval Radiological Defense Laboratory, February 1959.
7. W. B. Lane, Stanford Research Institute, private communication, July 1964.
8. C. F. Miller, Fallout and Radiological Countermeasures, Vol. I, Stanford Research Institute, Project IMU-4021, January 1963.
9. Samuel Glasstone (Ed.), *The Effects of Nuclear Weapons*, Revised Edition, U. S. Government Printing Office, Washington, D. C., 1962.
10. L. Machta, Meteorological Processes in the Transport of Weapon Radioiodine, *Health Phys.*, *9*(12): 1123-1132 (1963).

RADIOCHEMICAL-DATA CORRELATIONS ON DEBRIS FROM SILICATE BURSTS

GLENN R. CROCKER, FRANCIS K. KAWAHARA, and EDWARD C. FREILING
U. S. Naval Radiological Defense Laboratory, San Francisco, California

ABSTRACT

Local-fallout samples collected in 1962 in the Johnie Boy, Small Boy, and Sedan shots were analyzed radiochemically for ^{89}Sr, ^{90}Sr, ^{91}Y, ^{95}Zr, ^{99}Mo, ^{103}Ru, ^{106}Ru, ^{131}I, ^{132}Te, ^{136}Cs, ^{137}Cs, ^{140}Ba, ^{141}Ce, ^{144}Ce, ^{239}Np, and ^{239}Pu. These results, as reported by the project officers, have been correlated by plotting the log of the ratio of equivalent fissions of each nuclide, i, to equivalent fissions of ^{95}Zr, $r_{i,95}$, against the log of the similar ratio for ^{89}Sr and ^{95}Zr, $r_{89,95}$. The data were fitted to straight lines by linear regression; and slopes, intercepts, coefficients of correlation, and confidence limits were determined. The slope of such a line for a nuclide i is an indication of the degree of fractionation of the nuclide relative to the fractionation of ^{89}Sr. For all cases observed in these Nevada shots, the same group of nuclides (^{89}Sr, ^{90}Sr, ^{91}Y, ^{103}Ru, ^{106}Ru, ^{131}I, ^{132}Te, ^{136}Cs, ^{140}Ba, ^{137}Cs, ^{141}Ce, and ^{239}Np) fractionated from ^{95}Zr. The nuclides ^{99}Mo, ^{144}Ce, and ^{239}Pu did not fractionate appreciably from ^{95}Zr. For the Sedan shot the slope of the ^{137}Cs plot is near 1.0, but, for the remaining fractionating nuclides, the slopes lie within a narrow intermediate range. For the Johnie Boy and Small Boy shots, for which the results are quite similar, these slopes show much wider variation. The results of the correlation have been compared with those from similar correlations for a coral-surface burst and some air bursts. Aside from the fact that ^{99}Mo fractionated from ^{95}Zr in the air bursts and that ^{239}Np did not fractionate from ^{95}Zr in the coral-surface burst, the results indicate that differences in the fractionation behavior of the nuclides are of degree rather than of kind. Correlation of radiochemical results with particle size indicates increasing degree of fractionation with increasing particle size.

INTRODUCTION

In the summer of 1962, the U. S. Naval Radiological Defense Laboratory (NRDL) collected fallout from three shots at the Nevada Test Site (NTS)—Johnie Boy, Small Boy, and Sedan. Radiochemical studies were made of the debris from these shots and were reported.[1–3] During the past several months, we have made log–log correlations of these radiochemical results and have attempted some interpretation of them.

Before the results are discussed, it seems appropriate to review the shot conditions since important differences existed among the three events. These differences undoubtedly had effects on the fractionation behavior of the fallout.

SHOT CONDITIONS

Small Boy was a low-yield shot fired from atop a 10-ft-high wooden tower above alluvial soil in Area 5 at NTS. NRDL collected many fallout* samples of debris at 43 stations within 8.7 miles of ground zero and took other samples on a line 15 miles from ground zero. Further samples were supplied by the University of California at Los Angeles sampling network at distances of 18, 27, 36, 52, and 70 miles. Four cloud samples were supplied by Los Alamos Scientific Laboratory. The discussion in this report is mainly restricted to samples from within 8.7 miles of ground zero and from the cloud samples. The number of samples used from each station varied, and many samples were subdivided by sieving into seven fractions that were analyzed individually. A total of about 187 samples is dealt with here, all of which were analyzed for ^{89}Sr, ^{90}Sr, ^{91}Y, and ^{95}Zr. In addition, about one-third of them were analyzed for ^{99}Mo, ^{103}Ru, ^{106}Ru, ^{136}Cs, ^{137}Cs, ^{140}Ba, ^{141}Ce, ^{144}Ce, ^{239}Np, and ^{239}Pu. Some of this last group of samples were also analyzed for ^{131}I and ^{132}Te. The numbers quoted do not include a fairly large number of radiochemical analyses on samples used for solubility studies.

NRDL's participation in the Johnie Boy and Sedan shots was on a rather limited basis. Johnie Boy was a low-yield burst 23 in. below the surface of basaltic material in Area 18 at NTS. Forty-four fallout samples from the area out to about 1¼ miles from ground zero and two cloud samples were studied radiochemically. All of these were analyzed for ^{89}Sr, ^{90}Sr, ^{91}Y, and ^{95}Zr, and about one-third of them were analyzed for the long list of nuclides previously given for the Small Boy samples.

---

*As distinguished from cloud and air-filter samples.

Sedan was the well-known 100-kt cratering shot for the Plowshare program. The device was buried 635 ft below the surface in alluvial material in Area 10. NRDL collected samples at stations within 1 to 3.6 miles of ground zero. Analyses were performed on about 50 samples for the short list of nuclides previously given, and about one-third of these were analyzed for the long list.

TREATMENT OF THE DATA

The radiochemical analytical work was contracted out to three commercial laboratories since NRDL does not have facilities for handling a large volume of samples for routine analysis. The contractors were selected on the basis of qualification tests, which were also intended to serve for interlaboratory calibration purposes. It required nearly a year for all the contractors to complete and report the analyses. The results were reported to NRDL as disintegrations per minute or equivalent ^{235}U thermal-neutron fissions at shot time. NRDL then converted the values to equivalent fissions of the device at shot time, using mass-chain yield values supplied by the weapons laboratories. At the same time the calibration factors derived from the qualification-test analyses were applied.

As a reference nuclide ^{95}Zr was chosen for fractionation studies. Some such choice seems unavoidable if fractionation is to be discussed. Zirconium-95 belongs to a class of nuclides (other members are ^{99}Mo, ^{144}Ce, and ^{147}Nd) that are generally present in debris in equal quantities when expressed as equivalent fissions. Strontium-89, on the other hand, shows wide variation when compared with any of these. The ratio of equivalent fissions of ^{89}Sr to equivalent fissions of ^{95}Zr is, in fact, a fairly good indicator of the degree to which a sample is fractionated. The ratio will be 1 for an unfractionated sample, less than 1 for a sample depleted in ^{89}Sr, and greater than 1 for a sample enriched in ^{89}Sr.

The behavior of other fractionating nuclides can be correlated with that of ^{89}Sr by log–log plotting. The log of the ratio, $r_{i,95}$, of equivalent fissions of nuclide i to equivalent fissions of ^{95}Zr is plotted against the log of the similar ratio for ^{89}Sr and ^{95}Zr. The data so treated can be fitted more or less satisfactorily to a straight line. The slope of the line is then an indication of the extent of fractionation of nuclide i.

RESULTS AND DISCUSSION

For the Johnie Boy and Small Boy shots, the local-fallout collections were sufficient to define the geographical extent of the close-in fallout fairly well. The Small Boy field was the cigar-shaped downwind area typically associated with such shots. The Johnie Boy field was very, perhaps atypically, narrow with a very hot line down the center, which was visible on the ground as a darkened streak. The NRDL collection array at Sedan was not sufficiently widespread to define the limits of the close-in fallout field.

With each of these shots, one can associate a sort of average, or typical, value (or narrow range of values) for the ratio $r_{89,95}$ observed in gross samples. It is to be understood that this range of $r_{89,95}$ is much extended when cloud samples, sieve-fraction samples, and samples from the peripheral stations are considered. Nonetheless, the average value is useful for describing the overall degree of fractionation of the shot. For Johnie Boy a weighted average of this ratio for the hot-line stations is around 0.03, indicating very severe fractionation. For Small Boy the values for most stations are in the range 0.1 to 0.2, indicating more moderate fractionation. All Sedan samples were sieved, but the $r_{89,95}$ values for gross samples were reconstructed by properly weighting the values for the sieve fractions and were found to range from about 0.5 to 3.8. Values in this range would be anomalous for local fallout from a true surface burst, but they seem to be characteristic of cratering (buried) shots, venting underground explosions, and venting underwater bursts.

All of the Johnie Boy, Small Boy, and Sedan $r_{i,95}$ values have been log–log plotted against $r_{89,95}$. Figure 1 indicates how some of the data accommodate themselves to this treatment. These are the data on ^{140}Ba for the Johnie Boy shot, and they illustrate a particularly satisfactory fit. The slope, the y intercept at $\log x = 0$ ($x = 1$), and the coefficient of correlation* have been determined by linear regression to be 0.61, 2.4, and 0.98, respectively. Not all of the data, by any means, fit a log–log plot so neatly. Figure 2 shows a much less satisfactory and more typical example. These data are part of the results for ^{90}Sr in the Small Boy shot. The coefficient of correlation here is only 0.684.

The data were originally fitted by lumping together data points from all three contracting laboratories. In the process of investigating a poor fit of ^{141}Ce data for Small Boy, we noticed that points from Laboratory A could be fitted fairly well, whereas those from Laboratory B were scattered so badly as to suggest that Laboratory B was experiencing difficulty with this analysis. Figure 3 shows these data. Investigation of the ^{103}Ru and ^{106}Ru data showed a similar situation, but it was reversed with respect to the two laboratories—Laboratory B points correlated notably better than did Laboratory A points.

---

*The square of the coefficient of correlation reflects that part of the variation in one set of measurements which can be explained by their dependence on the other.

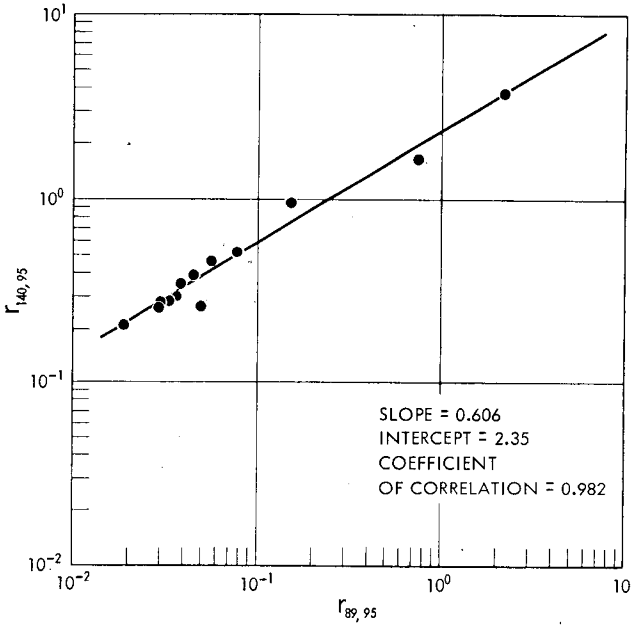

Fig. 1—Fractionation plot for ^{140}Ba in Johnie Boy.

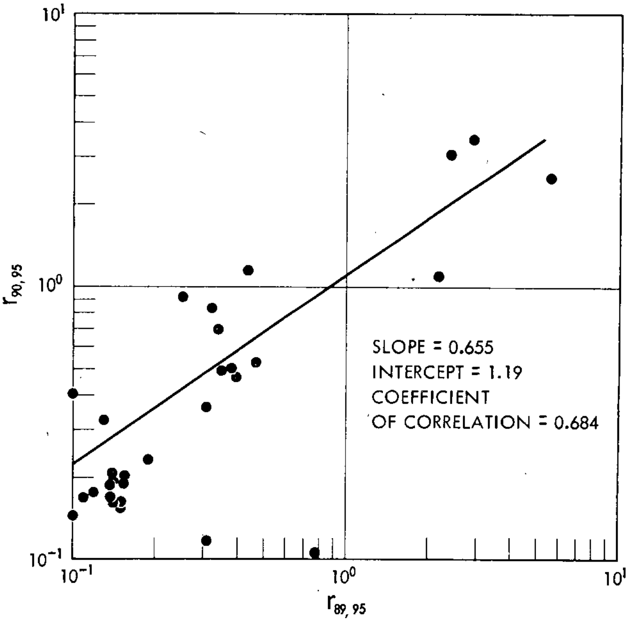

Fig. 2—Fractionation plot for ^{90}Sr in Small Boy.

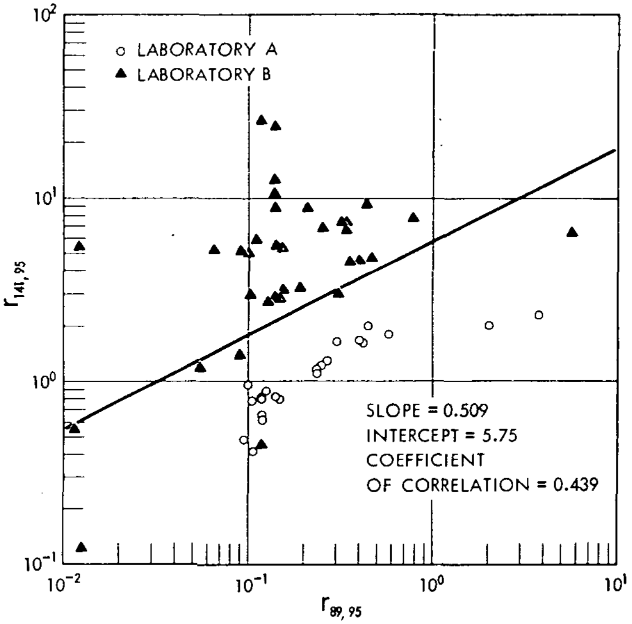

Fig. 3—Fractionation plot for ^{141}Ce in Small Boy.

All the data were reinvestigated by plotting and fitting the data points of each laboratory separately. Differences in the degree of correlation appeared which were sufficient to cast suspicion on part of the data for ^{132}Te, ^{136}Cs, and ^{137}Cs. Calibration differences among the laboratories also appeared to be obscuring the correlation in some instances. Figure 4 illustrates this effect. When the data from the three laboratories are treated separately, the three lines shown are obtained with a reasonable degree of confidence. Note that their slopes do not differ greatly. However, when the data are lumped together, the correlation is much less clear.

In spite of the difficulties involved in correlating the data, some facts emerge fairly clearly, as can be seen in Table 1. First, the same group of nuclides previously mentioned (^{89}Sr, ^{90}Sr, ^{91}Y, ^{103}Ru, ^{106}Ru, ^{131}I, ^{132}Te, ^{136}Cs, ^{137}Cs, ^{140}Ba, ^{141}Ce, and ^{239}Np) fractionated from ^{95}Zr in all three shots, whereas ^{99}Mo, ^{144}Ce, and ^{239}Pu did not. Second, ^{137}Cs appears to fractionate about as severely as ^{89}Sr. Beyond these basic points, the Sedan data display some differences from the data obtained in the other two shots. This is not surprising in view of the radical differences in the Sedan shot conditions. For Sedan the fractionating nuclides other than ^{137}Cs all showed a more or less intermediate degree of fractionation—the slopes of the log–log plots were between about 0.3 and 0.6—whereas, for Johnie Boy and Small Boy,

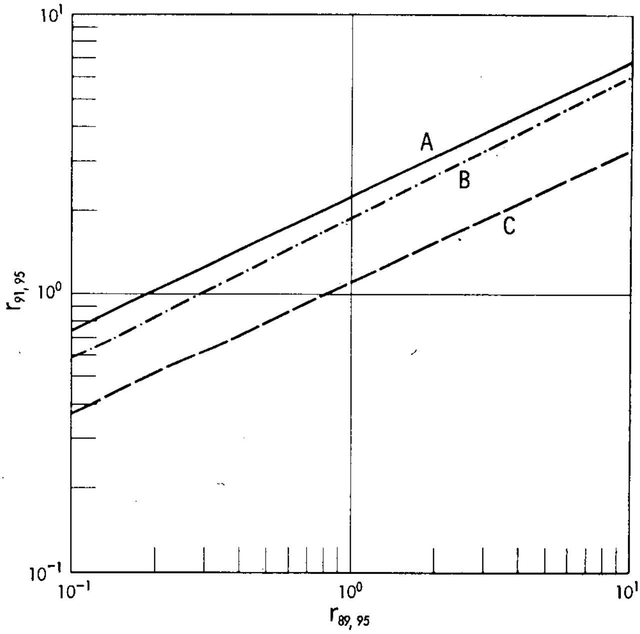

Fig. 4—Correlation lines for ^{91}Y *in Small Boy from three different laboratories.*

Table 1—SUMMARY OF SLOPES OF FRACTIONATION PLOTS

	Silicate-surface and subsurface bursts in 1962			High-yield coral-surface burst	
Nuclide	Sedan	Small Boy	Johnie Boy		Air bursts
^{137}Cs	0.99	1.19	1.11	1.03	0.90
^{89}Sr	1.0	1.0	1.0	1.0	1.0
^{132}Te	0.43	0.90*	1.08*	0.60	
^{106}Ru	0.58*	0.89*			
^{131}I	0.56	0.84	1.10		
^{90}Sr	0.54	0.73	0.73	0.76	0.92
^{136}Cs	0.38*	0.65*	0.83*		
^{140}Ba	0.48	0.53	0.61	0.63	0.62
^{103}Ru	0.50*	0.52*			
^{91}Y	0.44	0.51	0.54		0.56
^{239}Np		0.48	0.48	−0.02	0.80
^{141}Ce	0.23*	0.43*	0.39*		0.40
^{239}Pu	0.04	0.07	0.18		
^{144}Ce	0.17	0.03	−0.003	0.08	0.18
^{99}Mo	0.04	0.04	−0.017	−0.10	0.30
^{95}Zr	0.0	0.0	0.0	0.0	0.0

*Certain reservations relative to these values are expressed in the text.

the range was considerably wider. The slope values obtained from the Johnie Boy and the Small Boy data are in quite good agreement with each other. The Sedan data are also given for purposes of comparison along with slopes from previous correlations on a high-yield coral-surface burst[4] and on some air bursts. A few interesting points with regard to the table may be mentioned. The nonfractionating behavior of ^{239}Np in the coral-surface burst is at variance with its behavior in the air bursts and the silicate bursts. On the other hand, ^{99}Mo fractionates in the air bursts but not in the other shots. There is an indication of possible slight fractionation of ^{144}Ce in Sedan and in the air bursts. In the silicate bursts ^{136}Cs fractionates less than ^{137}Cs. The fractionation of the latter is explainable on the basis of its rare-gas precursor, ^{137}Xe. Cesium-136, on the other hand, is shielded; i.e., it has no precursors. A possible explanation of its fractionation behavior lies in the basicity of the alkali-metal oxide or hydroxide relative to the silicate soil medium.

A reservation should be noted for the slope values reported for the 103-, 106-, and 132-mass chains for Johnie Boy and Small Boy. There is some indication in each of these cases that the data points belong to two different families and should not be fitted to the same straight line. The available data are unfortunately inadequate to resolve the question.

Aside from the ^{99}Mo and ^{239}Np anomalies just mentioned, insofar as the table permits one to judge, the differences in fractionation in the various kinds of bursts are of degree rather than kind.

Analysis on many samples separated into sieve fractions displays the trend of fractionation with particle size in a rough way. Figure 5 shows an example of these data from the Small Boy shot and also illustrates the variability of the ratios observed. The ratio of ^{89}Sr to ^{95}Zr has been plotted against the sieve-opening diameter. There is, of course, no really accurate way of plotting these data. For example, any point on the right side of the 1580-μ line corresponds to a sample that passed a No. 7 sieve (2800-μ openings) and was caught on a No. 12 sieve (1580-μ openings); presumably the sample may contain particles up to 2800 μ. The scattering of the points is thought to be due to the combined effects of heterogeneity and very small sample size. At least two kinds of active particles, smooth spheres and irregular particles, were discernible in these samples. Since many of the sieve fractions consisted of only a few particles, their compositions may not have been truly representative of their particle-size classes. If an average weighted according to sample masses is taken, one obtains the points of Fig. 5 through which a line has been drawn. The figure is quite representative of the behavior of fractionating nuclides in both Small Boy and Sedan. The sieve data on the Johnie Boy samples were too few to draw any conclusions relative to particle size.

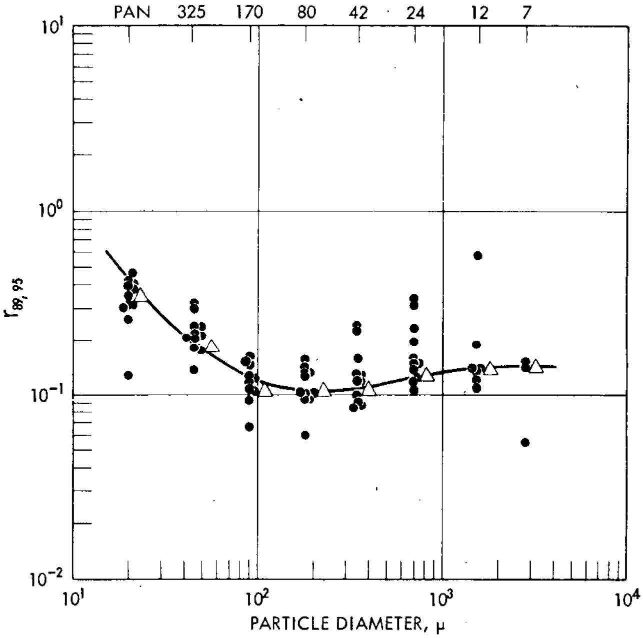

Fig. 5—Effect of particle size on fractionation ratio.

SUMMARY

Correlations indicate that the fractionation behavior of ^{89}Sr, ^{90}Sr, ^{91}Y, ^{137}Cs, ^{140}Ba, and ^{144}Ce relative to ^{95}Zr in silicate-surface bursts does not differ essentially from that observed in a coral-surface burst or in air bursts. Differences are noted for ^{99}Mo and ^{239}Np. For ^{103}Ru, ^{106}Ru, ^{131}I, ^{132}Te, ^{136}Cs, ^{141}Ce, and ^{239}Pu, some differences in degree of fractionation are indicated, and further study of these nuclides is recommended.

ACKNOWLEDGMENTS

In addition to the U. S. Atomic Energy Commission, the Defense Atomic Support Agency contributed generously to the support of this study. Some of the data were obtained from U. S. Air Force sources.

REFERENCES

1. D. E. Clark, F. K. Kawahara, and W. C. Cobbin, Fallout Sampling and Analysis: Radiation Dose Rate and Dose History at 16 Locations, Report POR-

2289, U. S. Naval Radiological Defense Laboratory, Oct. 24, 1963. (Classified)

2. E. C. Freiling, L. R. Bunney, and F. K. Kawahara, Physicochemical and Radiochemical Analysis, Report POR-2216, U. S. Naval Radiological Defense Laboratory, Oct. 28, 1964. (Classified)
3. W. B. Lane, Some Radiochemical and Physical Measurements of Debris from an Underground Explosion, USAEC Report PNE-229F, Jan. 7, 1964.
4. E. C. Freiling, Radionuclide Fractionation in Bomb Debris, *Science, 133* (3469): 1991–1998 (1961).

PHYSICAL CHARACTERISTICS OF SINGLE PARTICLES FROM HIGH-YIELD AIR BURSTS

P. BENSON, C. E. GLEIT, and L. LEVENTHAL
Tracerlab, A Division of Laboratory for Electronics, Inc.,
Richmond, California

ABSTRACT

Particles, isolated from high-altitude nuclear explosions, were separated and their physical parameters determined. The particles varied in color from colorless to black. They were generally spherical, and some had satellites that were a result of collisions of small particles with larger particles before complete solidification had occurred. Particles with diameters greater than 2 μ were isolated.

The beta radioactivity of the particles was measured at 25 days and was found to be related to the diameter expressed in the following way: $A = aD^b$, where b showed values of 3.06 ± 0.08, 3.22 ± 0.16, and 3.01 ± 0.30 for the three shots studied. Since the standard deviations were due to variations in activities of the particles and not in experimental errors, it was concluded that the activity was directly proportional to the particle volume. The standard deviations were found to be unrelated to particle size and color, but the value of a was found to be a function of the weapon yield. The value of b, however, was not related to weapon yield.

Individual particles were allowed to decay to determine the decay rate of the fission-product mixtures. On the average, the particles followed the relation $A = kt^{-1.10}$. Values of the decay slopes varied from 0.7 to 1.4. The distributions of the decay slopes of the individual particles from the average was found to be Gaussian. The deviations were not a function of particle size or color; they are explained as being a result of the widely different radionuclide content of the particles.

PHYSICAL CHARACTERISTICS

The fireball of a nuclear explosion contains material from two sources, the weapon itself and the explosion environment. In studies of the physical phenomena occurring during cloud cooling and of the precipitation of the vaporized materials and radioactivities in the form of a particulate aerosol prior to the Operation Dominic I test series, the processes have been hard to resolve because of incomplete vaporization of the environmental materials and the incorporation of new materials into the fireball as it rose. During the Operation Dominic I test series, however, it was possible to study high-altitude nuclear explosions in which the material incorporated into the fireball was only that of the weapon itself plus its ballistic casing. This relatively small amount of material was completely vaporized by the heat of the nuclear explosion.

As the fireball expands and cools, the vaporized materials condense in the form of small droplets that solidify, forming the small particles which we are examining in the investigation reported here. Figure 1 shows photomicrographs of particles isolated from high-yield air bursts from the Operation Dominic I series. These particles show the spherical-shape characteristic of solidified droplets. When viewed under the optical microscope, these particles show great differences in color, varying from colorless to black. This may be due to variation in matrix-element composition or to surface effects.

The radioactive part of the nuclear debris consists of fission products, radionuclides produced by neutron reactions with the matrix materials, and the unreacted fissile material of the nuclear device. The majority of the radionuclides are incorporated into the particles, with the fission products contributing the dominant part of the radioactivities. The composition of the fission-product mixtures varies with fission mode and time after fission. Table 1 shows the composition of an unfractionated ^{235}U fission-product mixture 25 days after the time of fission.

Figure 2 shows the activities of the isolated particles plotted as a function of particle diameter. The analysis of particle samples, 2 μ in diameter or larger, shows that the beta activity increases as the cube of the particle diameter. Three shots were analyzed in this study, and a least-squares fit of the logarithm of the activity vs. the logarithm of the particle diameter of the form $\log A = b \log D + a$ gave values of b of 3.06 ± 0.08, 3.22 ± 0.16, and 3.01 ± 0.30. The standard deviations observed are due to variations in the activities of the various particles and not to experimental errors in the measurement of these activities.

The cubic relation of beta activity to size is used to describe one of the important physical properties of particles, the activity per unit

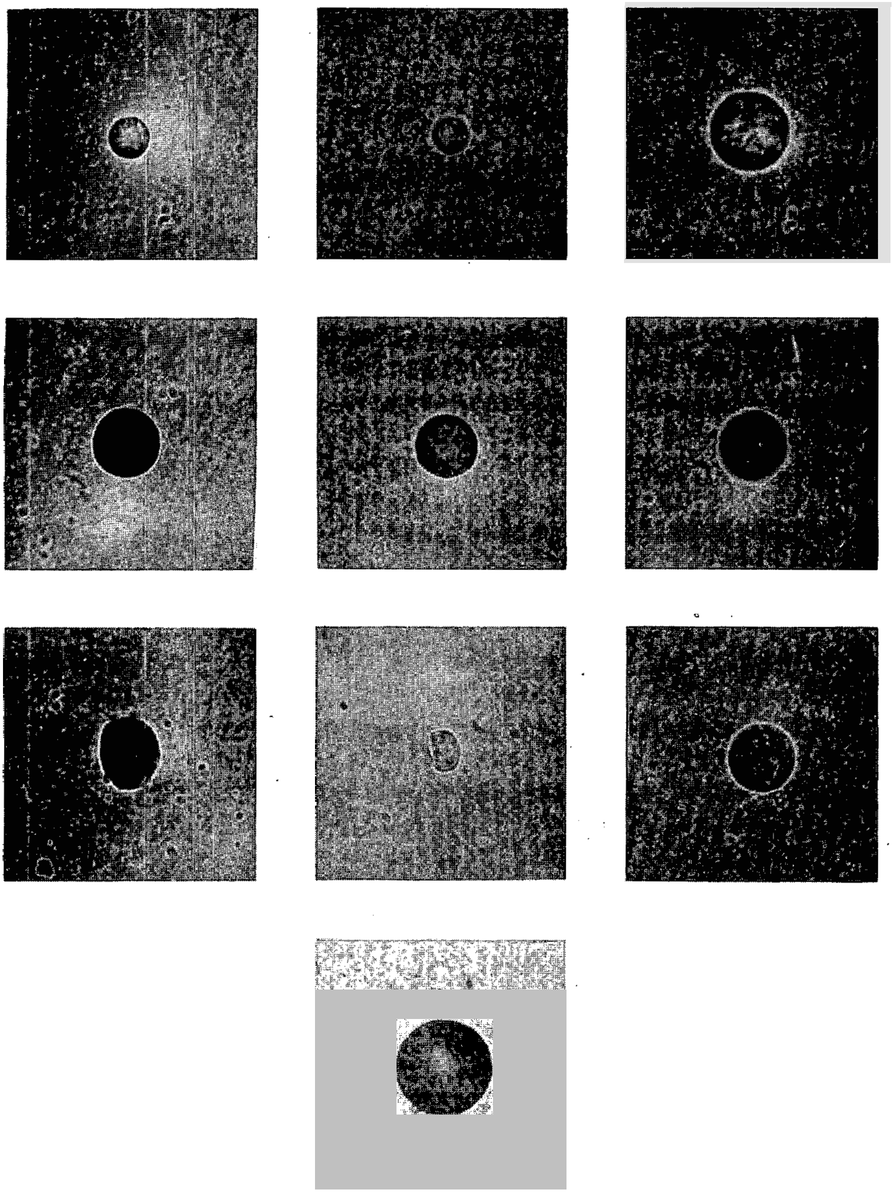

Fig. 1—Photomicrographs of particles.

Table 1 — THE RADIONUCLIDE CONTENT OF AN UNFRACTIONATED ^{235}U FISSION-PRODUCT MIXTURE AT 25 DAYS

Radionuclide	Activity, %	Radionuclide	Activity, %
^{89}Sr	5.4	^{131}I	1.7
$^{90}Sr-^{90}Y$	0.05	^{133}Xe	4.75
^{91}Y	6.4	^{137}Cs	0.05
^{95}Zr	6.5	^{140}Ba	8.1
^{95}Nb	2.8	^{140}La	9.2
$^{99}Mo-^{99}Tc$	0.3	^{141}Ce	9.1
^{103}Ru	3.8	^{144}Ce	1.5
^{106}Ru	0.08	^{143}Pr	25.6
^{129m}Te	1.4	^{147}Nd	12.5
$^{132}Te-^{132}I$	0.5	^{147}Pm	0.2

particle volume. Figure 3 shows the activity per unit particle volume as a function of particle diameter for two shots. As is to be expected, the activities per unit particle volume tend to fall at a common average for each of the three shots studied, depending on the fission yield of the nuclear device. For each case, however, there are particles that vary considerably from the norm. This variation appears not to be related to particle color, and on a fractional basis it appears to be as large in large particles as it is in small particles.

The beta-energy spectrum, of course, varies as a function of time as the composition of the fission-product mixture changes. Figure 4 shows aluminum absorption measurements on a particle sample at different times. Close to zero time the absorption curve approaches a straight line on semilog plots, but as time passes the absorption curve shows a shape of a low-energy component plus a high-energy component. When the sample has decayed 200 days, the major high-energy component is due to ^{144}Pr, the daughter of ^{144}Ce.

In the discussions so far, the similarities between particles have been noted. Striking dissimilarities become apparent, however, after decay. Figure 5 shows the beta decay of ^{235}U and ^{239}Pu fission-product mixtures as measured with a methane-end-window proportional counter. Although it is readily apparent that the rate of decay of these fission-product mixtures varies with time, a relation of $A = kt^{-1.2}$ is a close approximation of the decay from 3 to 4000 days.

The decay of isolated particles was followed and the data during the period 3 to 200 days were chosen to determine the decay rate by a least-squares curve fit. Figure 6 shows plots of the number of particles vs. the decay slope of those particles. As analytical aids the standard deviation of the decay slope, the standard error of the estimate, the variance in each variable, and the difference between each experimental value and the unfractionated fission-product mixtures, derived

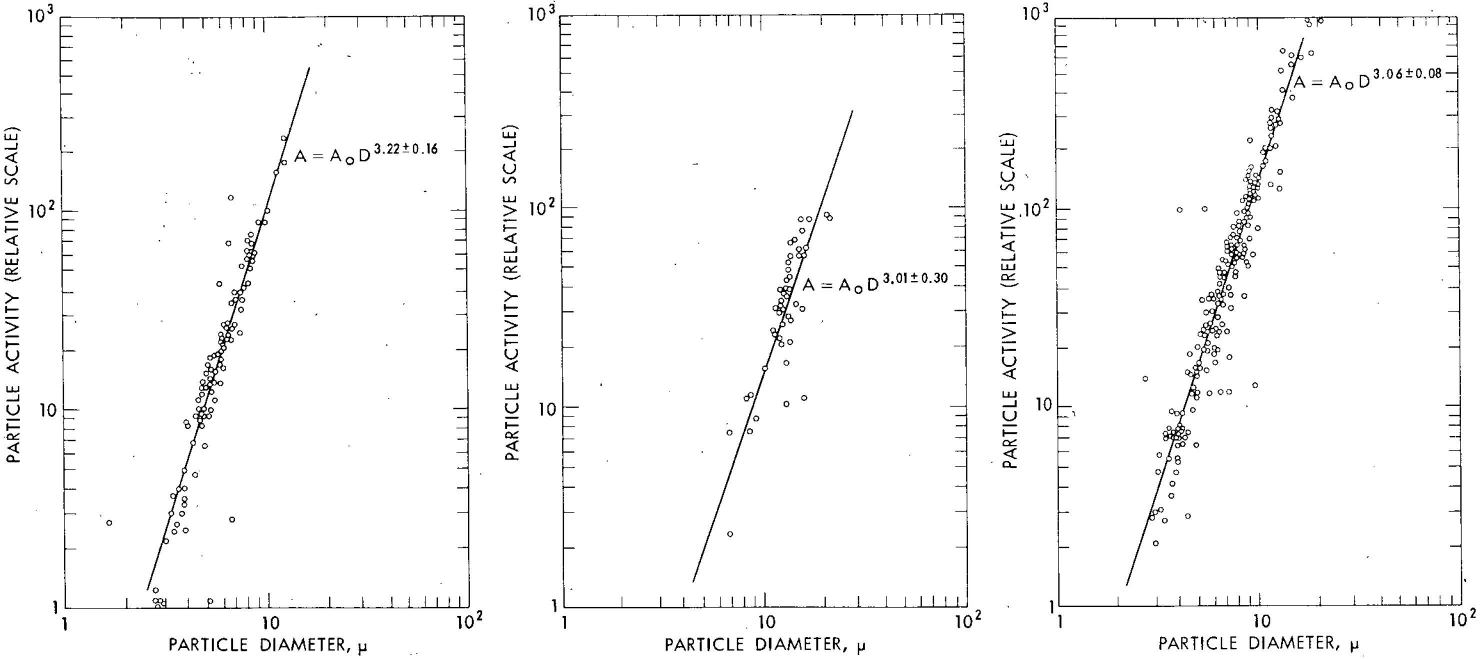

(a) (b) (c)

Fig. 2—Total beta activity as a function of particle diameter.

TCT ENLARGE ~~27~~ 46 % KILL ALL LETTERING

Conf 765

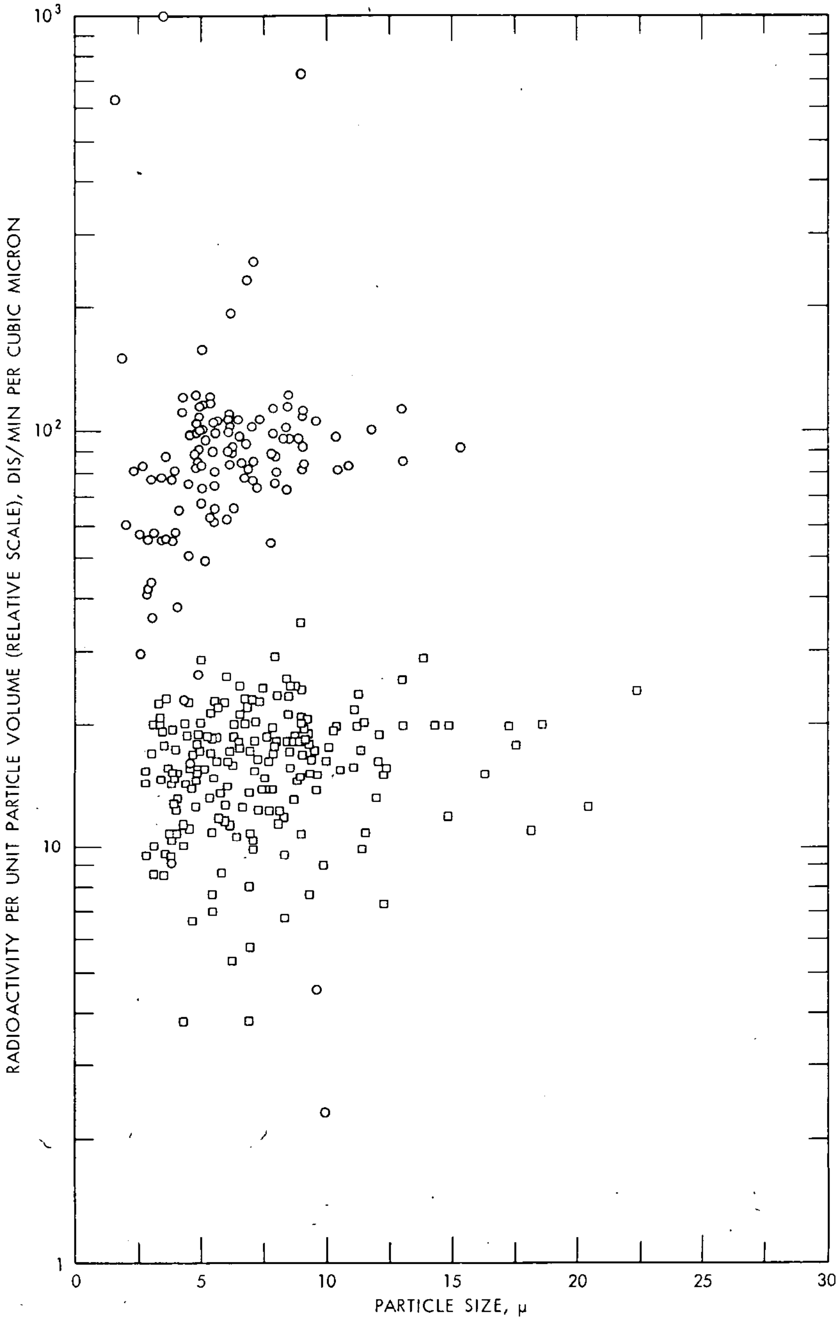

Fig. 3—Radioactivity per unit particle volume for two shots as a function of particle size.

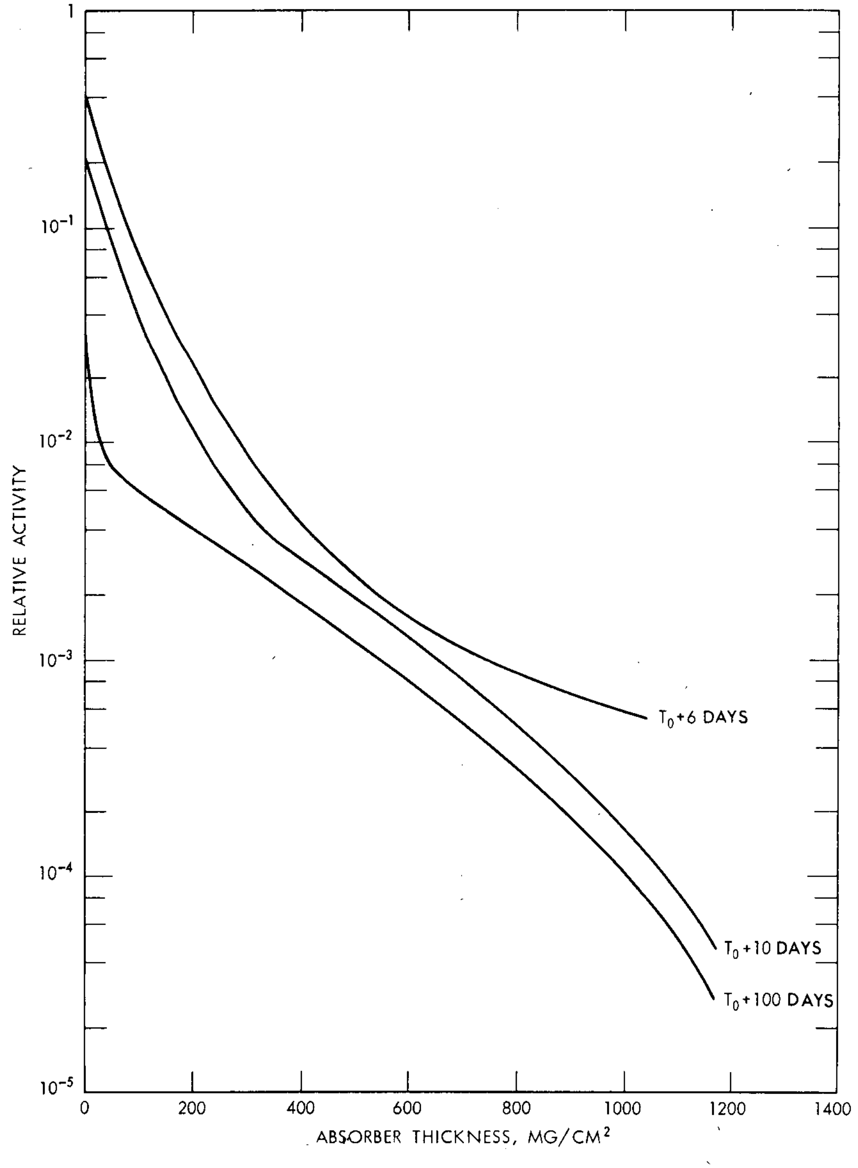

Fig. 4—Aluminum absorption measurements as a function of time.

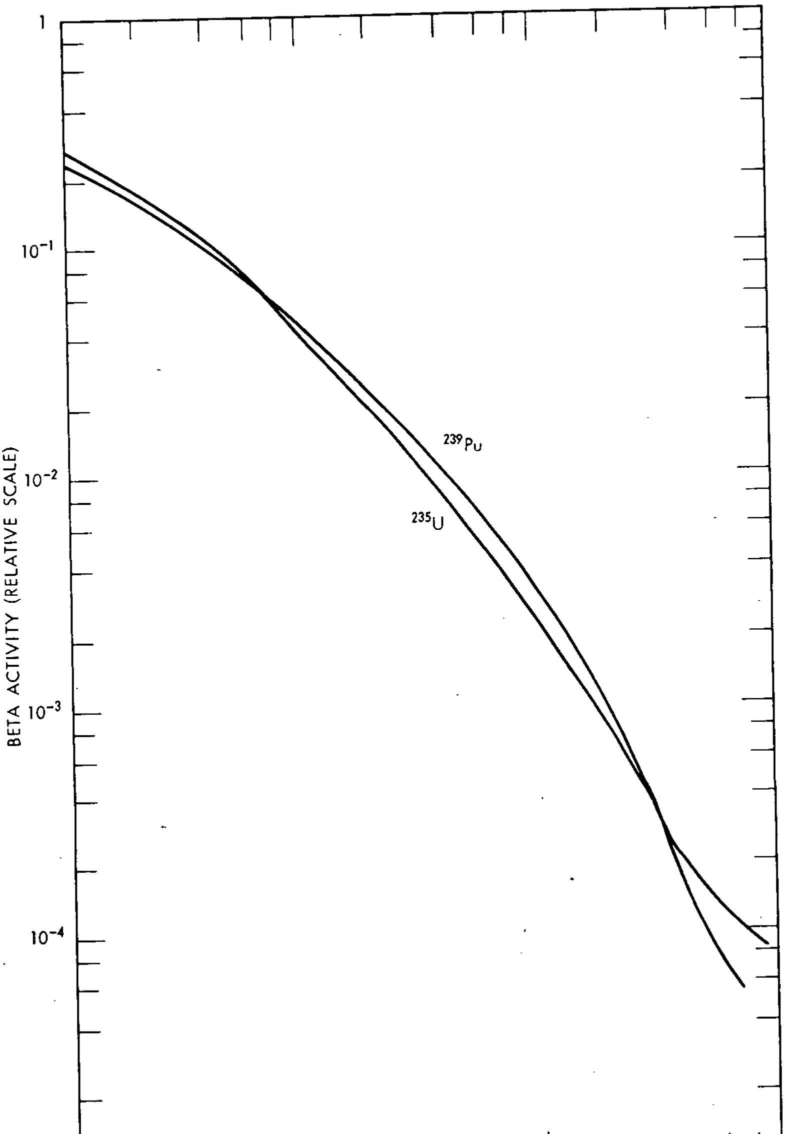

Fig. 5—Beta-activity decay of unfractionated ^{235}*U and* ^{239}*Pu fission-product mixtures.*

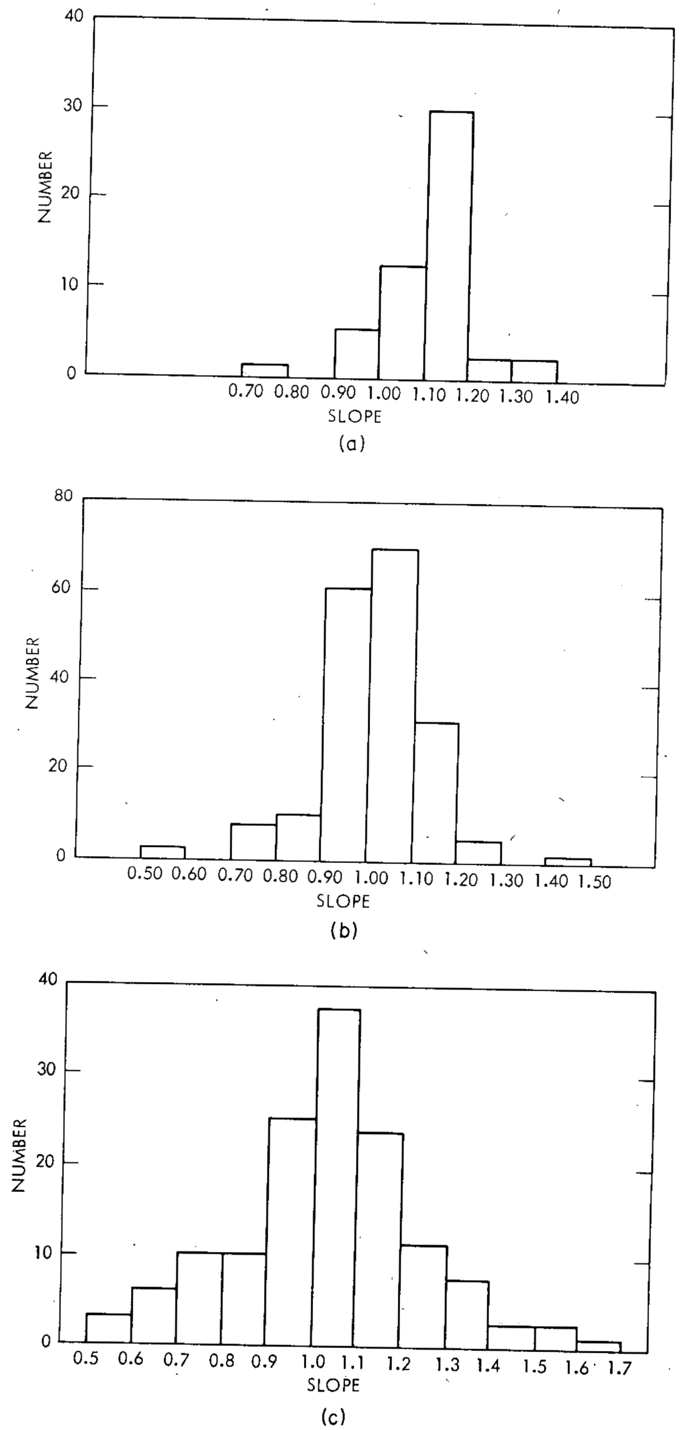

Fig. 6—The number of particles observed with various decay slopes.

from the straight-line approximation, were calculated. For over 90% of the decay curves, the standard error in the exponent was less than ± 3%. The excellence of the curve fit was further demonstrated by the magnitude of the correlation coefficient, which exceeded 0.99 for over 90% of the decay curves.

Values of the decay constant were 0.7 to 1.4, with an average value for all shots of 1.10. These variations were found among particles of approximately the same size from each shot. There was no correlation between the decay slope and the particle size or the color. A statistical analysis of the variance indicates that a negligible variation can be associated with experimental errors or statistical fluctuations, and it is concluded that the wide variations in the beta-decay rates result from widely varying fractionation patterns among the particles. These distributions appear to be Gaussian and independent of weapon yield.

The physical characteristics of single particles can yield information concerning the radiochemical content. Although single-particle beta and gamma decay curves, the beta-energy spectrum (as well as the gamma-energy spectrum), and the activity per unit particle volume can give valuable information from the health-hazard point of view, the radionuclide concentrations as a function of particle size are of prime importance for an understanding of the fractionation process. In any laboratory program dealing with single-particle analysis, it is desirable to provide simple test procedures to select those particles which will yield particles exhibiting the interesting radionuclide compositions. A correlation of the radionuclide compositions with the physical parameters of the particles will provide a field test-particle selection procedure. The radiochemical composition of these particles was also investigated, and the program concerned will be reported in the next paper.*

---

*P. Benson, C. E. Gleit, and L. Leventhal, this volume.

RADIOCHEMICAL FRACTIONATION CHARACTERISTICS OF SINGLE PARTICLES FROM HIGH-YIELD AIR BURSTS

P. BENSON, C. E. GLEIT, and L. LEVENTHAL
Tracerlab, A Division of Laboratory for Electronics, Inc.,
Richmond, California

ABSTRACT

The radiochemical fractionation characteristics from two Operation Dominic high-yield air bursts were studied. Particles measuring from 2.5 to 20.0 μ were isolated from filter-paper matrices by autoradiographic registration and confirmed by optical microscopy. After physical measurements radiochemical and/or gamma-spectroscopy studies were performed on individual and aggregates of particles. Of particular interest was the distribution of volatile and refractory nuclides for each particle size. The nuclides radiochemically analyzed were ^{99}Mo, ^{89}Sr, ^{90}Sr, ^{95}Zr, ^{129m}Te, ^{132}Te, ^{137}Cs, ^{140}Ba, ^{141}Ce, ^{144}Ce, ^{147}Nd, ^{237}U, and ^{239}Np. Gamma-spectra analysis was used to determine the ^{95}Zr and ^{140}Ba concentrations in 334 particles. A computer technique for resolving these nuclides and ^{99}Mo, ^{103}Ru, ^{131}I, ^{132}Te, ^{137}Cs, ^{141}Ce, ^{144}Ce, ^{147}Nd, and ^{239}Np was developed.

The particles were found to be extremely fractionated. A logarithmic fractionation correlation plot for ^{140}Ba was determined which compared within the limits of error with data plotted by Freiling for high-yield water bursts. The logarithms of ^{95}Zr and ^{140}Ba activities were plotted as functions of the particle diameters for the two shots. The slopes for the regression plot for ^{95}Zr were 3.41 ± 0.18 and 3.09 ± 0.37. These values imply a cubic relation. The slopes for the regression plot for ^{140}Ba were 2.63 ± 0.24 and 2.32 ± 0.50, somewhat between a square and a cubic relation. These results point toward condensation of the refractory nuclides initially with subsequent precipitation of the volatiles on the particles at later times.

These experiments have proved that important radiochemical fractionation information can be obtained from single particles. Both the limitations and the advantages of this technique have been delineated.

INTRODUCTION

The 1961 Dominic test series presented the first opportunity to study radionuclide fractionation in single particles from high-yield air bursts. In these air bursts the condensation matrices were dependent only on the weapon composition. Masses of contaminating materials such as tower, water, and salt, which would present indeterminable factors, were not present. The radionuclide distributions in selected particles obtained from several tests in this series were analyzed radiochemically and by gamma spectrometry. Of particular interest was the distribution of volatile and refractory nuclides for each particle size. The nuclides radiochemically analyzed were ^{99}Mo, ^{89}Sr, ^{90}Sr, ^{95}Zr, ^{129m}Te, ^{132}Te, ^{137}Cs, ^{140}Ba, ^{141}Ce, ^{144}Ce, ^{147}Nd, ^{237}U, and ^{239}Np. It soon became apparent that the radiochemical method was too time consuming, and as an alternative a nondestructive gamma-spectrometric technique, which also yielded the required data on radionuclide behavior, was employed. A computer technique was developed for resolving the spectra, and 334 of the particles were examined by this method. Analysis of the radionuclide concentrations in individual particles so far has been confined to the determination of correlations between the data and the particle diameters.

PROCEDURE

The radioactive particles were located by autoradiography and isolated from the filter-paper matrix. After particle size and other physical parameters were measured, the particles were subjected to sequential radiochemical analysis (see Fig. 1). Particles ranged in size from 4 to 20 μ and contained between 10^8 and 10^{10} fissions based on ^{99}Mo analysis. Aggregates of particles representing groups 4 to 5 μ and 4.5 to 9 μ were similarly analyzed to determine radionuclides that were in too low abundance to be measured in single particles. A complete study was made on integral papers. The nuclides were assayed by standard counting techniques, and the results were converted to R* values for fission products or atoms for induced radionuclides.

---

*An R value is defined as the ratio of the ratio (r) of calculated fissions in isotope (i) to fissions as calculated from ^{99}Mo to a similar ratio (r) determined from thermal-neutron fission of ^{235}U; i.e., $(r_{i,99})x/(r_{i,99})th$.

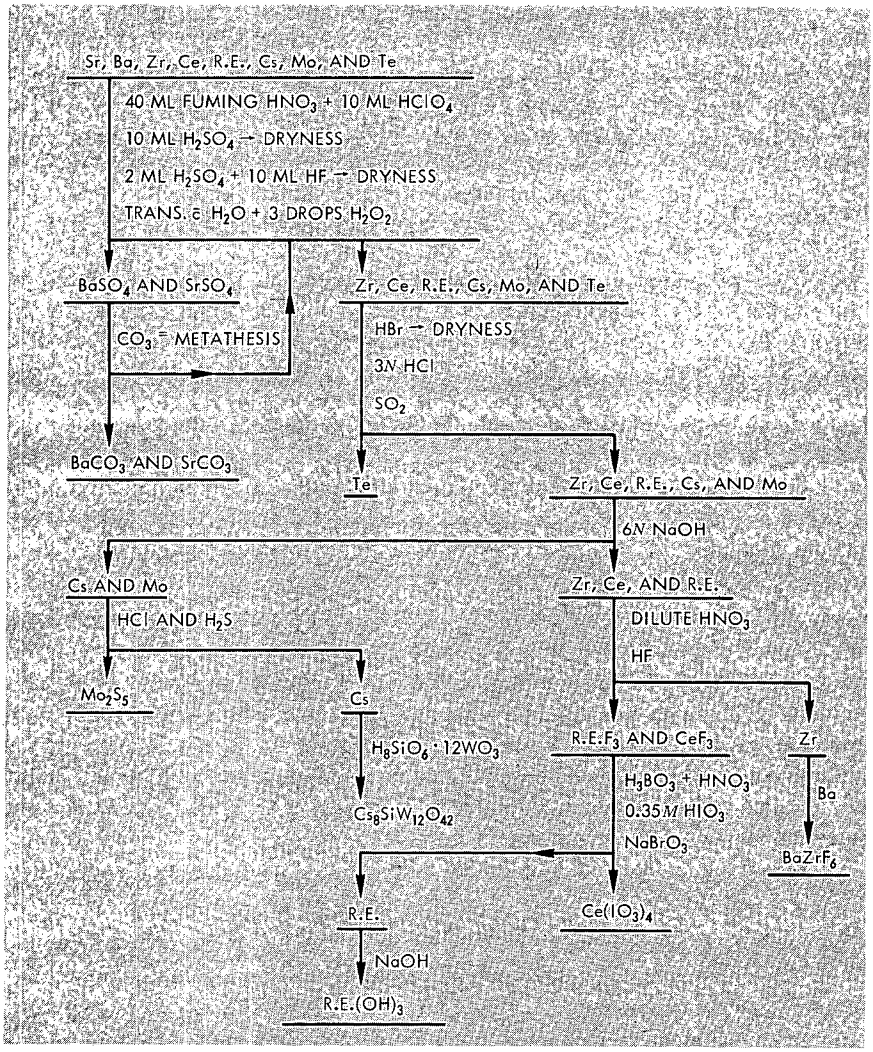

Fig. 1—Sequential separation of particle radionuclides.

Gamma spectra of individual particles were obtained with a 3- by 3-in. NaI detector and a 400-channel pulse-height analyzer. The particles were analyzed as early as two days after the shot and thereafter once every two particle half-lives.

In general, six spectra per particle were obtained over a two-year period. Particles studied ranged in size from 2.5 to 25 μ and contained 10^8 to 10^{11} ^{95}Zr fissions. The gamma spectra were normalized prior to gamma-spectra stripping by a computer program written in FORTRAN for the IBM-7094. This program has a capability for the determination of ^{95}Zr, ^{99}Mo, ^{137}Cs, ^{141}Ce, ^{144}Ce, ^{140}Ba, and ^{239}Np, as well as for others, and is based on the method proposed by Carnahan.[1] The isotopes mentioned represent the predominant peaks in the spectra obtained. Figure 2 indicates a typical gamma-spectrometer scan observed over a two-year period. The background radiation is the lowest line. The peaks of interest are singled out on the figure.

RADIOCHEMICAL STUDIES

Calculations of the counting-rate yield at zero time for a particle representing 10^8 fissions indicated that measurable activities would be obtained for the nuclides of interest if *no* fractionation is assumed (see Table 1). However, fractionation effects in single particles caused wide

Table 1—THEORETICAL RADIOCHEMICAL SENSITIVITY FOR A PARTICLE OF 10^8 FISSIONS

(Basis: Counting Rate at Zero Time for 100% Chemical Yield)

Nuclide	Counts/min	Remarks
^{89}Sr	23	R = 1
^{90}Sr	0.1	R = 1
^{95}Zr	10	R = 1
^{97}Zr	1000	110 abs, R = 1
^{99}Mo	562	R = 1
^{111}Ag	0.5	R = 1
^{115}Cd	2	R = 1
^{103}Ru	2	Zero abs, R = 1
^{106}Ru	0.2	Zero abs, R = 1
^{136}Cs	0.05	R = 1
^{137}Cs	0.09	R = 1
^{140}Ba	94	R = 1
^{141}Ce	24	Zero abs, R = 1
^{144}Ce	7.4	Zero abs, R = 1
^{91}Y	25	R = 1
^{156}Eu	0.06	74 abs, R = 1
^{147}Nd	40	R = 1
^{7}Be	0.004	N/f* = 100×10^{-5}
^{24}Na	44	N/f = 100×10^{-5}
^{64}Cu	200	N/f = 1000×10^{-5}
^{67}Cu	0.06	N/f = 1×10^{-5}
^{187}W	0.23	N/f = 1×10^{-5}
^{203}Pb	0.015	N/f = 1×10^{-5}
^{231}Th	900	N/f = 100×10^{-5}
^{237}U	690	N/f = 0.3
^{239}Np	2880	N/f = 0.3
^{240}U	2880	N/f = 0.1
^{238}Pu	0.00005	N/f = 10×10^{-5}
^{239}Pu/J†	0.0009	N/f = 0.5

*N = atoms, f = fissions.

†J = [atoms ^{239}Pu/atoms ^{240}Pu/(atoms ^{239}Pu/atoms ^{240}Pu) + 3.7].

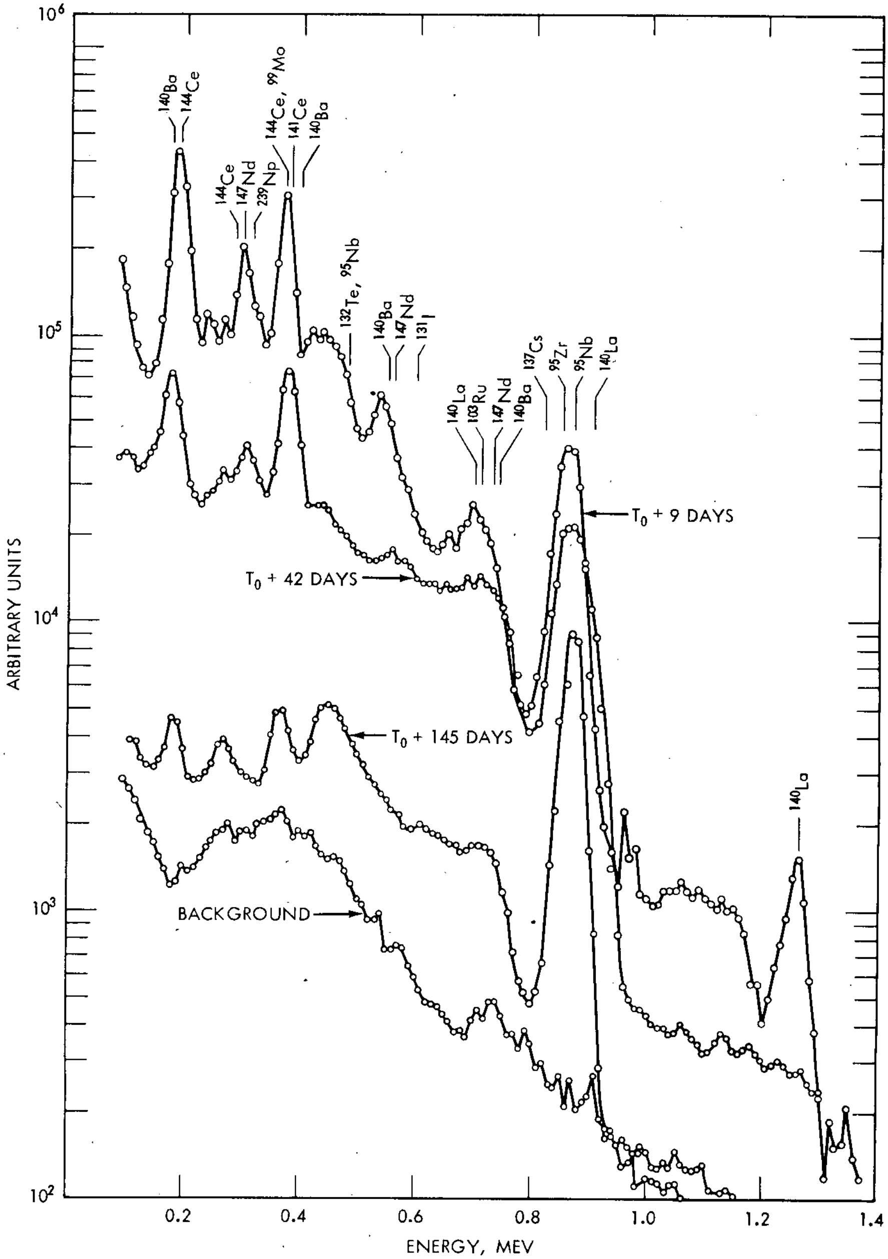

Fig. 2—Particle gamma spectrum.

variations from predicted values. Particles ranging in size from 5 to 20 μ were analyzed from each of two shots. Two sets of selected aggregate particles between 4 to 9 μ were also analyzed.[2]

A logarithmic fractionation correlation plot of $r_{140,89}$ vs. $r_{95,89}$* incorporating filter-paper aggregate particles and individual particle data from both shots fitted linearly (see Fig. 3). Freiling[3] has plotted $r_{140,89}$ data for megaton-range coral-surface bursts and three types of water bursts. Within the limits of error, the slope and intercept of the regression line of Fig. 3 are comparable with those of Freiling's plot.

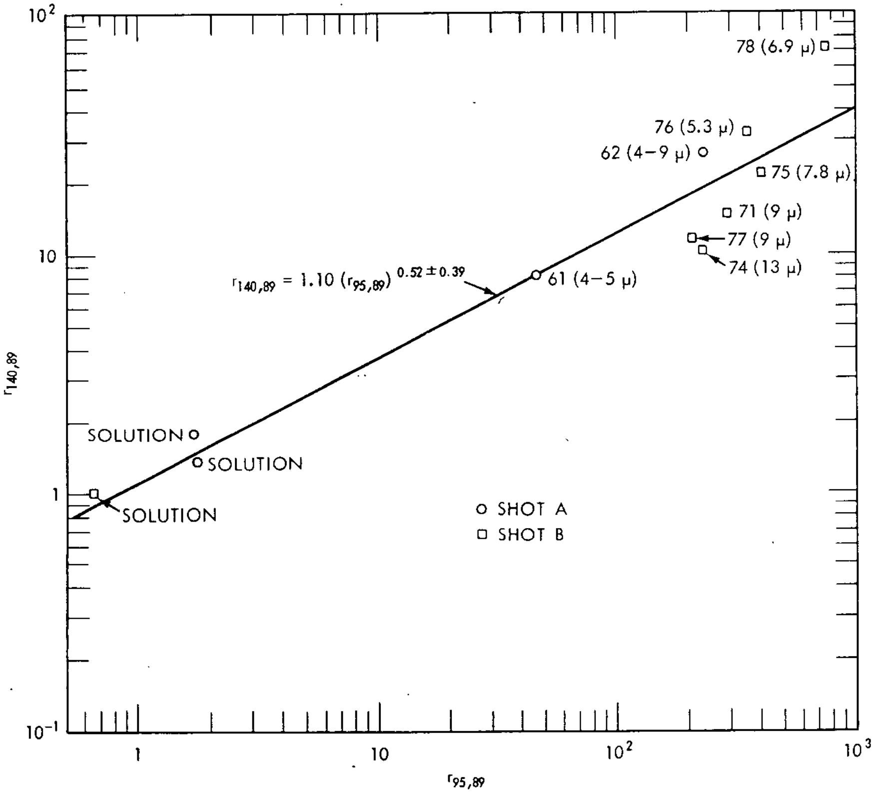

Fig. 3—Logarithmic fractionation correlation for ^{140}Ba.

The single particles are severely fractionated with respect to the total sample. It is interesting to note that for these particles the fractionation plot had to be extended another decade to include the particle r-value ratios.

---

*$r_{i,89}$ is defined as the ratio of calculated isotope (i) fissions to calculated ^{89}Sr fissions, f_i/f_{95}, where f equals fissions.

Table 2— PRINCIPAL GAMMA RAYS OF THE MAJOR FISSION PRODUCTS FOR A PARTICLE OF 10^8 FISSIONS

(Basis: Gammas Per Minute at Zero Time)

Radionuclide	Energy, Mev	Dis/min	Gammas/min
^{95}Zr – ^{95}Nb	0.717	47.0	47.0
	0.745	8.6	8.5
	0.235		0.17
^{99}Mo – ^{99m}Te	0.780	1050.0	210.0
	0.740		146.0
	0.180		10.5
	0.041		105.0
	0.141	930.0	930.0
^{103}Ru – ^{103m}Rh	0.498	38.0	36.0
	0.040		38.0
^{131}I	0.364	170.0	138.0
^{132}Te – ^{132}I	0.231	670.0	670.0
	1.40		76.0
	0.96		130.0
	0.777		490.0
	0.673		670.0
	0.528		170.0
^{137}Cs – ^{137m}Ba		0.29	
	0.661		0.270
^{140}Ba – ^{140}La	0.54	230.0	70.0
	0.30		23.0
	0.16		23.0
	0.03		230.0
	1.60		220.0
	0.815		67.0
	0.49		91.0
^{141}Ce	0.145	89.0	60.0
^{143}Ce	0.660	2100.0	325.0
	0.356		260.0
	0.289		1285.0
	0.126		260.0
^{144}Ce – ^{144}Pr	0.134	10.0	10.0
	0.081		10.0
	0.034		10.0
	1.480		0.20
	0.695		0.41
^{147}Nd	0.532	100.0	25.0
	0.318		1.50
	0.092		60.0

Similar graphs were prepared for ^{144}Ce and ^{237}U. The plot of the particle data for ^{144}Ce also had to be extended a decade higher. The uranium activity per particle was too low to get accurate data, and a linear fractionation plot could not be developed from these data.

Analyses were made for ^{90}Sr, ^{136}Cs, ^{132}Te, ^{143}Ce, and ^{239}Np, but they were not detected in the samples. Satisfactory values were obtained for ^{129m}Te, ^{141}Ce, and ^{147}Nd.

GAMMA-RAY SPECTRA

The individual radionuclides that are susceptible to gamma-spectra analysis in particles were determined. Limits of detection were obtained for the radionuclides of interest by assuming 10^8 thermal-neutron fissions. This was done by correction of the estimated gamma rays per minute for the efficiency of the 3- by 3-in. NaI crystal at a particular energy. Further selection was made by determining if interfering gamma energies were present that produced unresolvable spectra in the region of interest. Of the heavy elements, ^{239}Np was the only nuclide high enough in yield for analysis. However, because of its short half-life, no attempt was made to resolve this nuclide. The induced activities were too low for spectral analysis. Among the fission products listed in Table 2, ^{99}Mo also was too low for spectral analysis. The radionuclides ^{103}Ru, ^{131}I, and ^{137}Cs were not detected, but ^{95}Zr and ^{140}Ba were resolved. Also ^{132}Te, ^{141}Ce, ^{144}Ce, and ^{147}Nd can be resolved.

The ^{140}Ba and ^{95}Zr fissions for two high-yield shots have been calculated[4] from gamma spectra obtained from 21 particles from shot A and 45 particles from shot B. Peak resolution was confirmed by decay of the respective peaks. Three of the particles were sacrificed after gamma stripping and were radiochemically analyzed for ^{140}Ba and ^{95}Zr. Agreement between physical and radiochemical measurements was ± 5%.

The logarithm of ^{140}Ba fissions was plotted as a function of the logarithm of the particle diameter (Figs. 4 and 5), and a linear regression calculation was performed. The slopes of the regression line obtained for the shots A and B data were 2.63 ± 0.24 and 2.32 ± 0.50, respectively. The hypotheses that the populate slopes are square or cubic (equal 2.0 or 3.0) were tested. Because of the scatter of the points about the regression line, both hypotheses could not be rejected except for the hypothesis that the shot A slope was two, which was rejected at the 95% confidence interval. The intermediate value may be explained as due to the decaying of volatile precursors before particle condensation. The slopes obtained for the regression plots for ^{95}Zr (Figs. 6 and 7) for shots A and B were 3.41 ± 0.18 and 3.09 ± 0.37. For this nuclide a cubic relation appears to hold. An explanation for the large value for ^{95}Zr for shot A is not apparent. Spectra stripping of additional particles may reduce this value.

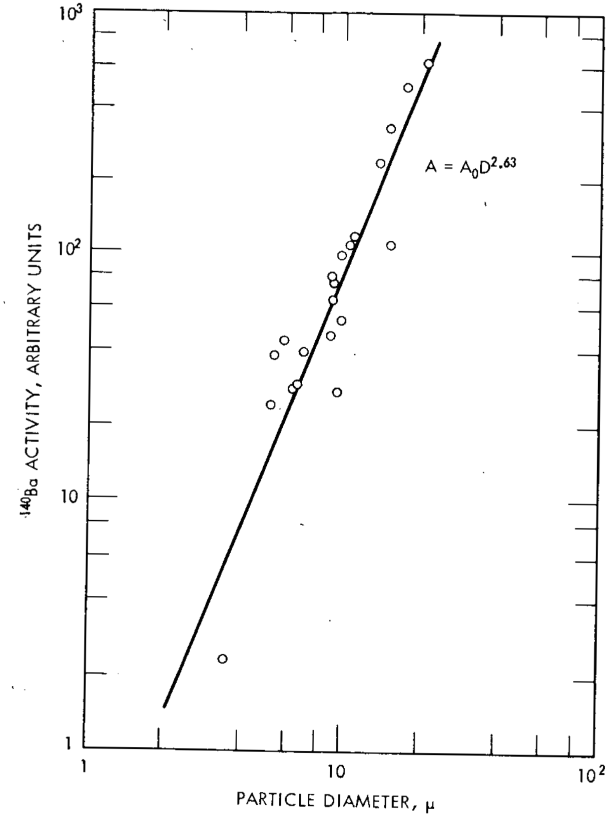

Fig. 4—Barium-140 activity as a function of particle diameter for shot A.

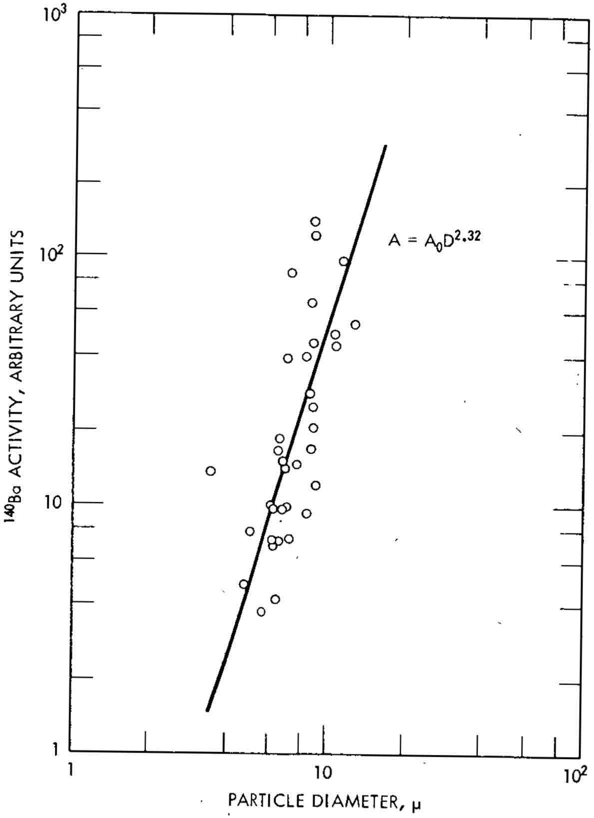

Fig. 5—Barium-140 activity as a function of particle diameter for shot B.

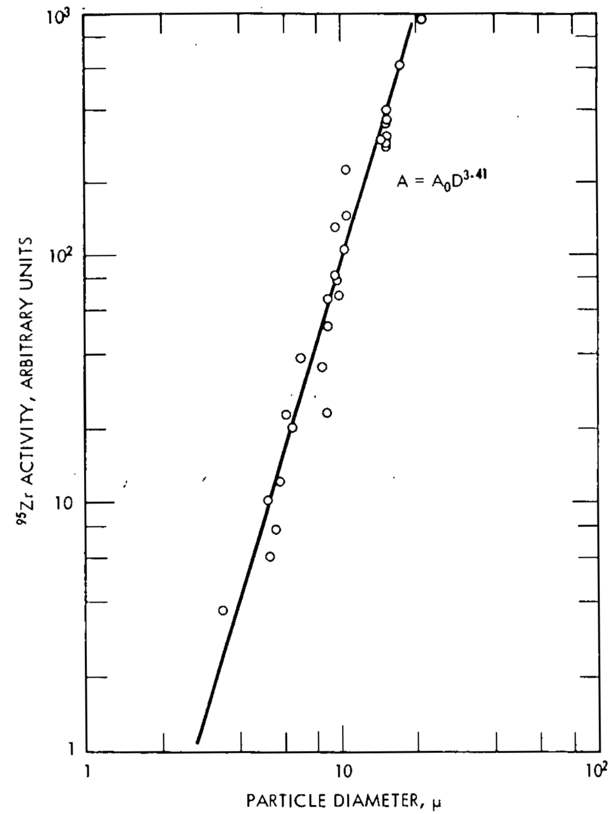

Fig. 6—Zirconium-95 activity as a function of particle diameter for shot A.

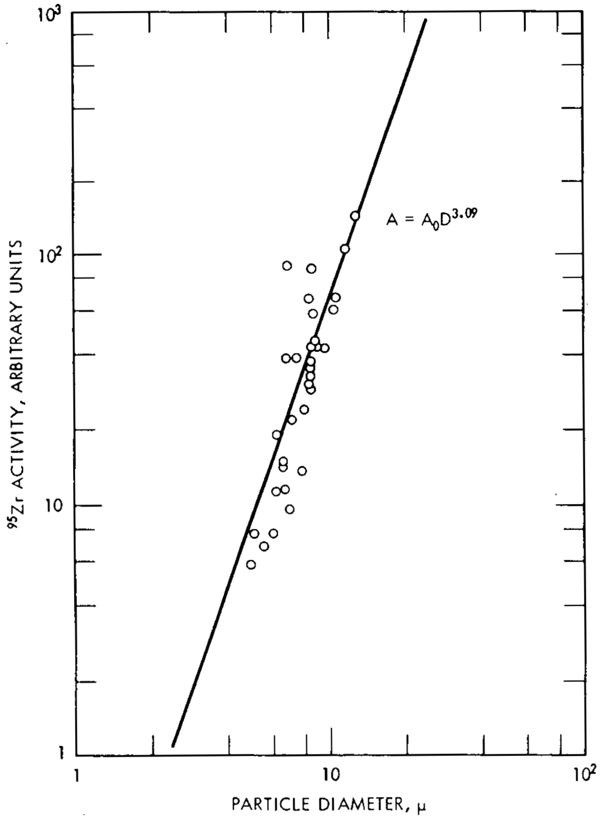

Fig. 7—Zirconium-95 activity as a function of particle diameter for shot B.

Although the surface relation between ^{140}Ba activity and particle size cannot be demonstrated on the basis of these data, the variance in the activity per unit area is quite obvious. One would expect this in nuclear-explosion clouds in which the particles form rather quickly and the volatile constituents precipitate on the particle surfaces much later. This hypothesis appears to be confirmed if one considers the ^{95}Zr as representative of a refractory nuclide. The cubic relation then would indicate that the ^{95}Zr is condensed initially and is distributed as a function of the volume of the particle. In effect, regularity is observed through approximately a hundredfold change in volume.

Another interesting observation that stems from a comparison of the shots A and B plots is that the intercept of the ^{140}Ba regression line of the nuclides of a particular particle size is a function of the yield to mass ratio.

CONCLUSIONS

The feasibility of isolating and analyzing individual particles by radiochemical and gamma-spectrometric techniques has been demonstrated.

Particles under 10 μ and as low as 10^8 fissions have yielded accurate values for the important volatile and refractory fission products. Heavy-element analysis is borderline for ^{237}U and ^{239}Np and is dependent on analysis at early times. Unless an induced activity is present in abnormally large amounts, the analyses of these radionuclides in single particles are not feasible.

Gamma spectrometry is a satisfactory technique for the resolution of nuclides in large numbers of individual particles and may be used to obtain ^{140}Ba and ^{95}Zr values to ± 5%.

Logarithm fractionation plots of particles from high-yield air tests have been found to correlate well with $r_{140,89}$ and $r_{95,89}$ values from a coral-surface burst and three types of water bursts.

Barium-140 fissions have been found to correlate with between a square and a cubic relation to particle diameter. Zirconium-95 fissions have demonstrated a cubic relation to particle diameter.

REFERENCES

1. C. L. Carnahan, A Method for the Analysis of Complex Peaks Occurring in Gamma Ray Pulse Height Distributions, Report USNRDL-TR-572, U. S. Naval Radiological Defense Laboratory, July 1962.
2. Tracerlab, A Division of Laboratory for Electronics, Inc., The Analysis of Particulate Debris from Pacific Air Shots, Final Report, Dec. 16, 1964.
3. E. C. Freiling, Radionuclide Fractionation in Bomb Debris, *Science 133:* 1991 (1961).
4. P. A. Benson, Sixth Quarterly Progress Report to USAEC, Tracerlab, A Division of Laboratory for Electronics, Inc., Apr. 1, 1964. (Classified)

PREDICTION OF FALLOUT FROM SUBSURFACE NUCLEAR DETONATIONS

JOSEPH B. KNOX
University of California, Lawrence Radiation Laboratory,
Livermore, California

ABSTRACT

A numerical simulation model has been developed for the prediction of fallout from subsurface nuclear detonations that produce craters through spall and the action of the cavity gas. The physical processes modeled are atmospheric transport, lateral eddy diffusion, and gravitational sedimentation of radioactive particulates. This cratering fallout model is normalized to the observed external gamma-dose-rate fields of the Sedan (100 kt) and the Danny Boy (0.43 kt) cratering shots conducted at the Nevada Test Site. Calculations of the fallout patterns for additional shots, used for testing the prediction capability of the cratering fallout model, indicate that the model gives estimates of the external gamma dose rate at H + 1 hr with a maximum error of a factor of 2 to 3 in the gamma dose rate vs. distance along the hot line of the pattern.

INTRODUCTION

During the past few years, a small but continuing effort has been expended in developing a model for predicting fallout from subsurface nuclear detonations. In this report the experience in predicting fallout from surface bursts that is transferable to the construction of a fallout model for subsurface detonation is summarized, the development of the fallout model for subsurface nuclear detonations (the cratering fallout model) is described, the predictive capability of the model is illustrated by means of independent test cases, and some of the problems associated with the prediction of fallout from row-charge subsurface nuclear detonations are discussed. This paper is limited to research or development in which the investigator has been personally involved within the Plowshare Program of the Lawrence Radiation Laboratory.

CRATERING FALLOUT MODEL

Basis of Model Construction

For prediction of the area affected by radioactive fallout from a subsurface detonation of a nuclear explosive and of the gross external gamma dose rate in the surface-fallout pattern, knowledge of the following factors are needed:

1. The heights of the base, the top, and the radius of each radioactive cloud (i.e., the main cloud and the base surge) formed by the detonation at the time the clouds cease to rise in the atmosphere. This time is defined as the time of cloud stabilization. The cloud heights are prescribed in terms of height above surface zero.
2. The total yield of the explosive, W_T; the fission yield of the explosive, W_f; the depth of burial of the explosive, z; the fraction of the fission-product gamma emitters expected to appear in the fallout pattern beyond the estimated radius of direct ejecta, F_c; and the equivalent fission-yield gamma needed to simulate the gamma dose from induced activities.
3. The activity–particle size distribution in both the main cloud and the base surge and the fraction of F_c in each.
4. The terminal fall velocity of the fallout particles (in still air) as a function of particle size and height in the atmosphere.
5. The time and space prediction of the horizontal wind at the level of each cloud top along with the specification of the wind-shear tangential and normal to the wind for the layer through which particles fall. This knowledge is required because in a fallout calculation involving two clouds (main cloud and base surge), the calculation of the fallout pattern for each cloud is done separately. The total surface-fallout pattern of the shot is found by summing the patterns from the base surge and the main cloud.
6. The effect of horizontal eddy diffusion on the growth of the horizontal radius of the disks of radioactive particles as the disks fall earthward. The initial debris cloud is subdivided into disks of debris in the model as a function of initial height in the cloud and of particle size.

The preceding information (items 1 through 6) provides the simplest, but still adequate, basis for constructing a cratering fallout model. In addition to this information, it is assumed that the fission-product radioactivity is unfractionated and that 1 kt of unfractionated fission products spread uniformly over 1 sq mile corresponds to an (H + 1)-hr dose rate of 3380 r/hr at a height of 3 ft above an infinite plane.[1] This normalization constant of 3380 r/hr is corrected for terrain shielding by a factor of 0.8.

Certain atmospheric processes or effects have been neglected in developing the cratering fallout model, just as these same effects were neglected in developing the land surface-burst fallout model:[2]

1. The effect of synoptic-scale vertical motions on the vertical displacement of the falling disk of particles.
2. The effect of the mean divergence of the horizontal wind on the radius of the disk of falling particles during descent.
3. The effect of vertical eddy diffusion.
4. The time from detonation to cloud stabilization.
5. The development of subsynoptic-scale wind systems.
6. Changes in time and space of the shear tangential and normal to the horizontal wind at cloud-top level.
7. The effect of water products of condensation on the size and fall rate of radioactive particles.

Fraction of Gamma Activity in the Close-in Pattern

For calculation of the close-in fallout pattern from a subsurface detonation, the fraction of the gamma activity produced by the fission yield and appearing in the close-in fallout pattern, F_c, must be known. Thus far, experimental data from the Sedan, the Teapot ESS, the Jangle U, the Neptune, the Jangle S, and other surface-burst shots have provided a basis for estimating F_c. The measured fallout patterns from these shots have been integrated[3] from the radius of direct throwout to the limit of the measured pattern. The results are shown in Table 1.

These F_c calculations were performed by assuming a normalization constant of 3380 r/hr per kiloton of fission yield per square mile at H + 1 hr and a terrain shielding factor of 0.8. The graphical presentation of F_c as a function of z/W is shown in Fig. 1. In construction of the experimental F_c curve, the following asymptotes were used: (1) an

Table 1—EXPERIMENTAL DATA

Shot	W, kt	z, ft	F_c	Medium
Sedan	100	635	~0.10	Alluvium
Teapot ESS	1.2	67	0.46	Alluvium
Jangle U	1.2	17	0.64	Alluvium
Neptune	0.115	100	0.005	Tuff
Jangle S	1.2	0	0.50	Alluvium
Danny Boy	0.43	109	0.04	Basalt
Blanca	19	835	0.0005	Tuff

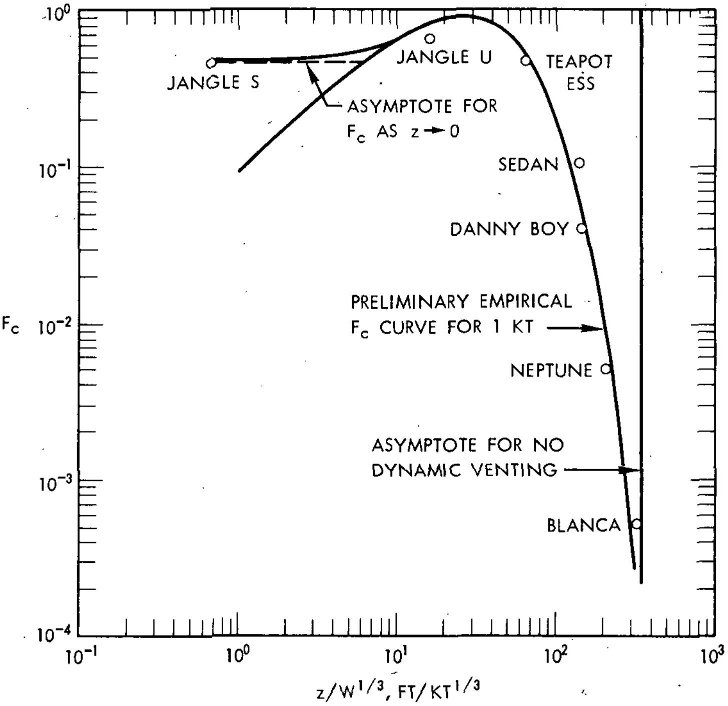

Fig. 1—Fraction of gamma activity appearing in the close-in fallout pattern.

asymptote of $F_c = 0.50$ for $z = 0$, suggested by the Jangle S data in Table 1 and supported by previous work,[4] and (2) an asymptote of no dynamic venting for $z/W^{1/3} = 330$ ft/kt$^{1/3}$, supported by experimental evidence[5] and by studies of containment physics.[6]

It should be noted that the value of F_c (estimated by pattern integration) for the Sedan shot departs considerably from the curve fitted to the whole sample of F_c data. This departure could arise because of an F_c yield dependency that is inadequately known at this time. In the absence of knowledge of such a dependency, F_c estimates made from the curve in Fig. 1 for high-yield cratering events (of the order of 100 kt and above) should be considered as uncertain by a factor of 2. It should be further stated that F_c estimates derived from Fig. 1 are made with the tacit assumption that the nuclear explosive is fully tamped and that no additives for fission-product gamma-radiation suppression have been placed around the explosive.

It should also be mentioned that the maximum value of F_c (0.75 at $z/W^{1/3} \approx 30$) occurs at very nearly the same value of $z/W^{1/3}$ as the maximum base-surge radius (crosswind) in a neutral atmosphere, reported in Ref. 7. The author believes that this coincidence of maximums at $z/W^{1/3} \approx 30$ is physically consistent.

Cloud Geometries

The geometrical definition of the top, the base, and the radius of both the main cloud and the base surge at the time of cloud stabilization is shown in Fig. 2. In addition to the definitions given in Fig. 2, the height of the base of the main cloud is defined as being equal to the height of the base-surge top, H_b, in the model.

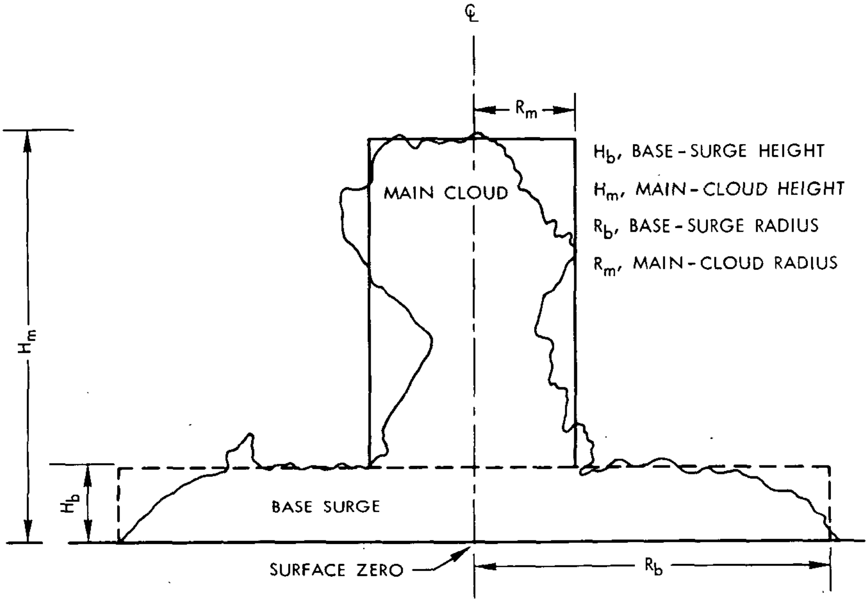

Fig. 2—Definition of cloud dimensions and symbols.

Evidence suggests that the geometry of these two clouds at the time of stabilization is a function of the total explosive yield, the material in which the detonation occurs, the depth of burial of the explosive, and the meteorological conditions existing during the development of the clouds.[7] At present, the cloud-geometry parameters (R_b, H_b, R_m, and H_m) must be evaluated experimentally as functions of total yield and depth of burial. Reasonable samples of experimental data exist for alluvium and basalt materials. Examples from one of the most useful summaries of cloud-geometry data for alluvium[8] are shown in Figs. 3b to 3g. (Figure 3a is a computational aid to the acquisition of input to Figs. 3b to 3g. In these figures, z denotes depth of burial and D_a denotes the depth of apparent crater.) This summary utilizes all the known

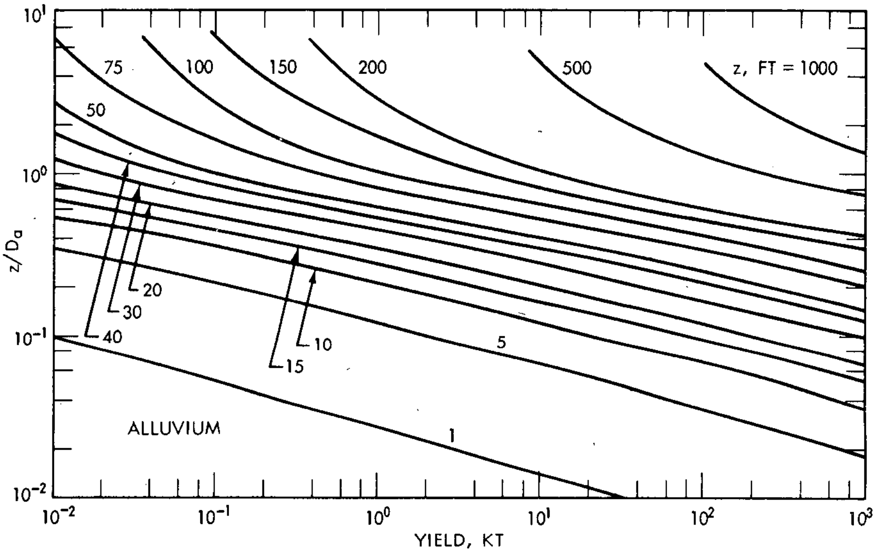

Fig. 3a—Computational aid to the acquisition of input data to the cloud-dimension graphs of Figs. 3b to 3g.

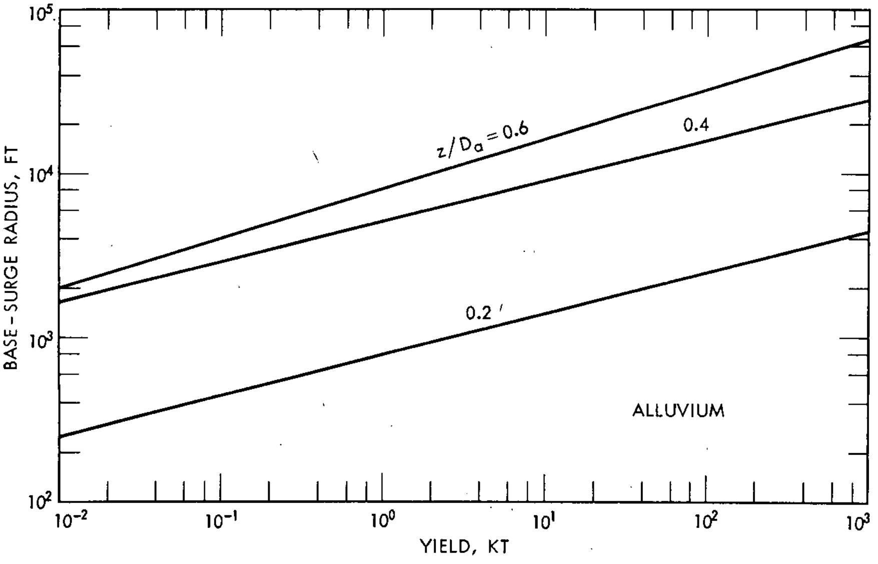

Fig. 3b—Base-surge radius as a function of the total yield and the parameter z/D_a.

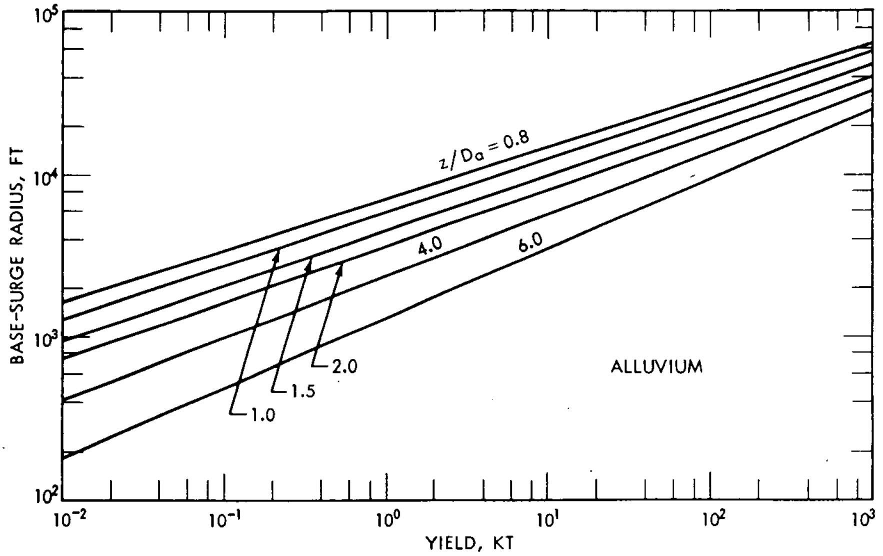

Fig. 3c—Base-surge radius as a function of the total yield and the parameter z/D_a.

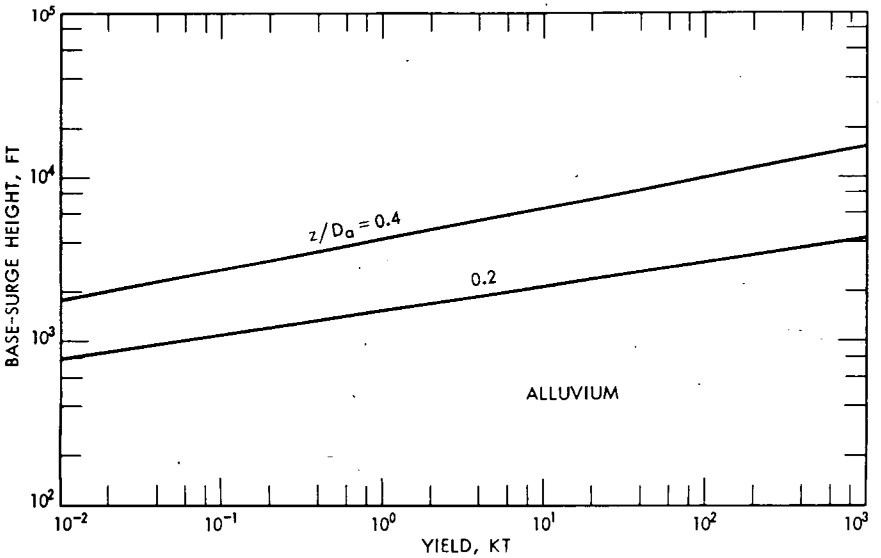

Fig. 3d—Base-surge height as a function of the total yield and the parameter z/D_a.

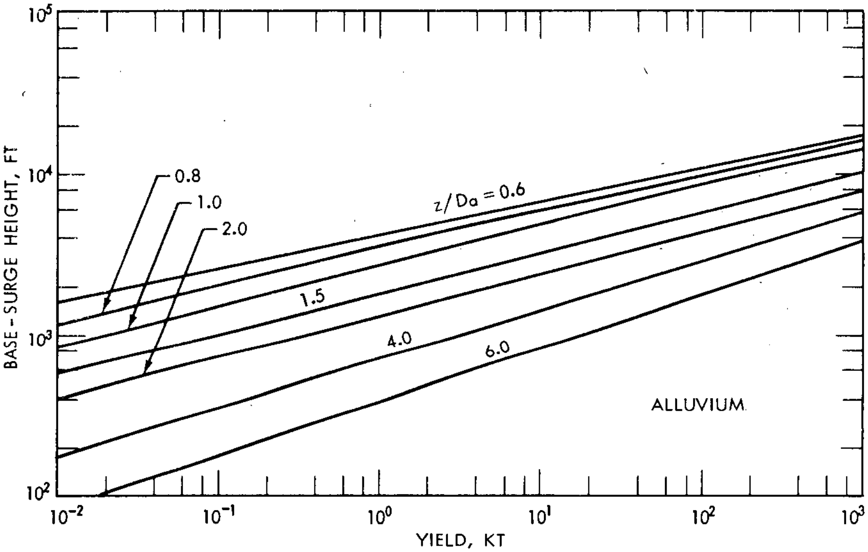

Fig. 3e—Base-surge height as a function of the total yield and the parameter z/D_a.

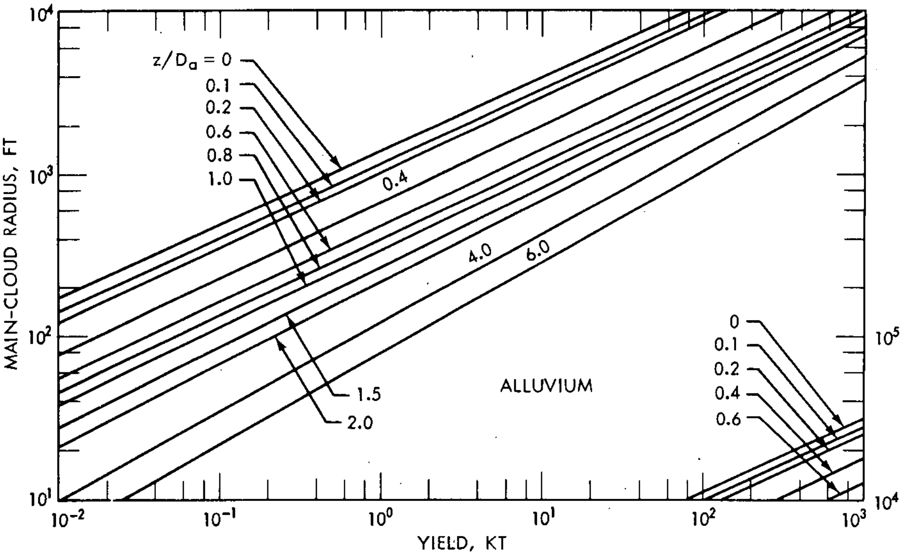

Fig. 3f—Main-cloud radius as a function of the total yield and the parameter z/D_a.

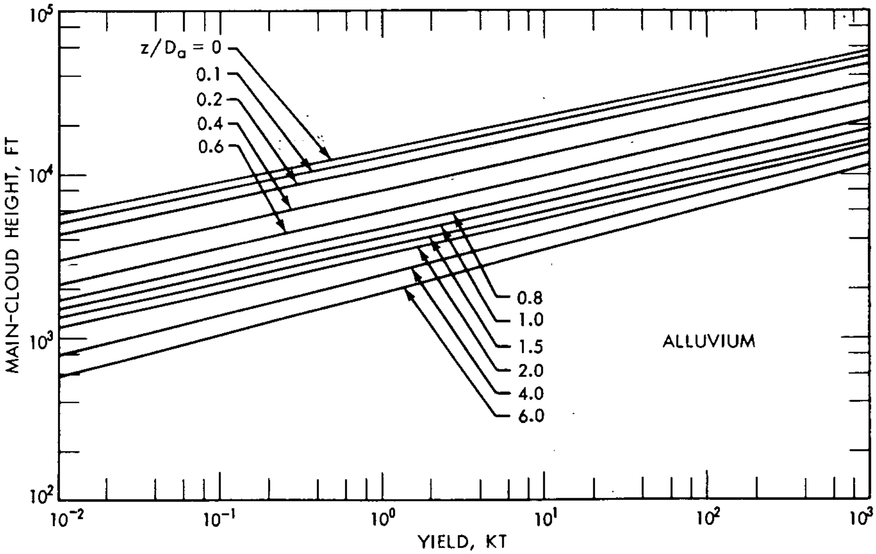

Fig. 3g—Main-cloud height as a function of the total yield and the parameter z/D_a.

cloud-geometry data from high-explosive and nuclear-explosive detonations conducted by the U. S. Atomic Energy Commission in alluvium and basalt. Implicit in the summary is the assumption that a high explosive and a nuclear explosive detonated in the same material at identical depths of burial and under similar meteorological conditions produce the same cloud geometries.

Activity–Particle Size Distributions

In a typical subsurface nuclear detonation in alluvium, two clouds are formed. The main cloud is composed mostly of vented cavity gas and particulates (originating from either condensation or injection and entrainment of soil). The base surge is composed of ejecta and suspended fine particulates. For a nuclear cratering shot in alluvium, it is assumed that 80% of the F_c gamma activity is in the main cloud and 20% is in the base surge. The 0.8 F_c main-cloud activity is assumed to be subdivided between two lognormal activity–particle size distributions. The first activity–particle size distribution contains the activity 0.8 $w_m(1)F_c$ and is characterized by the mean $\ln \bar{r}_m(1)$ and the standard deviation $\sigma_m(1)$. The second activity–particle size distribution contains the activity 0.2 $w_m(2)F_c$ and is characterized by the mean $\ln \bar{r}_m(2)$ and the standard deviation $\sigma_m(2)$. The activity of the first distribution is assumed to be homogeneously mixed through the whole main cloud, whereas that of the second distribution is assumed to be homogeneously mixed only in the lower fifth of the cloud. A similar prescription of activity–particle size is used for the base surge. Figure 4 summarizes the parameters governing the activity–particle size distributions in the two clouds at the time of cloud stabilization. These parameters governing the activity–particle size distributions in the cratering fallout model have been determined by mathematical experimentation with the model in the re-creation of the observed fallout patterns for the Sedan and the Danny Boy shots. Results of these calibration calculations will be discussed in a later section.

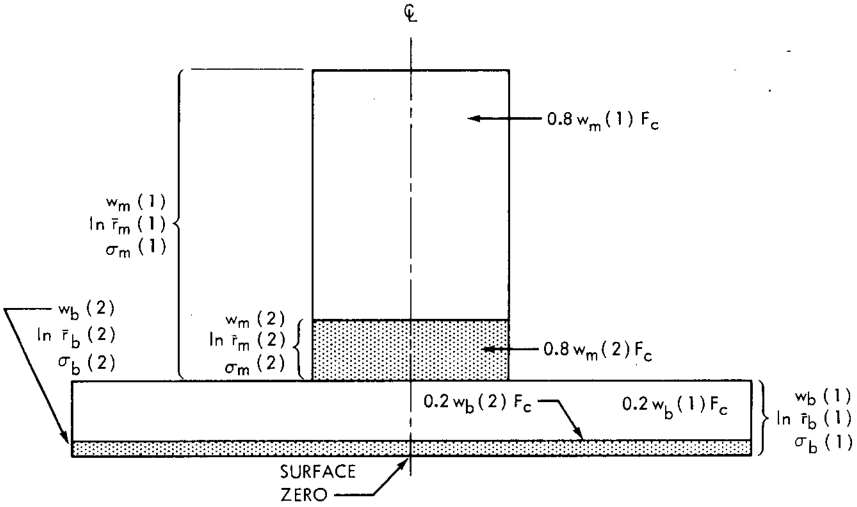

Fig. 4—Schematic drawing of an idealized cloud from a subsurface detonation showing spatial relations of the activity–particle size distribution assumed in the model.

Terminal Fall Velocity of Fallout Particles

The vertical fall velocities of the fallout particles are modeled as the terminal fall velocities of smooth spheres of density 2.5 g/cm^3 in an International Civil Aeronautical Organization standard atmosphere as computed by McDonald[9] for both the Stokes'-law region and the aerodynamic region (wherein the Reynolds number exceeds 1). If some fallout particles are a cluster of small spheres attached to a large central particle, these complex particles are assumed to fall with the speed of the equivalent smooth spherical particle of the same mass. Experimental evidence has been obtained by Rapp and Sartor[10] to support this assumption.

Specification of the Horizontal Wind Field for the Model

The horizontal wind field that transports the debris-disk centroids during their fall to the earth's surface may be specified in two ways in the cratering fallout model:

1. Idealized Wind Hodograph. If H denotes height above surface zero, then the horizontal wind, $\underset{\sim}{v}_h$, at height H for a simple wind hodograph (see Fig. 5) is

$$\underset{\sim}{v}_h(H) = \underset{\sim}{v}_h(H_m)\,\frac{A(p)}{A(p_m)} - S(H_m - H)\underset{\sim}{n}$$

where $\underset{\sim}{v}_h(H_m)$ = steady-state wind at cloud-top level H_m (or it can be specified as a function of time and space in either wind component form or by means of a stream function)

$A(p)$ = wind-shear component tangential to the horizontal wind at cloud-top level and is evaluated from shot-time winds in a diagnostic fallout calculation or from preshot wind information for a predictive fallout calculation (it is held constant in time for the period of fallout deposition)

$A(p_m)$ = value of A(p) at cloud-top level (normally it is set equal to 1)

S = wind-shear component normal to the horizontal wind at cloud-top level (it is evaluated from shot-time winds or preshot wind information, depending on the purpose of the fallout calculation, and is held constant in time)

$\underset{\sim}{n}$ = unit vector normal to $\underset{\sim}{v}_h(H_m)$ in a right-handed system

p = atmospheric pressure corresponding to H

2. Arbitrary Hodograph. The horizontal wind can be specified in wind-component form for as fine a vertical interval as desired or for which wind information exists.

Debris-disk Radius as a Function of Time

For estimation of the radius of a debris disk expanding by horizontal eddy diffusion during its fall to earth, it is proposed that the disk radius as a function of time $R_e(t)$ be represented by

$$R_e(t) = (R_{e,0} + 2Dt')^{1/2}$$

where t' is the distance traveled by the disk centroid divided by the mean horizontal wind speed in the layer through which the disk has settled, $R_{e,0}$ is the debris-disk radius at time of stabilization, and D is the horizontal eddy-diffusion coefficient.[2] The diffusion coefficient D is estimated as the Richardson's diffusion coefficient $0.2 \times \ell^{4/3}$, where

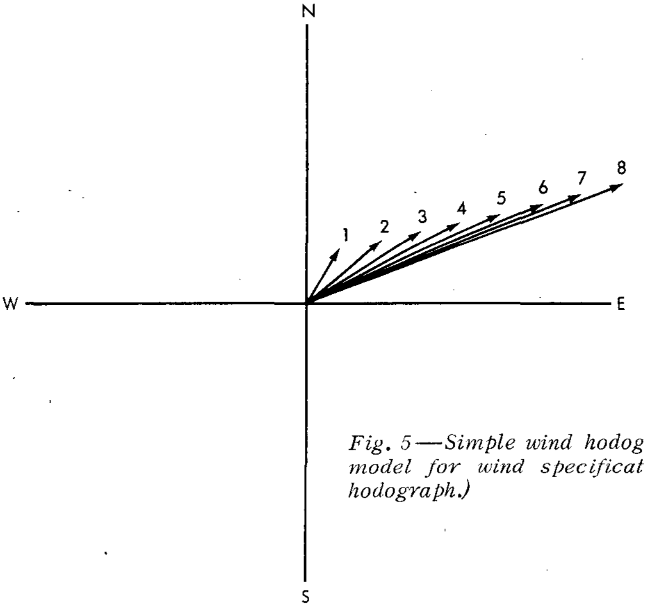

Fig. 5—Simple wind hodograph assumed in the model for wind specification. (Idealized wind hodograph.)

ℓ is the standard deviation of the position of the particles (in the disk) from the disk centroid. Since ℓ is poorly known in nuclear-debris clouds, it is usually set equal to $R_{e,0}$ or $2R_{e,0}$ if accelerated relative diffusion is to be approximated in the fallout model.

Physical Processes Simulated in the Model

The principal physical or meteorological processes simulated by the cratering fallout model are (1) the transport of the debris disks by the mean wind in the layer through which the disks are falling, (2) the relative advection of the debris disks by the horizontal wind field containing both a speed and a directional shear, and (3) the lateral eddy diffusion, which expands the disks falling earthward.

The first two processes are simulated by calculating the transport of the disk centroids by the ambient horizontal wind field during the disk's earthward fall until the disk centroid is on the ground surface by using either the idealized wind hodograph or the arbitrary hodograph for the horizontal wind specification. The result of this calculation is the position vector from surface zero to the predicted ground position of each disk centroid and the time of arrival at the ground surface of each disk. The lateral eddy-diffusion process is modeled by the expression for $R_e(t)$ which estimates the debris-disk radius at the time of arrival of the disk centroid on the ground surface.

The debris disks tracked earthward are defined as follows: In each cloud (main cloud and base surge), 11 disks of particle size r_I are defined at each isobaric surface p_p such that

$$\ln r_I = \ln r_L - \frac{I}{10} (\ln r_L - \ln r_s)$$

where I is equal to 0, 1, 2, ..., 10; r_L is the radius of the largest particle modeled in the cloud; and r_s is the radius of the smallest particle modeled in the cloud. The term p_p is equal to $p_B - [P/10(p_B - p_m)]$, where P is equal to 0, 1, 2, ..., 10; p_B is the pressure at the base of the cloud at the time of cloud stabilization; and p_m is the pressure at the top of the cloud at the time of cloud stabilization.

The (H + 1)-hr external gamma dose rate (for a height 3 ft above an infinite plane) is calculated by using the method of Batten, Iglehart, and Rapp[11] modified to account for the effect of normal shear and lateral eddy-diffusive disk growth.

The following quantities are calculated in the model and are output in the indicated modes:*

	Printout	Cathode-ray-tube display
Position of surface zero		x
(H + 1)-hr dose rate at the predicted ground position of each disk centroid for each cloud	x	
Predicted ground position of each disk centroid for each cloud	x	x
Envelope containing the area affected by the fallout from each cloud		x
Time of beginning and end of fallout deposition at each ground-position centroid for each cloud	x	
Isopleths of the (H + 1)-hr dose rate for any specified interval of dose rate (each contributing cloud and total pattern)		x
(H + 1)-hr dose rate as a function of distance along the hot line (each cloud and total pattern)		x

DIAGNOSTIC CALCULATION FOR SEDAN

For calibration of the cratering fallout model on the Sedan shot, the observed shot-time winds, the observed cloud geometry of the main cloud and the base surge, the estimated $F_c = 10\%$, and the appropriate fission yield were input to the model. A first guess of the 12 activity–particle size parameters, to be discussed later, was also input to the

---

*About 0.25 min of IBM 7094 computer time is required for the calculations for a two-cloud nuclear-cratering fallout problem, and 2.4 min of Livermore Advanced Research Computer time is required for the cathode-ray-tube displays indicated above.

model. The main cloud was assumed to contain 80% of F_c; the base surge, 20%. The parameters governing the activity–particle size distributions have been determined from the observed Sedan gross gamma fallout pattern by mathematical experimentation. The values of these parameters are as follows:

$$w_m(1) = w_b(1) = 0.9$$

$$w_m(2) = w_b(2) = 0.1$$

$$\ln \bar{r}_m(1) = \ln \bar{r}_b(1) = 2.9$$

$$\ln \bar{r}_m(2) = \ln \bar{r}_b(2) = 5.0$$

$$\sigma_m(1) = \sigma_b(1) = 0.69$$

$$\sigma_m(2) = \sigma_b(2) = 0.59$$

Figure 6 shows the calculated and the observed gamma dose rate* at H + 1 hr from fission products vs. distance along the hot line for the Sedan shot.

DIAGNOSTIC CALCULATION FOR DANNY BOY

The Danny Boy shot was a 0.42-kt nuclear cratering detonation emplaced at a depth of 109 ft in dry basalt. The observed gamma fallout pattern for Danny Boy has been published.[4] By mathematical experimentation with the cratering fallout model, the activity–particle size distribution parameters can be adjusted to duplicate the observed Danny Boy fallout pattern. In this shot no visible main cloud was observed.[4] Thus, in the diagnostic calculation with the cratering fallout model, it is assumed that 100% of the F_c gamma activity is in the base surge and that there is a preliminary value of 0.05 for F_c. The activity–particle size distribution parameters determined in this calculation are given below:

$$w_b(1) = 0.9$$

$$w_b(2) = 0.1$$

$$\ln \bar{r}_b(1) = 3.0$$

$$\ln \bar{r}_b(2) = 5.7$$

$$\sigma_b(1) = 0.69$$

$$\sigma_b(2) = 0.59$$

---

*The observed (H + 1)-hr gamma dose rate for fission products derived from the observed total gamma dose rate at H + 24 hr, assuming that 52% of the (H + 24)-hr gamma dose rate was from tungsten.[12]

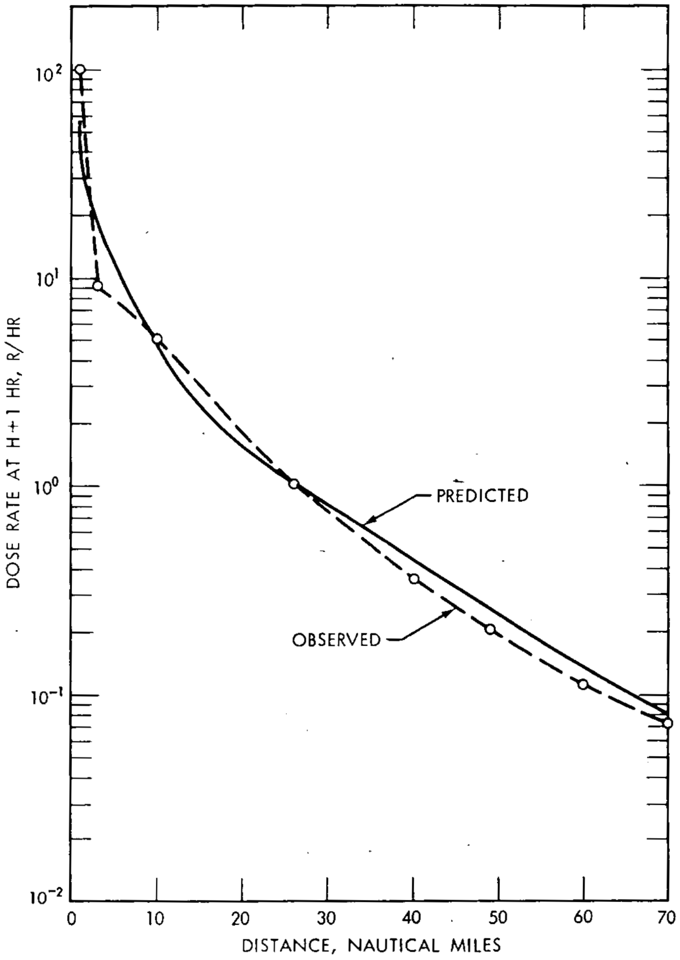

Fig. 6—The calculated and observed gamma dose rate at H + 1 hr as a function of distance along the hot line of the Sedan pattern (diagnostic calculation).

Figure 7 shows the calculated (H + 1)-hr dose rate vs. distance curve from the model, and the observed (H + 1)-hr dose rate vs. distance. As was previously mentioned, the value of F_c used in the cratering-fallout-model calculation was 0.05. If a value of 0.04 for F_c (as reported in Ref. 4) had been used, the agreement between the calculated (H + 1)-hr dose rate and the observed (H + 1)-hr dose rate vs. distance would have been better than shown in Fig. 7.

Recently effort has been expended to obtain machine capability of plotting the calculated (H + 1)-hr dose-rate patterns for an arbitrarily selected interval of dose rate. Figure 8 shows the machine-plotted dose-rate pattern for the Danny Boy diagnostic calculation. The computer-

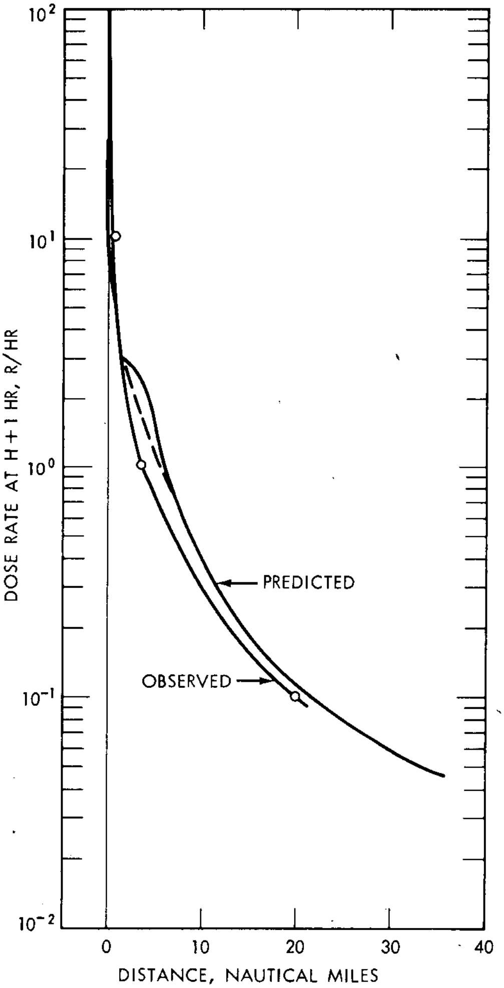

Fig. 7—The calculated and observed gamma dose rate at H + 1 hr as a function of distance along the hot line of the Danny Boy pattern (diagnostic calculation).

pattern breadth at 25 miles downwind is about 7 miles; the observed-pattern breadth at 25 miles downwind is 5.5 miles. It should be noted that the closure of the isodose-rate line of 10^{-4} r/hr at H + 1 hr in the plotted pattern is artificial and is the result of the logic used for the computer plotting rather than of the logic used for the cratering fallout model. All isodose-rate lines will apparently be closed at the downwind edge of the pattern if computed dose-rate information is insufficient for their appropriate extension downwind. The observed (H + 1)-hr gamma-dose-rate pattern for Danny Boy is shown in Fig. 9 for comparison with the computer-plotted pattern.

INDEPENDENT TESTS OF THE MODEL

An independent test calculation of the cratering fallout model (calibrated on Sedan) was performed by using data from the Teapot ESS

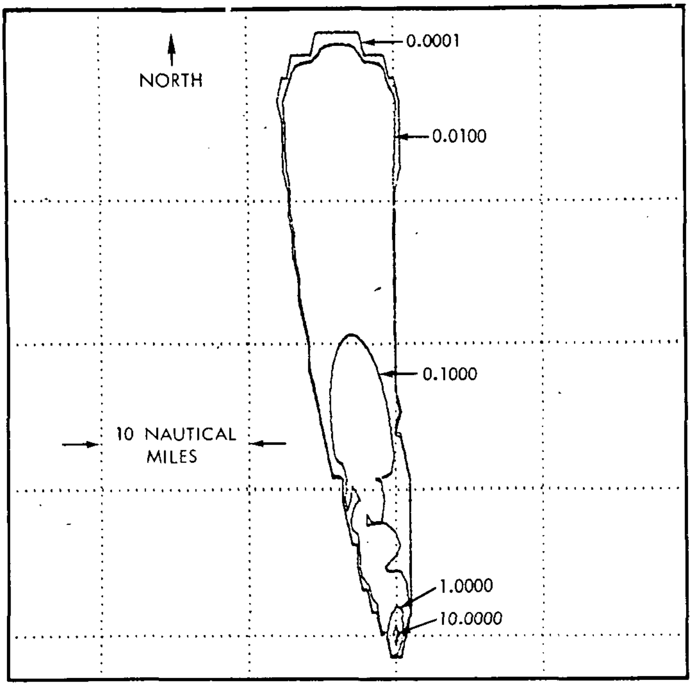

Fig. 8—The machine-plotted (H + 1)-hr gamma-dose-rate pattern for the Danny Boy shot (diagnostic calculation), roentgens per hour.

shot. The observed winds at shot time, the observed cloud geometry, the published fission yield of 1.2 kt, and a value of 0.85 (an early preliminary value) for F_c were input to the model. Figure 10 shows the calculated and the observed (H + 1)-hr gamma dose rate as a function of distance along the hot line of the pattern. A comparison of these two dose rate vs. distance curves shows that the largest error between calculation and observation is of the order of a factor of 2.5. An examination of the radiosonde observation near shot time at the Nevada Test Site indicates that the vertical temperature distribution of the layer through which the particles were falling was slightly superadiabatic. Under such conditions, it is possible that the vertical eddy diffusion on the day of the Teapot ESS shot was larger than average. If enhanced vertical eddy diffusion were operative, the dose rate would have been slightly less near ground zero and would have been enhanced downwind.

Other model confirmation tests have been performed. These include calculations with the surface-burst version of the model on the Apple II and the Zucchini shots[2] and on several other atmospheric shots for which the data are still classified. The results of these additional tests were satisfactory.

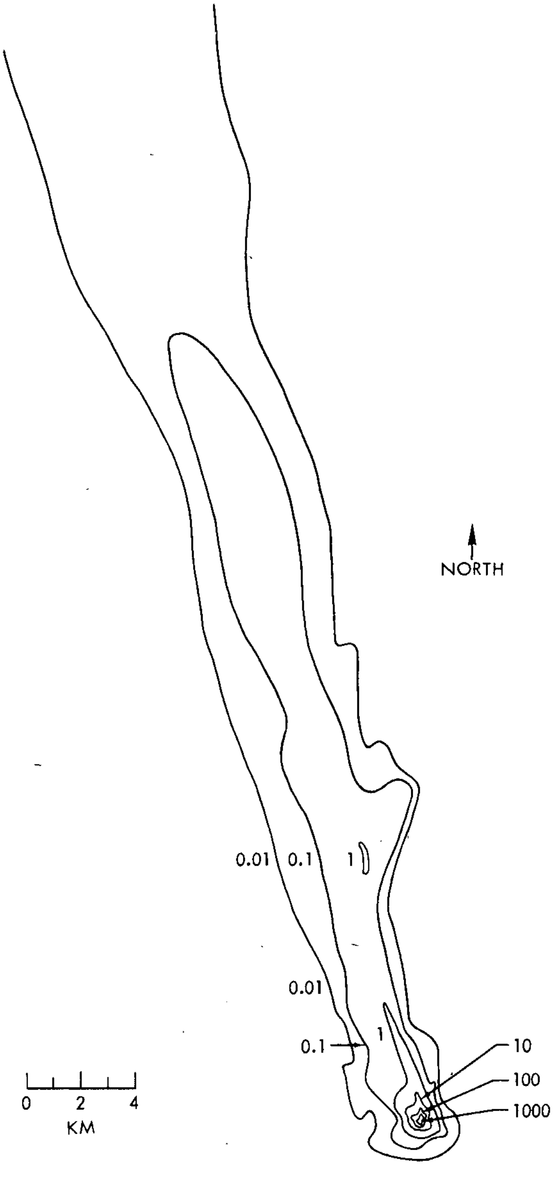

Fig. 9—Preliminary gamma-isodose-rate contours observed at H + 1 hr.[4] *Readings in roentgens per hour minus H + 1 hr. Data taken from Nuclear Defense Laboratory ground surveys (close in); Edgerton, Germeshausen & Grier, Inc., aerial surveys (intermediate range); and U.S. Geological Survey aerial survey (long range).*

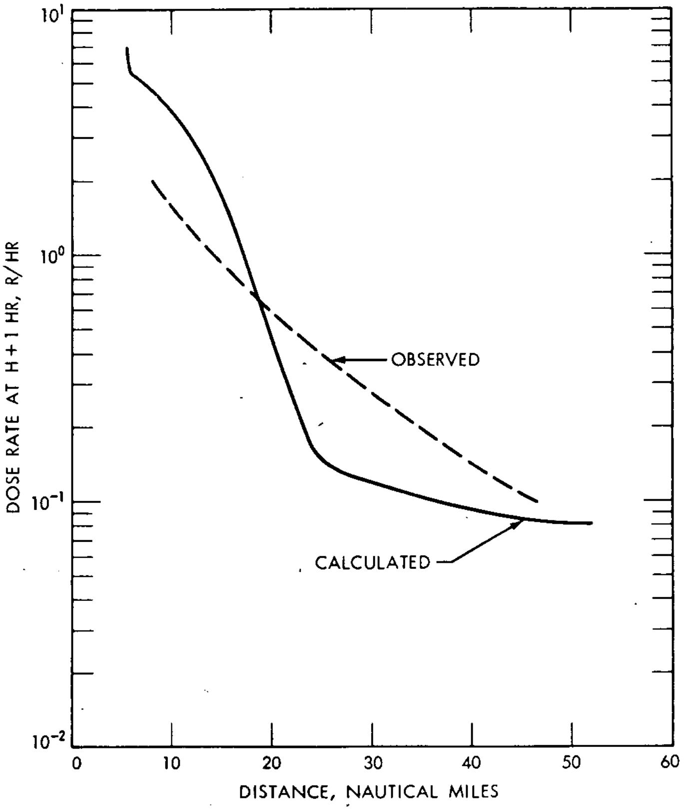

Fig. 10—The calculated and the observed gamma dose rates at H + 1 hr as a function of distance along the hot line of the pattern (predictive calculation) from the Teapot ESS shot.

PREDICTION OF FALLOUT FROM ROW-CHARGE SHOTS

In principle, the fallout pattern from a row of subsurface nuclear detonations may be estimated with the cratering fallout model, provided the model input parameters are adequately known for row-charge events. In the current state of knowledge, the cloud-geometry input parameters and the value of F_c appear to be the most difficult to specify. Study of time-lapse photography of the main-cloud and the base-surge evolution from past high-explosive row-charge tests give significant experimental information on the cloud-geometry parameters. For example, empirical methods of predicting crosswind radius and height of the base surges originating from high-explosive row-charge shots have been studied.[7] In this study it was shown that for five equal-weight charges, equally spaced and emplaced at the same depth of burial, the resulting base surge has approximately the same radius as the base surge from a large single shot of the same total yield and emplaced at the same scaled depth. The base-surge height for a five-charge row shot is reasonably well approximated by scaling the height of the base surge for a single-charge event by the 0.2 power of the total yield of the row-charge shot.

A first approximation to the geometries of the individual main cloud may be obtained by treating each main cloud independently and estimating the top and the radius of each cloud from the work of Day.[8] Examination of the high-explosive row-charge documentary photographs of the Rowboat, the Dugout, and the Pre-Buggy shots indicates that such an approximation is reasonable. This approximation can, of course, be in error if main-cloud interactions occur. There is a need to evaluate the uncertainty in fallout prediction for multiple-charge shots in cases where cloud interactions lead to the injection of radioactivity at levels higher in the atmosphere than predicted.

Concerning the F_c for row-charge shots, preliminary experimental results for high-explosive single- and row-charge shots have been reported previously.[13] In this study, results of the measured vented fraction of ^{140}La tracer from single- and row-charge high-explosive shots were given. The experimental evidence suggests that the vented fraction from row-charge shots may be about twice that from single-charge shots. One of the most pressing needs for fallout prediction from row-charge shots is the establishment, through either experiment or theory, of the dependency of the F_c on yield, depth of burial, or charge spacing.

The development of computer aids for the row-charge fallout-prediction problem, however, can proceed independently of the solution of the two previously cited problems: (1) the specification of initial cloud geometry and (2) the specification of F_c. Therefore the capability of plotting fallout patterns for multicloud and/or multidetonation events has been developed. Figures 11 and 12 show, respectively, the (H + 1)-hr dose-rate patterns computed for 10 Danny Boy detonations on an east to west line with charge centers separated by 33.5 m and for 10 Danny Boy detonations on a north to south line with charge centers separated by 33.5 m. For the purpose of these calculations, each detonation is assumed to vent 5% (e.g., $F_c = 0.05$), each cloud is assumed to be the same as that for Danny Boy, and the input wind for each cloud fallout problem is assumed to be the same as the shot-time wind for Danny Boy. These two row-charge fallout patterns, although detectably different as determined from the printout, appear to be very similar. Calculational results suggest that the fallout pattern from a small-scale row-charge shot is not sensitive to the orientation of the wind to the alignment of the charges.

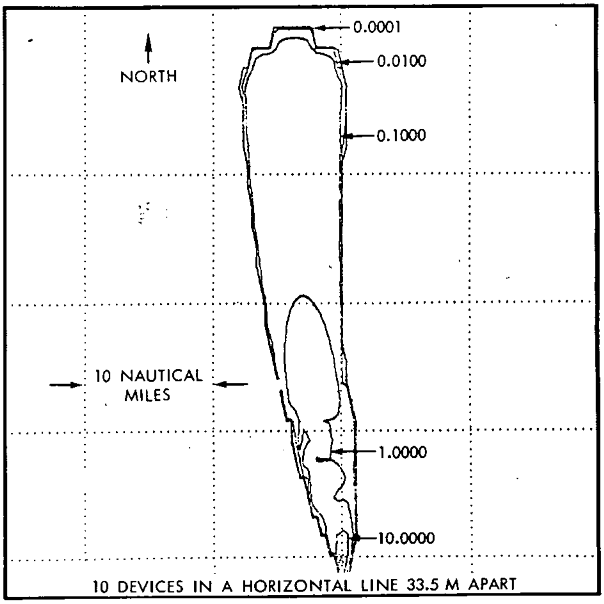

Fig. 11—The (H + 1)-hr gamma-dose-rate pattern computed for 10 Danny Boy detonations on an east to west line with charge centers separated by 33.5 m. Values are in roentgens per hour.

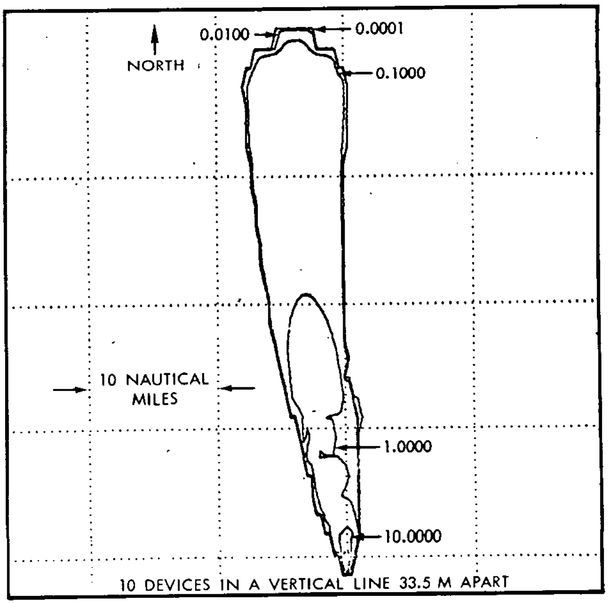

Fig. 12—The (H + 1)-hr gamma-dose-rate pattern computed for 10 Danny Boy detonations on a north to south line with charge centers separated by 33.5 m. Values are in roentgens per hour.

CONCLUSIONS

In conclusion, it may be stated that the cratering fallout model developed gives reasonable results for the prediction of the area of the pattern, the geometry of the dose-rate contours, and the (H + 1)-hr dose rate vs. distance along the hot line. The independent testing of the model should be extended to include more than the Teapot ESS case described and the several others cited.

Meteorological improvements in the cratering fallout model could well include the following items:

1. The prediction of synoptic-scale changes in the normal- and tangential-shear components.
2. A better understanding of the growth of the debris disks through horizontal eddy diffusion during their earthward fall.
3. The prediction of diurnal change of wind at low levels and close to ground zero.
4. The inclusion of the effects of topography on the evolution of the horizontal wind field.
5. The effect of terrain-induced circulations on fallout deposition.
6. A better solution to the cloud-rise problem for cratering detonations.

Before embarking on the development of these meteorological improvements in fallout predictions, however, one must consider potential improvements that may come from other areas. Areas of promise are cratering physics and filtration theory for the vented-fraction problem, special emplacement for control of vented fraction, and improvement of nuclear explosives.

ACKNOWLEDGMENTS

The author wishes to acknowledge the interest often expressed by Gary Higgins and the late A. Vay Shelton in the work herein reported, as well as programming support given by Mrs. Leota Barr and Roger Fulton.

REFERENCES

1. G. H. Higgins, Calculation of Radiation Fields from Fallout, USAEC Report UCID-4539, University of California Lawrence Radiation Laboratory, Jan. 25, 1963.
2. J. B. Knox, The Prediction of Wind and Fallout, USAEC Report UCID-4662, University of California Lawrence Radiation Laboratory, November 1962.
3. M. M. Williamson, private communication, 1964.
4. M. D. Nordyke and W. Wray, Cratering and Radioactivity Results from a Nuclear Cratering Detonation in Basalt, *J. Geophys. Res.*, *69*(4): 675-689 (1964).
5. G. H. Higgins, University of California Lawrence Radiation Laboratory, private communication, 1964.

6. J. B. Knox, University of California Lawrence Radiation Laboratory, unpublished data, 1963.
7. J. B. Knox and R. Rohrer, Project Pre-Buggy. Base Surge Analysis, USAEC Report PNE-304, University of California Lawrence Radiation Laboratory, Sept. 1, 1963.
8. W. Day, University of California Lawrence Radiation Laboratory, private communication, 1964.
9. J. D. McDonald, Rates of Descent of Fallout Particles from Thermonuclear Explosions, *J. Meteorol., 17:* 380-381 (1960).
10. R. R. Rapp and J. D. Sartor, Rate of Fall Through the Atmosphere of Irregularly Shaped Particles, Report RM-2006, RAND Corporation, Nov. 1, 1957.
11. E. S. Batten, D. L. Iglehart, and R. R. Rapp, Derivation of Two Simple Methods for the Computation of Radioactive Fallout, Report RM-2460, RAND Corporation, Feb. 18, 1960.
12. J. B. Knox, Status Report on Cratering Fallout Models, USAEC Report UCID-4663, University of California Lawrence Radiation Laboratory, Jan. 30, 1963.
13. E. Graves, W. R. Wray, and R. B. Pierce, Scope of Chemical Explosive Cratering Experiment, USAEC Report PNE-300, University of California Lawrence Radiation Laboratory, May 15, 1963.

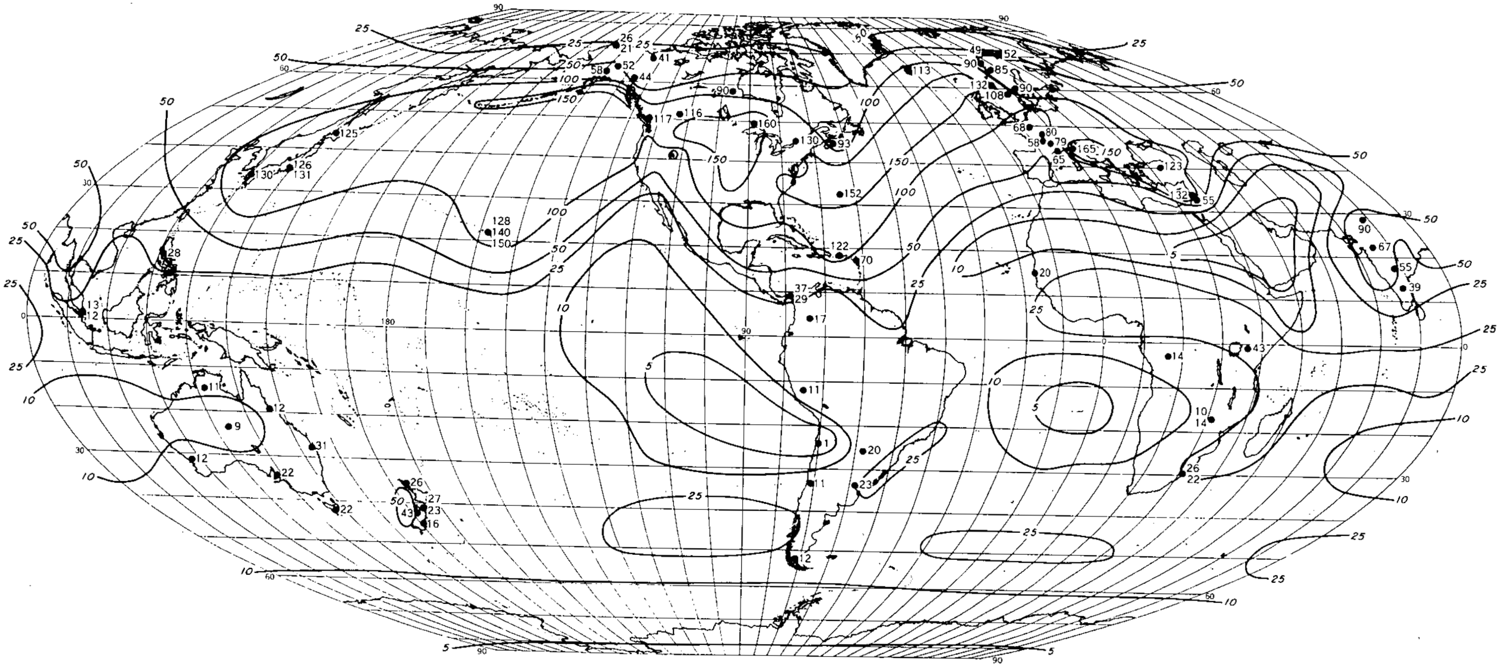

Fig. 5—Strontium-90 in soil determined from the 1963 and early 1964 survey, millicuries per square mile. Isolines are based on observed data and mean precipitation patterns.

DISTRIBUTION OF RADIOACTIVITY WITH HEIGHT IN NUCLEAR CLOUDS

GILBERT J. FERBER
U. S. Weather Bureau, Washington, D. C.

ABSTRACT

During Operation Dominic I at Christmas Island in 1962, aircraft sampling of nuclear clouds was done soon after cloud stabilization to investigate the amount of radioactive debris that stabilizes in the troposphere and its distribution with height. The detonations studied were all air bursts over water. Some data for surface bursts obtained during Operation Redwing in 1956 are used for comparison. Results indicate that for air bursts less than 1% of the total radioactivity is present in the stem of the nuclear cloud. It is estimated that about one-third of the total debris from the Christmas Island clouds initially stabilized in the troposphere.

Project Stemwinder has shown that in-cloud dose-rate monitoring by aircraft is a relatively simple and economical way to obtain information on the distribution of radioactive debris in a nuclear cloud. Used in conjunction with limited radiochemical analysis of samples, this type of monitoring could produce a reliable inventory of the debris in a nuclear cloud.

INTRODUCTION

The objective of Project Stemwinder was to probe and sample nuclear clouds as soon as possible after cloud stabilization to investigate the amount of radioactive debris that stabilizes in the troposphere and its distribution with height. Sampling was done with RB-57 aircraft of the 1211th Test Squadron under the scientific direction of the Atmospheric Radioactivity Research Branch, U. S. Weather Bureau.

The detonations investigated were all air bursts over water during Operation Dominic I at Christmas Island in 1962. Some data for surface detonations obtained by aircraft sampling during Operation Redwing in 1956 are used to compare with the Project Stemwinder data.

The project was conceived as an attempt to utilize available sampling aircraft to narrow the area of uncertainty involved in two related problems. The first problem was concerned with the operational need for prediction of the possible local hazards due to rainout of radioactive debris from a portion of a nuclear cloud that might pass over Christmas Island shortly after an air burst. Since the tops of rain clouds in the Christmas Island area were generally below 20,000 ft. and often below 10,000 ft, the amount and distribution of activity in the stem of the mushroom cloud was of primary concern. The second problem was concerned with the partitioning of nuclear debris between the stratosphere and the troposphere as a function of nuclear yield, tropopause height, burst height, and, possibly, other factors. Such partitioning has been an important consideration in estimating the long-range fallout from nuclear tests since nuclear debris has a mean residence time of several weeks in the troposphere (intermediate fallout) as opposed to many months or years in the stratosphere (worldwide fallout), depending on the latitude and altitude of injection. The fraction of the debris which remains in the troposphere may be particularly important in considering the possible hazards from relatively short-lived nuclides such as ^{131}I since the stratospheric portion usually decays to insignificant amounts before it can return to the surface of the earth.

It is emphasized that the preceding remarks apply only to the very small particles that contribute to the intermediate and the worldwide fallout. In the case of surface detonations, much of the radioactivity is associated with relatively large particles that comprise the local fallout. These large particles are not affected by the tropopause and appear in the local fallout regardless of whether they are initially injected into the troposphere or into the stratosphere.

CLOUD HEIGHTS OF AIR BURSTS IN A TROPICAL ATMOSPHERE

Operation Dominic I shot data (including those for yield, burst height, and cloud-top, base, and tropopause heights) are given in the Project Stemwinder final report.[1] Since there was no scientific program to document cloud heights, a "best guess" was made for each cloud by evaluating estimates made by observers on the ground and in the sampling aircraft and by using the dose rates reported at the various sampling altitudes to verify, where possible, the visual observations. Variations in the burst heights did not appear to have any consistent effect on the cloud heights. Evidently, the effect of the burst height was masked by the influence of meteorological factors and/or the errors in the cloud-height estimates.

Selected data[2] were added from other Pacific test series to aid in drawing the mean curve and the curves for the estimated range of cloud heights (see Fig. 1). Almost all the detonations in previous U. S. tests in the Pacific had been surface bursts, and the documentation of nuclear cloud dimensions had been generally poor. The curves shown in Fig. 1 are intended to be valid only for air bursts in a tropical atmosphere and for burst heights less than about 15% of the expected cloud-top heights. For this purpose, an air burst may be defined as a detonation at an altitude equal to or greater than $180Y^{0.4}$, where Y is the total yield in kilotons. It is emphasized that there are no reliable cloud-top data for yields greater than about 5 Mt, and the extrapolation of the curves beyond this point represents little more than an educated guess. Indeed, over the entire range of yields shown in Fig. 1, the dashed curves indicate only the expected range of cloud heights for the stated conditions and should not be interpreted as representing absolute limits.

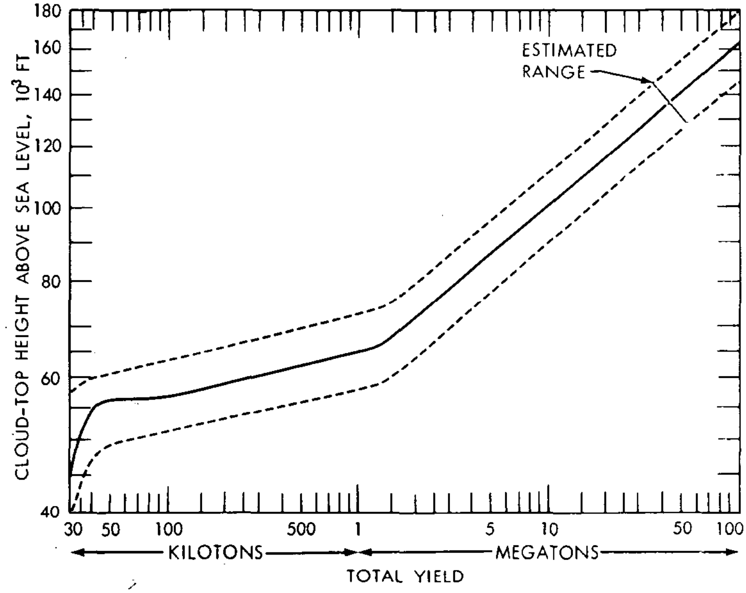

Fig. 1—Cloud-top heights and estimated range for air bursts ($180Y^{0.4}$ < burst height < $0.15\ H_T$) in a tropical atmosphere.

STEM-CLOUD PENETRATIONS

An RB-57 aircraft was available for stem-penetration missions immediately following seven of the Dominic I detonations. The navigator was provided with a dose rate meter with a range from 0.01 to 2000 mr/hr and was instructed to record the dose rate as the aircraft penetrated the stem cloud at specified altitudes. The dose rates measured in the cockpit were then used to estimate the amount of activity in the cloud.

The relation between cloud concentration and dose rate in a uniform infinite cloud[3] is given by

$$C = \frac{D\rho}{\rho_0} \frac{84\rho_0}{(3.7 \times 10^4)(1.6 \times 10^{-6})E} \tag{1}$$

where C = cloud concentration, $\mu c/cm^3$
D = dose-rate, r/sec
ρ_0 = standard density of air at sea level = 1.293×10^{-3} g/cm^3
ρ = density of air at sampling altitude, g/cm^3
E = average gamma energy, Mev
84 = energy absorbed per roentgen, ergs per gram of air
1.6×10^{-6} = ergs/Mev
3.7×10^4 = dis/sec per microcurie

If the unit of dose rate is converted to roentgens per hour and the concentration to megacuries per cubic mile,

$$C = 2.1 \frac{\rho}{\rho_0} \frac{D}{E} \tag{2}$$

For stem penetrations within an hour after the burst, E was assumed to be 1 Mev. For the sampling missions between 2 and 5 hr after the burst, a value of 0.86 Mev was used.[4] Figure 2 gives the value of ρ/ρ_0 as a function of altitude for a typical tropical atmosphere.[5] With the use of appropriate values for E and ρ/ρ_0 in Eq. 2, the dose rates recorded during stem penetration were converted to cloud concentrations. An estimate of the stem diameter was then used to estimate the total volume of cloud in a 1000-ft-thick layer. The total amount of activity in the layer and the fraction of the bomb represented by that activity was then determined by multiplying the concentration by the volume. The results are shown in Fig. 3 as a plot of the fraction of the bomb present in a 1000-ft-thick layer of the stem cloud vs. height (indicated as percent of the total stem height). The three highest Dominic I data points are derived from the extended sampling missions described later in this paper. The Redwing data used for the figure

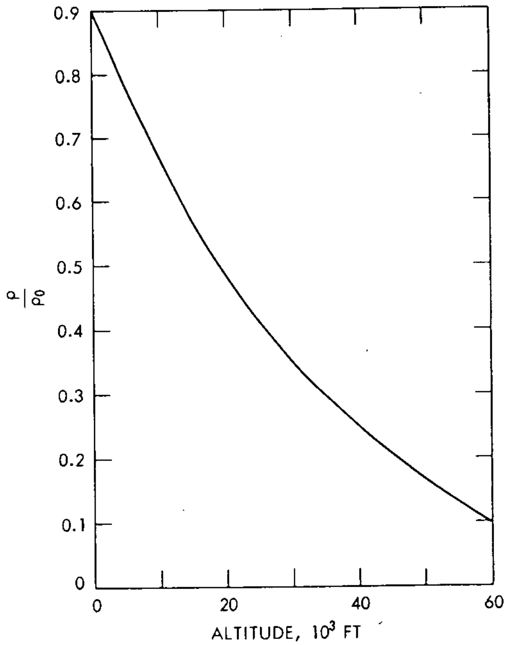

Fig. 2—Ratio of air density (ρ) to standard sea-level air density ($\rho_0{}' = 1.293 \times 10^{-3}$ g/cm^3) as a function of altitude.

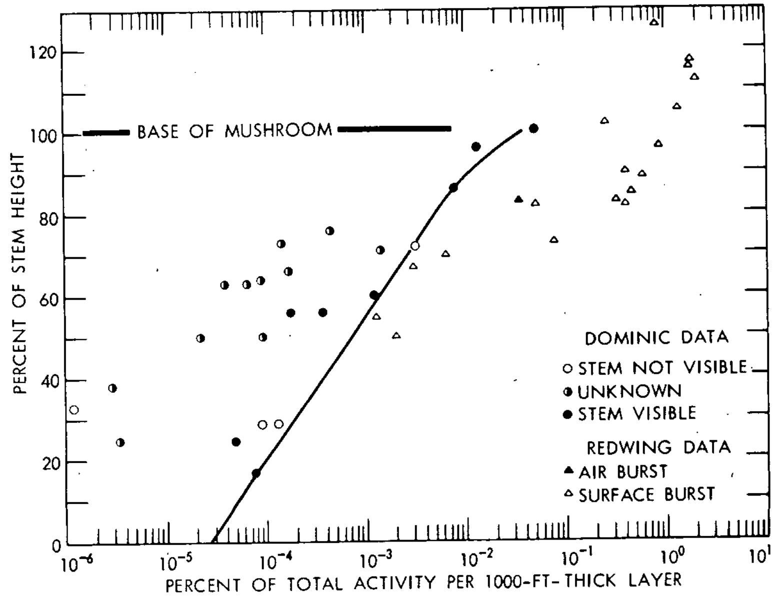

Fig. 3—Variation with height of the percent of the total activity residing in a 1000-ft-thick horizontal layer of the cloud.

also are discussed later. The curve is intended to represent a conservative estimate (for safety considerations) of the stem activity as a function of height for air bursts.

The rather large scatter in the data may be attributed to several factors. It appears that stem visibility may be the most important of these. Most of the higher activity readings occurred during penetrations when the stem cloud was visible to the pilot. The relatively low readings were obtained when the cloud was not visible or when it was not known whether the cloud was visible. It is quite possible that the aircraft did not actually penetrate the stem on these occasions. The dose rates measured inside the aircraft may have been due to "shine" from the stem cloud or to activity from diffuse material outside of the stem core. In those cases where the stem was not visible and where several passes were made at the same altitude, only the highest reading has been used.

Unfortunately, for the lower 80% of the stem, virtually all the data for the larger detonations are questionable because of the stem-visibility problem. Therefore it is impossible to say whether or not the low stem activity found for these shots indicates a real decrease in the fraction of activity in the lower part of the stem with increasing nuclear yield.

The following factors also contribute to the uncertainty in the results:

1. Stem-volume estimates. For the determination of the total activity present in a 1000-ft-thick layer, the stem diameter at the penetration altitude was estimated. The values used were based on visual estimates made by observers on the ground and in the sampling aircraft or, where necessary, on estimates for other detonations in the same yield range. The estimated diameter could be in error by as much as a factor of 2 in some cases.

2. Stem-height estimates. The stem was considered to extend from sea-level to the base of the cloud regardless of the burst height. The cloud bases used were based on visual observations from the ground and from the sampling aircraft and verified, where possible, by radiation readings taken in the sampling aircraft. The uncertainty in the height of the cloud-base (stem height) is about 10%.

3. Representativeness of dose-rate readings. The measured dose rates are assumed to represent those in a uniform, infinite cloud. The assumption appears to be reasonably valid for those penetrations where the stem was visible. The aircraft required 20 sec or more to traverse the cloud at a speed of about 7 miles/min while the mean free path of gamma radiation in air is on the order of a few hundred feet. The navigator reported that the dose rate usually rose sharply on entering the cloud, remained fairly steady (within a factor of 2) during

penetration, and then dropped sharply. (It would be advantageous to use automatic time–intensity recorders in future operations.)

The effect of aircraft shielding on the dose rate in the cockpit is also uncertain. Tests made at the ground, using a point source outside the aircraft, indicated that there was no appreciable shielding effect on gamma radiation by the aircraft. Equation 2 assumes that the receptor is completely surrounded by a uniform radiation field. Actually, of course, the receptor was surrounded by a "blank space" equivalent to the volume of the aircraft. No attempt has been made to correct for this. However, the effect should be small, probably less than a factor of 2, since the mean free path of the gamma radiation is large compared to the dimensions of the aircraft. Experimental determination of the correction factor should be planned in connection with any future operation of this type.

AIRCRAFT SAMPLING IN THE VICINITY OF THE CLOUD BASE

Aircraft equipped with Los Alamos Scientific Laboratory air-filter tanks were used for sampling after five Dominic I detonations. Approximately 1-hr sampling missions were flown at altitudes from 35,000 to 48,000 ft at 2 to 5 hr after detonation. The two sampling tanks were opened simultaneously when contact with the cloud was made and remained open for the entire sampling period. As the sampling patterns were flown, readings in the cockpit were made at 1-min intervals with a hand-held AN/PDR-27J Radiacmeter capable of measuring activity in a range from 0.01 to 500 mr/hr. Sampling missions were successful after four of the five detonations. The radiochemical analyses of the samples are reported elsewhere.[6]

The dose-rate readings obtained during three extended sampling missions were sufficient for estimations of the distribution and the amount of activity in the clouds at the sampling altitudes. Similar analyses were done for all three missions. The results are included in Fig. 3.

One of the clouds was sampled at an altitude of 45,000 ft at approximately 3 to 4 hr after detonation. The base of the cloud was reported to be at about 45,000 ft. Both the shot-time wind data and the position of the cloud indicate east-southeast cloud travel at about 15 knots. For correction for the movement of the cloud during the sampling period, the reported aircraft positions were adjusted to the sampling midtime of $3\frac{1}{3}$ hr after detonation. The corrected radiation field and the actual unadjusted sampling track are shown in Fig. 4. If a decay exponent of -1.2 is assumed, integration of the pattern yields 520 r/hr-cu mi at 1 hr in a 1000-ft-thick layer. From Eq. 2 this is equivalent to 270 Mc, or 4.9×10^{-4} of the total fission products produced by the detona-

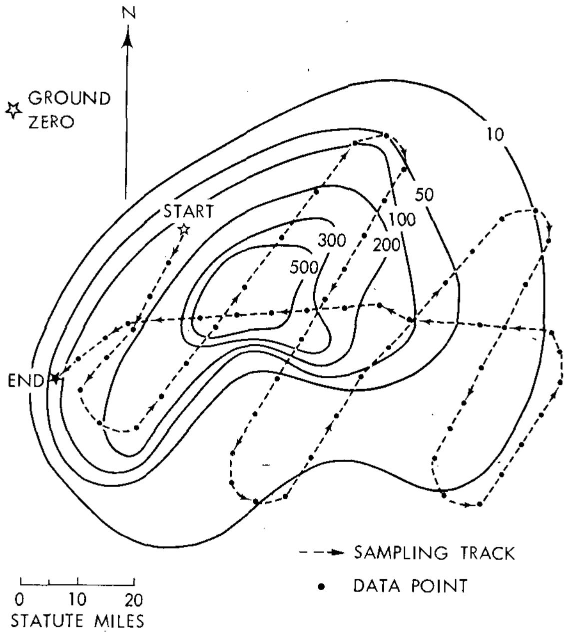

Fig. 4—Sampling track and radiation pattern in a nuclear cloud at 45,000 ft. Values given are in milliroentgens per hour at H + 3⅓ hr.

tion. The cloud covered an area of 5200 square miles at the 45,000-ft altitude.

The sampling track appears to have covered the cloud very well. However, the pilot reported shine from higher portions of the cloud during the last few minutes of sampling when the aircraft was outside the visible cloud. The readings due to shine were about 100 mr/hr. It is possible that a significant fraction of the in-cloud readings may also have been due to shine from the upper portions of the cloud; therefore the estimate of the amount of activity at 45,000 ft may be high.

COMPARISON WITH RADIOCHEMICAL RESULTS

The radiochemical analyses of the samples obtained on the three extended sampling missions provide a check on the method of calculating the amount of debris present from the dose-rate readings in the cloud. The total number of fissions collected in each sample has been determined,[7] based on the number of atoms of ^{99}Mo present corrected for the fission yield of ^{99}Mo for thermal fission of ^{235}U. If the total volume of air passing through the sampling tank and the average dose rate along the sampling path are known, the fissions per sample can be estimated by the same method that was used to estimate the fraction of the bomb in a 1000-ft-thick layer. The volume sampled is determined from the altitude, the air temperature, the aircraft speed, the sampling time, and the sampling-tank and filter-paper characteristics.[8] The average dose rate is determined from the readings taken in the cockpit at 1-min intervals during the sampling period. From Eq. 2 the gamma megacuries in the sample can be calculated. If it is assumed that 1 kt of fission (1.4×10^{23} fissions) is equivalent to 550 gamma megacuries at 1 hr, the following conversion factor can be used: 1 Mc (H + 1) = 2.64×10^{20} fissions. Table 1 gives the pertinent data and the fissions per sample as calculated from dose-rate readings and as determined from radiochemical analyses of the samples.

Table 1 — COMPARISON OF CALCULATED AND ANALYZED FISSIONS PER SAMPLE

Mission	Altitude, ft	Sample volume, cu ft	Average dose rate, mr/hr at H + 1	Calculated fissions per sample	Fissions per sample (radiochemical analyses)
A	43,000	1.06×10^6	190	1.9×10^{14}	3.3×10^{14}
B	48,000	1.11×10^6	270	2.3×10^{14}	4.9×10^{14}
C	45,000	1.10×10^6	560	5.6×10^{14}	5.8×10^{14}

The agreement between the calculated values and the results of the sample analyses is remarkably good, considering the uncertainties due to the possibility of shine from other portions of the cloud, aircraft shielding, and aircraft contamination. The calculated values for the samples from missions A and B are low by about a factor of 2, possibly because of the effect of the blank space previously mentioned. The calculated value for the sample from mission C is in almost perfect agreement with the result of the sample analysis. Mission C is the one depicted in Fig. 4 and for which there was reason to suspect a shine contribution to the dose rates which may have compensated for the blank-space effect.

Additional experimental data are needed to evaluate all the factors involved, but the results indicate that the method employed on these missions is a practical and promising way to obtain the distribution of activity in a nuclear cloud.

REDWING IN-CLOUD DOSE-RATE DATA

The doses and dose rates at various altitudes in several nuclear clouds (all but one from surface bursts) were investigated by aircraft penetrations[9] during Operation Redwing in 1956. Some of these penetrations were complete traverses through the cloud. Since the altitude, the mean speed of the aircraft, the time in the cloud, and the average dose rate are reported, these data can be utilized in the same manner as the Dominic I stem penetrations to compute the device fraction contained in the cloud at the penetration altitudes. The computed device fractions are plotted in Fig. 3 for comparison with the Dominic I data.

Several interesting features may be noted. It appears that the activity in the upper half of the stem is greater for surface bursts than for air bursts and that the difference increases with altitude. The largest gradient of activity with altitude appears at about 70 to 80% of the stem height; this implies that for surface bursts the "radiological base" lies below the visual cloud base. However, this inference may not be warranted since the high activities encountered below the base may be due to the descent of fallout particles.

The values computed for the lower portion of the mushroom indicate about 1 to 2% of the total fission products per 1000 ft. Since the mushroom portion of the clouds investigated averaged about 30,000 ft in vertical extent, the average activity in the mushroom must have been about 3% per 1000 ft. Thus we have some basis for believing that this admittedly crude method can give at least the right order of magnitude for the activity at a given altitude, even when the average dose rate recorded during a single pass through the cloud is used.

We note that the one Redwing data point for an air burst gives about five times the activity indicated by the curve estimated from the Dominic I data. This greater activity might be attributed to the fact that the detonation took place at a lower scaled height than any of the Dominic I air bursts. The burst height was somewhat below the minimum altitude for a true air burst according to our definition (burst height > $180Y^{0.4}$); therefore the activity distribution might be expected to be intermediate between those for air bursts and surface bursts. Although the close-in fallout measured after this detonation was very light, it was considerably more than that found after any Dominic I shot, where shipboard dose rates never exceeded 0.1 mr/hr. However, since only one surface vessel was available for fallout measurements during the Dominic I tests, the very limited number of measurements obtained does not permit the drawing of firm conclusions.

RESULTS AND CONCLUSIONS

Activity in the Stem Cloud for Air Bursts

Although the Dominic I stem-penetration data leave a good deal to be desired for defining the distribution of activity in the stem, the curve in Fig. 3 represents a best estimate based on our interpretation of these data. A major uncertainty lies in the assumption that the distribution in the stem does not vary with yield. As indicated previously,

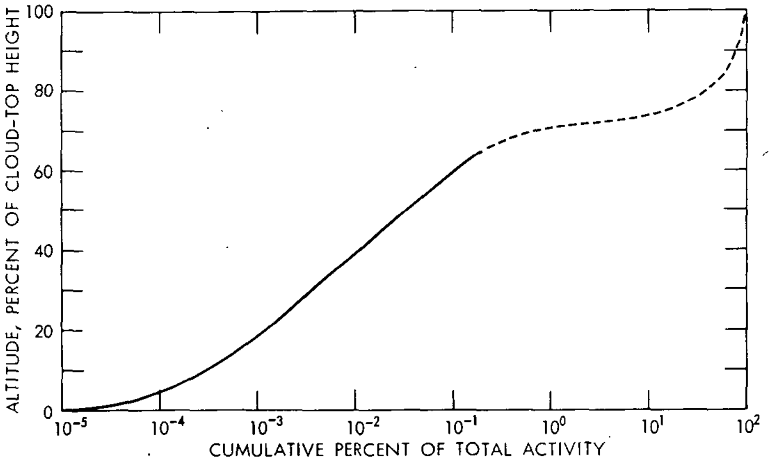

Fig. 5—Cumulative activity as a function of height in the nuclear cloud for air bursts.

this curve may represent an overestimation of the activity in the lower part of the stem for the larger yields (above about 200 kt).

Cumulative Activity with Height in the Nuclear Cloud for Air Bursts

With the use of the stem-activity curve in Fig. 3, an estimate of the cumulative activity with height in the nuclear cloud was derived. The solid portion of the curve in Fig. 5 was obtained from the stem-activity curve by using an average stem height of 40,000 ft and by assuming the stem-top height (or visual cloud base) to be 63% of the cloud-top height (the average for the Dominic I series). Since the entire stem appears to contain less than 1% of the total activity, it is obvious that the activity must increase rapidly with height at or above the base of the cloud. The dashed portion of the curve represents a subjective estimate (based, in part, on the Redwing data for surface detonations) of the distribution of activity in the mushroom portion of the cloud. The activity in the mushroom is assumed to be distributed as follows:

Layer, % of cloud-top height	Fraction of total activity, %
65 to 70	0.6
70 to 75	14
75 to 80	25
80 to 85	25
85 to 90	15
90 to 95	15
95 to 100	5

For air bursts it appears reasonably certain that less than 1% of the total activity is present in the stem and that less than 0.1% stabilizes between the surface of the earth and one-half of the cloud-top altitude. The fraction of activity per unit altitude increases with height throughout the stem, and the region of maximum vertical gradient, which might be termed "the radiological base of the cloud," probably occurs somewhat above the visual cloud base. The peak activity per unit altitude is assumed to occur between 75 and 85% of the distance from the surface to the cloud top. It is also assumed that for air bursts the distribution of activity relative to the cloud-top height does not vary with nuclear yield, burst height, or atmospheric conditions.

Actually, the interaction of these factors must exert some influence on the activity distribution. The estimated top and base heights of the Dominic I clouds indicate that the ratio of base height to top height has a tendency to decrease with increasing yield. However, it is uncertain to what extent these indications are valid since the variation among detonations of about the same yield is almost as great as that for the range of yields from 40 kt to several megatons. The mean ratio is 63%, with individual clouds varying from 53 to 73%. Some of the variation may be attributed to errors in the estimates of the base and top heights, but part of it is undoubtedly real. There is a similar uncertainty concerning the height of the radiological base.

Partition of Activity Between Stratosphere and Troposphere

The height of the tropopause varies with latitude, season, and daily atmospheric changes. The daily and seasonal variations are less in tropical latitudes than elsewhere. The tropopause heights averaged about 54,000 ft above sea level for the Dominic I tests, varying between 50,000 and 58,000 ft on individual shot days. This variation is representative of the tropical tropopause.

With the use of the activity distribution in Fig. 5, a mean tropopause height of 54,000 ft, and the mean cloud-height curve in Fig. 1, a typical curve of the percent of total debris in the troposphere as a function of yield has been calculated. The curve, shown in Fig. 6, is intended to be valid at the time of cloud stabilization for air bursts in a tropical atmosphere. Another curve has been drawn to indicate the likely maximum tropospheric fraction, based on a high tropopause (58,000 ft) and low cloud heights (from the lower curve in Fig. 1). These extremes do not represent absolute maximums since higher tropopauses and lower clouds may occur occasionally. In addition, the uncertainties in the activity–height curve (Fig. 5) make it impossible to define a meaningful and useful absolute maximum tropospheric fraction. No attempt has been made to estimate the minimum tropospheric fraction, but, in the megaton-yield range, it could be several orders of magnitude below the typical fraction.

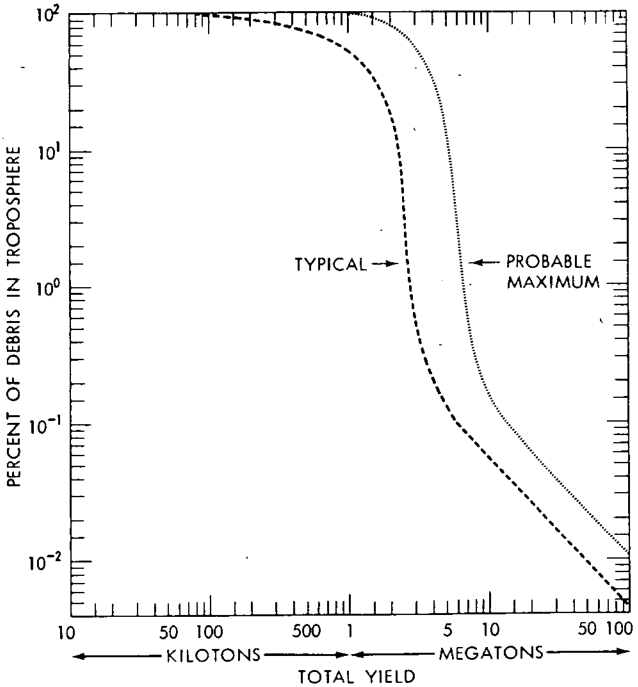

Fig. 6—Percent of total activity initially injected in the troposphere as a function of total yield for air bursts in a tropical atmosphere.

The most critical uncertainty in the estimates is for the range of yields from about 700 kt to about 5 Mt, where the radiological cloud base may lie in the vicinity of the tropopause. For yields less than 700 kt, the tropospheric fraction (at cloud stabilization) can be estimated to within a factor of 2 or less. For yields above about 5 Mt, the fraction in the troposphere becomes very small, although precisely how small it may be has not yet been determined.

An estimate of the kiloton equivalent of fission products stabilized in the troposphere as a function of total yield for air bursts is shown in Fig. 7. The typical and maximum curves are derived from the curves in Fig. 6, based on the assumption that the yield is entirely due to fission. Several interesting features may be noted. The maximum tropospheric contamination is produced by bursts in the low megaton range (assuming 100% fission yield). With typical cloud heights and an average tropopause height of 54,000 ft, the maximum tropospheric contamination is about 500 kt for yields between about 800 kt and 2 Mt. As the yield increases, the tropospheric debris decreases rapidly and then levels off at about 5 kt of fission equivalent for yields from 10 to 100 Mt. The maximum curve, based on a high tropopause and low cloud heights,

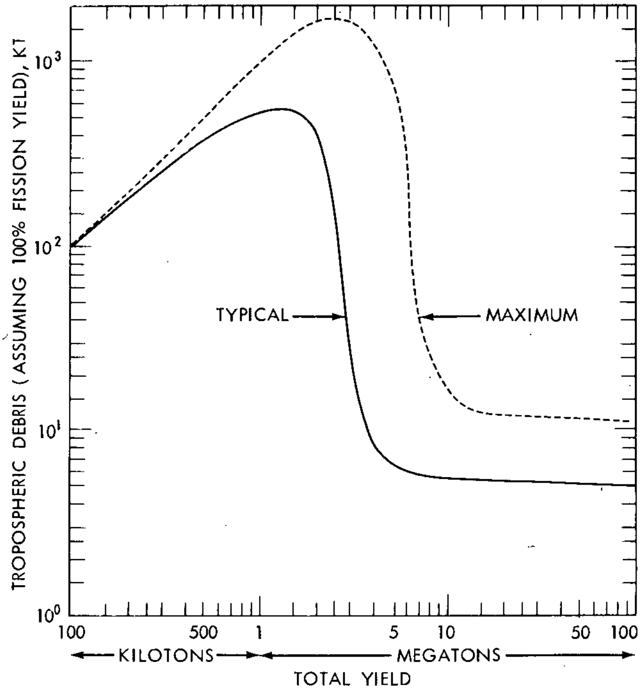

Fig. 7—Amount of debris (kilotons equivalent) initially injected in the troposphere as a function of total yield for air bursts in a tropical atmosphere.

is quite similar with a maximum tropospheric contamination of about 1.5 Mt for yields between 2 and 3 Mt, all fission. This curve also decreases rapidly and then levels off at about 12 kt of tropospheric debris for yields between 15 and 100 Mt. It should be recalled here that these curves are based on the activity–height curve given in Fig. 5 and are subject to the same uncertainties. For thermonuclear devices the amount in the troposphere should be multiplied by the fission fraction of the device.

Dominic I Debris in the Troposphere

With the use of the estimated tropospheric fraction and the fission yield for the individual Christmas Island detonations, it is estimated that about one-third of the total radioactivity initially stabilized in the troposphere. Since a half-residence time of one month is generally accepted for tropospheric debris,[10] about one-sixth of the total activity might be expected to be deposited at the surface, mostly in tropical latitudes, within a month after the conclusion of this test series. A rough integration[11] of the activity found in the AEC Health and Safety Laboratory monthly fallout-deposition collections indicated that only about half this amount was deposited in the latitude band from 30°N to 30°S through August 1962. The difference between the expected and the measured amounts may be due to the uncertainties in the estimates of the tropospheric fraction and the deposition. However, there are several reasons for believing that the amount deposited in the latitude band was actually less than that estimated from the tropospheric fraction at time of cloud stabilization.

First, some of the debris which initially stabilized below the tropopause may have ascended into the stratosphere in convective cells or as a result of thermally induced direct circulation. Second, some debris was transported to mid-latitudes at altitudes below the tropical tropopause. Since there is a polar tropopause in mid-latitudes, generally between 30,000 and 40,000 ft, the debris which was transported away from the equatorial region at altitudes from about 40,000 to 55,000 ft would have become incorporated into the mid-latitude stratosphere. An interesting example of such transport was provided by the interception of one of the Dominic I clouds by sampling aircraft over the western United States.[12] In addition, sampling of the lower stratosphere over the United States indicates that it contained fresh debris from the Dominic I tests during most of the month of May 1962. Finally, the evidence for a half-residence time of one month for tropospheric debris may actually apply only to debris below the polar tropopause. The residence time for debris in the troposphere, above 40,000 ft, in tropical latitudes has not been established. Only a very small fraction of the debris from the Dominic I tests stabilized below 40,000 ft. The fraction was much smaller than that for previous Pacific test series, which consisted primarily of surface bursts.

In any case, it has become increasingly evident that the potential hazard due to short-lived fission products is not attributable solely to the portion initially injected in the troposphere since there is an exchange of air between the stratosphere and troposphere. Therefore the three-dimensional trajectory of the debris-laden air would have to be considered in determining the fate of a particular debris cloud.

It has also been shown[12] that severe thunderstorms that penetrate the lower stratosphere provide an effective mechanism for bringing stratospheric debris directly to the ground. It appears that thunderstorm scavenging of stratospheric debris from the Dominic I tests accounted for most of the ^{131}I found in milk in the midwestern United States in May 1962.

RECOMMENDATIONS FOR FUTURE WORK

Project Stemwinder has shown in-cloud dose-rate monitoring by aircraft to be a relatively simple and economical way to obtain information on the distribution of radioactive debris in nuclear clouds.

Through the use of this technique, it may be possible to greatly reduce the amount of radiochemical analyses which would be required to obtain a reliable inventory of radioactivity in a nuclear cloud. This type of monitoring might be particularly well suited to clouds from large nuclear cratering detonations such as those contemplated for the Plowshare program. Such clouds should be visible for at least several hours and would probably be confined to the troposphere.

Tentative answers have been found for the questions that led to Project Stemwinder, but large uncertainties still exist. The experience gained in the project indicates that for air bursts the lower stem should be monitored soon after cloud stabilization while it is still visible and that several penetrations should be made at each altitude to ensure that representative readings are obtained. Additional data are particularly needed for yields in the megaton range.

An obvious limitation of Project Stemwinder was the aircraft ceiling of 50,000 ft. A determination of the amount of debris initially stabilized in the troposphere requires sampling to an altitude of 60,000 ft. Aircraft with the capability of operating at this altitude have been used for cloud sampling, but they were not available for Project Stemwinder.

The following recommendations are offered for any future operations:

1. A continuous-recording gamma-intensity instrument package with a range from 1 mr/hr to 1000 r/hr should be used for aircraft cloud penetrations.
2. Experimental determination of the dose-rate reduction due to the aircraft should be attempted.
3. An attempt should be made to monitor the entire cloud from a low- or an intermediate-yield detonation. Thus the distribution of activity throughout the cloud can be ascertained, and the total computed activity can be compared with the fission yield of the device as a check on the method.

ACKNOWLEDGMENTS

Project Stemwinder was originally conceived and coordinated by Joshua Holland, Chief, Fallout Studies Branch, Division of Biology and Medicine, U. S. Atomic Energy Commission, whose vigorous efforts brought the project into being in the space of a few weeks prior to the start of Operation Dominic I. The ideas and efforts of the late A. Vay Shelton, Lawrence Radiation Laboratory (Chief, Hazards Evaluation Branch for Dominic I, Joint Task Force 8) and of Robert J. List, Kosta Telegadas, and Jerome L. Heffter, Atmospheric Radioactivity Research Branch, U. S. Weather Bureau, were instrumental in planning and carrying out the project. The excellent cooperation and high skill of Paul Guthals, Los Alamos Scientific Laboratory, and Harry Hicks and Edward Fleming, Lawrence Radiation Laboratory, in directing and controlling the sampling aircraft contributed much to the success of the project. Our thanks are also due to Col. Templeton Walker, Commander, 9th Weather Reconnaissance Wing, and to all the members of the 1211th Test Squadron who displayed great enthusiasm and a high degree of professional competence in carrying out the sampling missions.

REFERENCES

1. G. J. Ferber, Operation Dominic I — Project Stemwinder, Operation Dominic Report, WT-2060, U. S. Weather Bureau, May 1964. (Classified)
2. L. Fussel, Jr., Cloud Photography, Operation Redwing Report, ITR-1343, Edgerton, Germeshausen and Grier, Inc., March 1957. (Classified)
3. J. Healy, Radioactive Cloud Dose Calculations, in *Meteorology and Atomic Energy*, D. Slade (Ed.), Chap. 6, U. S. Weather Bureau, Washington, D. C., in preparation.
4. G. Higgins, Calculation of Radiation Fields from Fallout, USAEC Report UCID-4539, Lawrence Radiation Laboratory, University of California. Jan. 25, 1963.
5. E. G. Reid, Average Atmospheric Characteristics at the Eniwetok Proving Ground (April–June 1956), Stanford University, private communication, July 1958.
6. P. A. Benson, The Analysis of Particulate Debris from Pacific Air Shots, Quarterly Progress Reports, 1962–1964, various pages, Tracerlab, Division of Laboratory for Electronics, Inc.
7. P. A. Benson, Total Fissions Collected in Dominic Samples, Tracerlab, Division of Laboratory for Electronics, Inc., private communication, November 1963.
8. K. Telegadas and R. J. List, B-57 Air Sampling Program (1960), USAEC Report HASL-105, Health and Safety Laboratory, Jan. 9, 1961.
9. E. A. Pinson et al., Operation Redwing — Project 2.66a, Early Cloud Penetrations, Report WT-1320, Air Force Special Weapons Center, Kirtland AFB, February 1960. (Classified)
10. United Nations, Report of the Scientific Committee on the Effects of Atomic Radiation, Supplement No. 16, General Assembly, 17th Session, p.248, New York, 1962.
11. R. J. List, U. S. Weather Bureau, private communication, January 1964.
12. R. J. List, K. Telegadas, and G. J. Ferber, Meteorological Evaluation of the Sources of Iodine-131 Contamination in Milk, *Science*, *146:* 59(1964).

CESIUM-137 AND STRONTIUM-90 RETENTION FOLLOWING AN ACUTE INGESTION OF RONGELAP FOOD

EDWARD P. HARDY, Jr.,* JOSEPH RIVERA,* and ROBERT A. CONARD†
*Health and Safety Laboratory, U. S. Atomic Energy Commission, New York, New York, and †Brookhaven National Laboratory, Upton, New York.

ABSTRACT

Marine and plant foods used by natives living on Rongelap in the Marshall Islands contain higher levels of long-lived fission-product radionuclides than do diets of people living in the United States due to residual contamination from fallout in 1954. During the 1963 medical survey of the Rongelap population, three food items indigenous to the Rongelap diet were brought back to the United States and consumed over a seven-day period by a member of the medical team. The ingestion of these foods introduced levels of ^{90}Sr and ^{137}Cs which were 20 and 60 times higher, respectively, than in the normal diet and was therefore considered in terms of an acute intake of two fission-product radionuclides that are important from a radiological standpoint. Urinary and fecal collections were analyzed separately, and whole-body ^{137}Cs measurements were made with a whole-body counter. The urine was the principal excretory route for the ^{137}Cs, whereas the feces was the main removal means for the ^{90}Sr. The retention of ^{90}Sr could be represented by a series of exponentials, whereas the retention of cesium as determined by whole-body counting indicated that a single long-term component with a biological half-life of 74 days describes the removal process. Reasonably good agreement was obtained between retention as determined by whole-body counting and by excretion measurements. It is estimated that about 25% of the ^{90}Sr from the Rongelap food was retained by the body at the end of 190 days. The

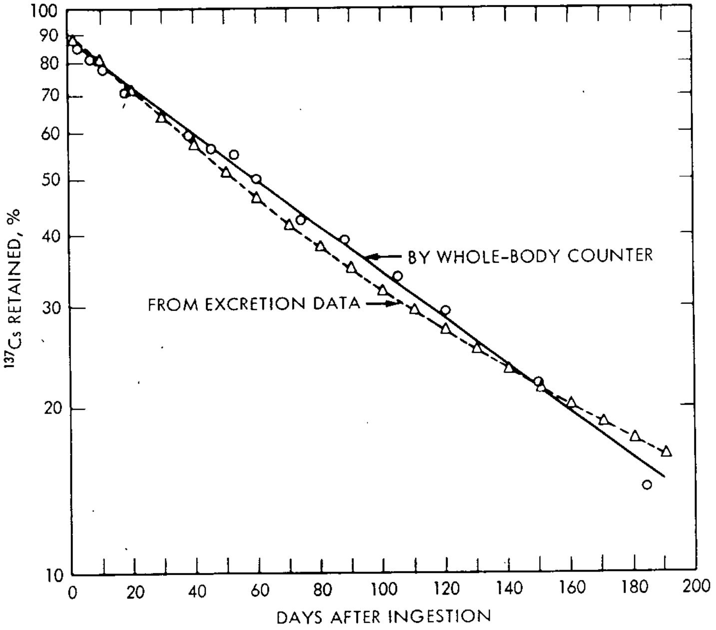

Fig. 5 — Percent retention of ^{137}Cs from Rongelap food.

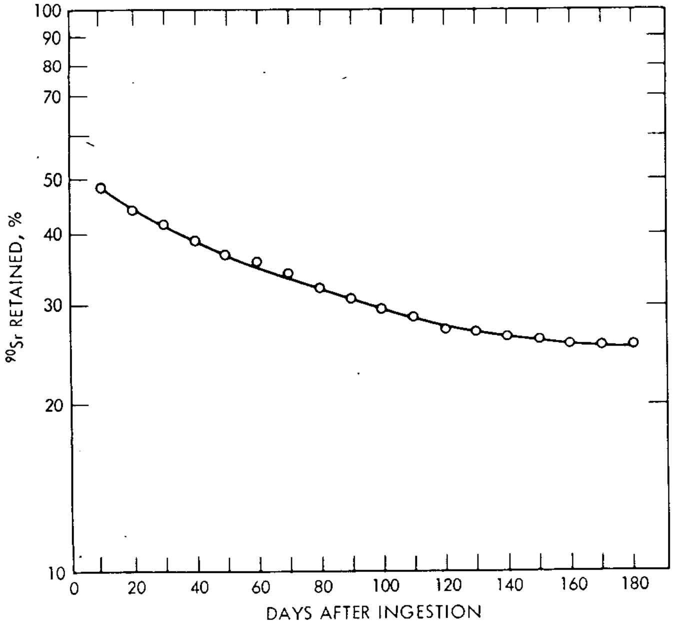

Fig. 6 — Percent retention of ^{90}Sr from Rongelap food as measured from excretion.

EARLY FOOD-CHAIN KINETICS OF RADIONUCLIDES FOLLOWING CLOSE-IN FALLOUT FROM A SINGLE NUCLEAR DETONATION

WILLIAM E. MARTIN
University of California at Los Angeles, Los Angeles, California

ABSTRACT

Plant samples and rabbits were collected from representative locations in the Sedan fallout field before and at various times after the detonation. Radiochemical and statistical analyses indicated highly significant correlations between estimates of gamma dose rates and maximum concentrations of ^{89}Sr or ^{131}I in plant samples and in the stomach contents, bone ash, or thyroids of rabbits collected between 15 and 110 miles from ground zero.

The effective half-lives of ^{89}Sr and ^{131}I on fallout-contaminated plants were approximately 18 and 5.0 to 5.5 days, respectively. Maximum concentrations of ^{89}Sr in rabbit bone ash occurred about 30 days after the detonation and remained high for at least 60 days; but maximum concentrations of ^{131}I in rabbit thyroids occurred by or before five days and then declined to pre-Sedan levels in less than 60 days after the detonation.

Deterministic exponential models were formulated and found to function satisfactorily, with parameter values derived from the data, in providing a partial explanation of the quantitative kinetic relations between initial concentrations of ^{89}Sr and ^{131}I on plants and subsequent concentrations in the bone ash or thyroids of rabbits collected in the Sedan fallout field. Major sources of error in the estimation of input-parameter values and in the use of such models to make predictions are described and discussed.

Similar models were proposed for the study of radionuclide kinetics in human food chains (i.e., pasture plants, cow milk, and human

tissues or organs) following environmental contamination by a single fallout event. The results of hypothetical calculations were compared with the Radiation Protection Guides recommended by the Federal Radiation Council.

INTRODUCTION

To explain the kinetics of radionuclide transfers in a given food chain, it is first necessary to describe the routes and rates of transfer affecting specific food-chain compartments. The major route and some of the minor routes of radionuclide transfer and exchange in a terrestrial ecosystem are shown in Fig. 1.

Some of the fallout particles initially deposited on soil surfaces may be redeposited by wind or rain on plants,[1] but most of them are mechanically trapped and not susceptible to redeposition.[2] Material deposited on soil may enter food chains by stem-base absorption,[3] by downward leaching in the soil profile and subsequent root uptake,[4,5] or by accidental ingestion, especially by burrowing animals.[6] Most of the fallout deposited directly on soil can be regarded as unavailable for rapid entry into major food chains.

Some of the radioactivity contained in the fallout particles, mostly < 44 μ in diameter,[1,7] retained on foliage may be assimilated by foliar absorption,[8,9] but a much larger fraction is subject to fairly rapid removal by wind or rain.[10,11] While it remains on plant surfaces, this material may be ingested by herbivores.

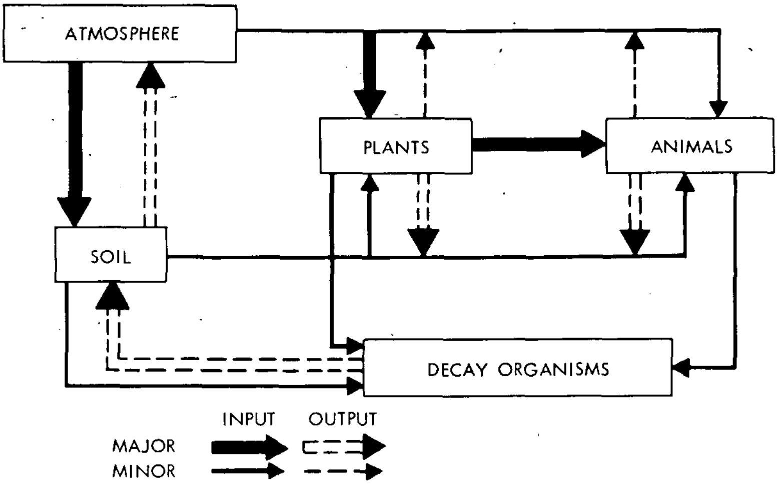

Fig. 1—Major and minor routes of radionuclide transfer and exchange in a terrestrial ecosystem contaminated by radioactive fallout.

Herbivorous mammals may be externally contaminated by direct exposure to fallout or by contact with contaminated plants or soils. Radionuclides may accumulate in animal tissues via inhalation, which, in many cases, is relatively unimportant or via ingestion of contaminated materials. Although inhalation, ingestion of contaminated soil or water, and ingestion of fallout particles while the animal is preening cannot be dismissed entirely, it is probably reasonable to assume that externally contaminated plants are the major sources of radionuclides for assimilation by herbivorous mammals (e.g., jackrabbits or dairy cattle) feeding in a fallout-contaminated environment during the first 30 to 90 days after close-in fallout.

The summer of 1962 provided an excellent opportunity to study the food-chain kinetics of ^{89}Sr and ^{131}I in relation to desert shrubs and rabbits in the Sedan fallout field. These studies included the formulation and testing of mathematical models that can be shown to provide at least a partial explanation of the kinetic relations between initial concentrations of ^{89}Sr and ^{131}I on fallout-contaminated plants and subsequent concentrations of ^{89}Sr in the bone ash or of ^{131}I in the thyroids of rabbits collected in the Sedan fallout field. Although the results of these studies[11–17] are not conclusive, partly because the causes of variation are imperfectly understood, they do provide evidence that mathematical models similar to those used by radiochemists to explain decay-chain kinetics,[18] by physiologists to explain tracer kinetics,[19] and by the International Commission on Radiological Protection (ICRP) to establish maximum permissible concentrations[20] can also be used to study food-chain kinetics under field conditions.

The objectives of this paper are (1) to summarize some of the data related to ^{89}Sr and ^{131}I on desert shrubs and in rabbit tissues following fallout from Project Sedan, (2) to present the deterministic models that provide a partial explanation of these results, and (3) to illustrate the potential value of similar models in studying the food-chain kinetics of radionuclides on pasture plants, in cow milk, and in human tissues following a single fallout event.

METHODS

Project Sedan, a peaceful nuclear-explosives test, involved the detonation of a 100 ± 15 kt thermonuclear device at a depth of 635 ft in alluvium and tuff at the north end of the Nevada Test Site on July 6, 1962. As predicted, the early fallout was relatively light and occurred primarily within a 150-mile sector, N60°W to N60°E, from ground zero in Yucca Flat.

Before and at various times after the detonation, plant samples and rabbits were collected from representative locations in the Sedan fallout field (see Fig. 2). Each sampling station was marked by a metal

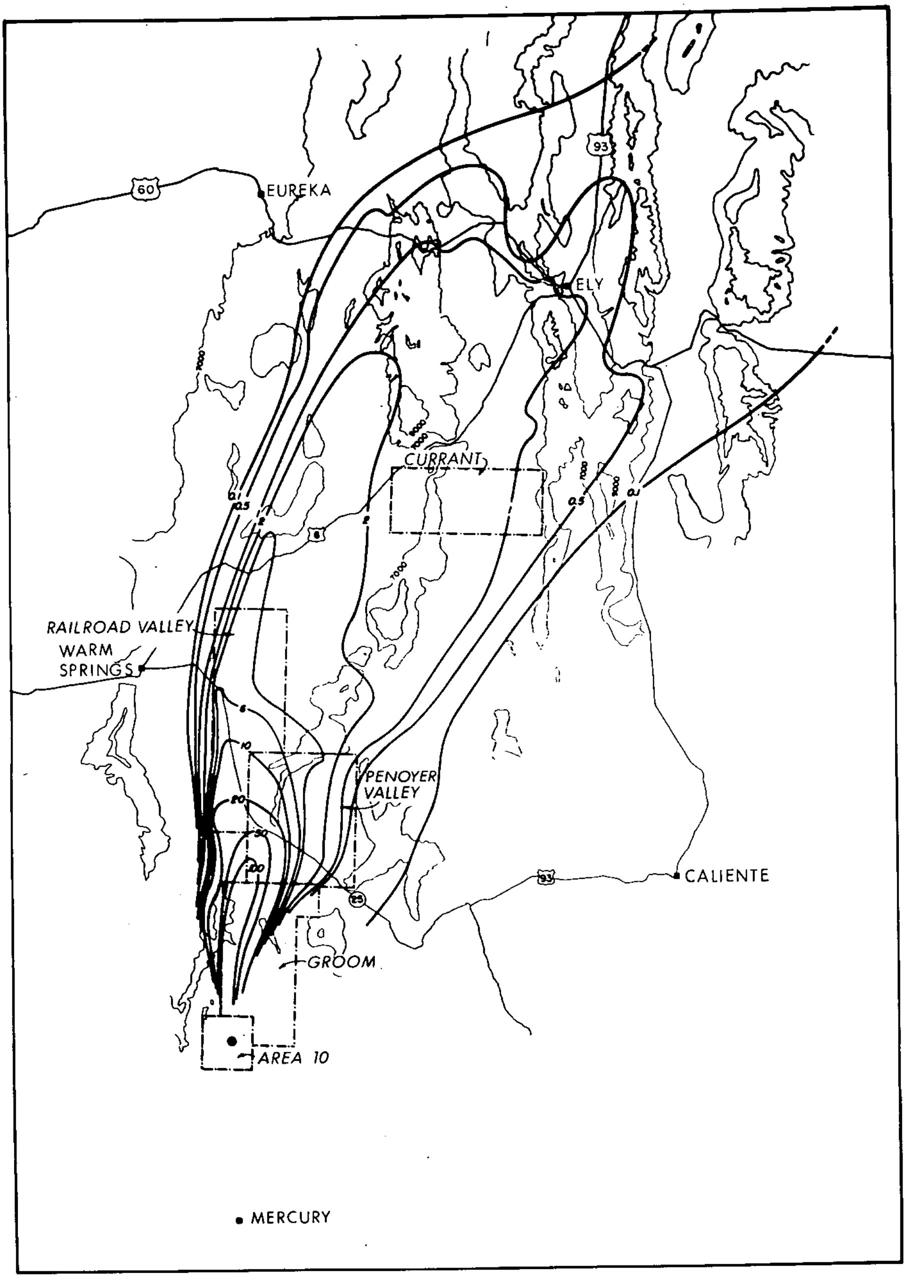

Fig. 2—Approximate locations of study areas and sampling stations in the Sedan fallout field. Dose-rate contours (mr/hr at H + 24) are based on aerial surveys.[22]

post to facilitate its relocation and positive identification. Plant samples were collected by clipping twigs and foliage from the crowns of desert shrubs growing within a radius of 150 ft from each station marker. *Artemisia tridentata* (sagebrush) was the species collected at all stations in Groom Valley and the Currant Area, and *Atriplex confertifolia* (shadscale) was collected at all but three of the stations in Penoyer and Railroad valleys. Most of the rabbits representing a given location were shot within a few hundred yards of a station marker, but rabbits taken within a 1-mile radius were accepted as representatives of the general location. Most of the rabbits collected were blacktailed jackrabbits (*Lepus californicus*), but a few cottontail rabbits (*Sylvilagus auduboni*) were taken in mountainous areas where jackrabbits were not always available.

Radiochemical analyses were made to determine the ^{89}Sr and ^{131}I contents of plant samples, the ^{89}Sr content of rabbit bone ash, and the ^{131}I content of rabbit thyroids. The stomach contents of rabbits were analyzed for ^{131}I, but the samples remaining after aliquots were removed for this purpose were too small to be used in making analyses for ^{89}Sr. Following each determination, a decay correction was made to indicate the ^{89}Sr or ^{131}I concentration at the time the sample was collected. The procedures followed in making these analyses are described elsewhere[11,16,21] in considerable detail.

For simplicity, the only samples considered in this paper are those collected at the 20 representative locations indicated in Fig. 2. Additional data are given in other publications.[13,16] Estimates of the initial gamma dose rates (R_0 = mr/hr at 3 ft aboveground at H + 24) were obtained from a tracing of Guillou's[22] original large-scale map prepared from aerial surveys made before and after the detonation.

Correlation and regression analyses were made to examine the relation between initial gamma dose rates, R_0, and initial concentraations of ^{89}Sr or ^{131}I on plants, P_0; between P_0 and maximum concentrations of ^{89}Sr in rabbit bone ash, B_{30}; and between P_0 and maximum concentrations of ^{131}I in rabbit thyroids, A_5. Similar analyses were also made to determine the relations between S_0 and R_0, A_5, and S_0, where S_0 represents the initial concentration of ^{131}I in rabbit-stomach contents.

Estimates of ^{89}Sr and ^{131}I retention by plants in relation to theoretical deposition rates, different parts of the fallout field, and different plant species were based on Eq. 1:

$$f_p = \frac{a_p}{a_s} \qquad (1)$$

where f_p = retention index of N_i deposited on plants, sq ft/g [N.B. This index multiplied by G = g (dry weight) of plants per square foot would give the fraction of N_i deposited on plants]

a_p = pc N_i/g (dry)/R_0 deposited on plants

a_s = pc N_i/sq ft/R_0 deposited on uniform plane
N_i = a given radionuclide (e.g., ^{89}Sr or ^{131}I)

Estimates of a_p were based on the results of radiochemical analyses, P_t, and estimates of a_s (theoretical values) were based on Eq. 2:

$$a_s = \frac{0.693 F_k Y}{T_r D_d C R_k} \tag{2}$$

where F_k = 1.43 × 10^{23} fissions (^{235}U)/kt (Ref. 23)
Y = percent fission yield (atoms/fission) of N_i (4.79% ^{89}Sr, 3.1% ^{131}I) (Ref. 24)
T_r = radioactive half-life of N_i in days (50.5-day ^{89}Sr, 8.04-day ^{131}I)
D_d = 3.2 × 10^3 dis/pc/day
C = 2.79 × 10^7 sq ft/sq mile
R_k = 4.5 × 10^4 mr/hr/kt/sq mile at 3 ft aboveground at H ± 24 (Ref. 25)

The relations between initial gamma dose rates, R_0, and initial concentrations of ^{89}Sr or ^{131}I on fallout-contaminated plants, P_0, were tentatively defined by linear regression formulas. For example, where $\overline{P}_0$ and $\overline{R}_0$ are the means of P_0 and R_0 and b_{xy} is the coefficient of regression of P_0 on R_0,

$$P_0 = \overline{P}_0 \pm b_{xy} (R_0 - \overline{R}_0) \tag{3}$$

The deterministic exponential models used to describe and explain the time-specific relation between ^{89}Sr or ^{131}I concentrations on plants, P_t, and of ^{89}Sr in bone ash, B_t, or of ^{131}I in thyroids, A_t, are given (if at $t = 0$, $P = P_0$, $B = 0$, and $A = 0$) by Eqs. 4 to 6:

$$P_t = P_0 e^{-\lambda_p t} \tag{4}$$

$$B_t = P_0 \frac{W_p f_b}{W_b} \left(\frac{e^{-\lambda_p t}}{\lambda_b - \lambda_p} + \frac{e^{-\lambda_b t}}{\lambda_p - \lambda_b} \right) \tag{5}$$

$$A_t = P_0 W_p f_a \left(\frac{e^{-\lambda_p t}}{\lambda_a - \lambda_p} + \frac{e^{-\lambda_a t}}{\lambda_p - \lambda_a} \right) \tag{6}$$

where t = days after fallout deposition
P_t = pc ^{89}Sr/g (dry) or pc ^{131}I/g (dry) on plants at $t > 0$
B_t = pc ^{89}Sr/g of rabbit bone ash at $t > 0$
A_t = pc ^{131}I (total) in rabbit thyroid at $t > 0$
W_p = g (dry) of contaminated plant material consumed per rabbit per day
W_b = g (dry) of bone ash per rabbit

f_b = fraction of ingested ^{89}Sr deposited in the rabbit's skeleton
f_a = fraction of ingested ^{131}I deposited in the rabbit's thyroid
$\lambda_p = 0.693/T_p$ where T_p = effective half-life of ^{89}Sr or ^{131}I on plants
$\lambda_b = 0.693/T_b$ where T_b = effective half-life of ^{89}Sr in rabbit's skeleton
$\lambda_a = 0.693/T_a$ where T_a = effective half-life of ^{131}I in rabbit's thyroid

RESULTS

Estimates of average gamma dose rates, of ^{89}Sr concentrations in plant samples and in the bone ash of rabbits, and of ^{131}I concentrations in plant samples, in the stomach contents of rabbits, and in rabbit thyroids are given in Tables 1 and 2. The approximate locations at which these samples were collected are shown in Fig. 2.

The wide range of values and the relatively large standard errors of the means given in Tables 1 and 2 indicate a high degree of apparently inherent variability.* The wide range of ^{89}Sr and ^{131}I concentrations in plant samples and in rabbit tissues or stomach contents is partly a reflection of the wide range of initial contamination levels as indicated by estimated gamma dose rates; but much of the inherent variability is undoubtedly related to the probabilistic nature of the environmental and biological processes that influence the external contamination of plants and the accumulation of radionuclides in animal tissues. The probabilistic approach to the study of food-chain kinetics and the use of stochastic models to simulate these processes are considered in this symposium by Turner.†

The results of correlation and regression analyses given in Table 3 show that the quantitative interrelations of initial dose-rate estimates and estimates of maximum ^{89}Sr or ^{131}I concentrations in plants and animal tissues are highly significant in spite of their inherent variability. As might be expected, the correlation between initial gamma dose rates, R_0, and initial concentrations of ^{89}Sr or ^{131}I on plants, P_0, are highly significant. The correlations and regressions of plant contamination on maximum concentrations of ^{89}Sr in bone ash, B_{30}, and of ^{131}I in thyroids, A_5, are also highly significant. The somewhat higher correlation between ^{131}I concentrations in stomach contents, S_0, and in thyroids, A_5, suggests some difference between the plants collected for radiochemical analyses and those actually eaten by the rabbits in the Sedan fallout field.

---

*Since the standard deviations (= sx $\sqrt{n}$) are large in relation to the means, the frequency distributions of these variates are sharply skewed. Preliminary investigations indicate that they may be lognormal rather than normal.

†See paper by Frederick B. Turner, this volume.[15]

Table 1—AVERAGE GAMMA DOSE RATES, R_0, AND AVERAGE CONCENTRATIONS OF ^{90}Sr IN PLANT SAMPLES AND IN THE BONE ASH OF RABBITS COLLECTED FROM DIFFERENT PARTS OF THE SEDAN FALLOUT FIELD AT VARIOUS TIMES AFTER THE DETONATION*

Study areas	Initial gamma dose rates†			Days after detonation	Plant samples, pc ^{89}Sr/g (dry)			Rabbit bone ash, pc ^{89}Sr/g (dry)		
	$\bar{x}$	s$\bar{x}$	n		$\bar{x}$	s$\bar{x}$	n	$\bar{x}$	s$\bar{x}$	n
Groom Valley	45.0	±30%	5	5	4059	±30%	5	1459	±42%	5
				15	2716	±38%	5	3648	±62%	5
				30	1544	±50%	5	3667	±41%	5
				60	788	±38%	5	3581	±74%	5
Penoyer Valley	16.8	±45%	5	5	948	±37%	5	1363	±51%	5
				15	470	±30%	5	2024	±37%	5
				30	332	±39%	5	2283	±61%	5
				60	283	±44%	5	552	±34%	5
Railroad Valley	6.8	±32%	5	5	397	±14%	5	334	±30%	5
				15	269	±13%	5	620	±68%	5
				30	164	±19%	5	783	±33%	5
				60	127	±30%	5	462	±33%	5
Currant Area	1.5	±33%	5	5	318	±20%	5	295	±54%	5
				15	183	±23%	5	323	±31%	5
				30	136	±18%	5	427	±26%	5
				60	55	±15%	5	280	±31%	5
All areas	17.5	±30%	20	5	1436	±32%	20	863	±29%	20
				15	909	±37%	20	1680	±38%	20
				30	544	±40%	20	2097	±30%	20
				60	313	±32%	20	1389	±34%	20
				Pre-Sedan concentrations	30	±17%	14	56	±30%	16

*$\bar{x}$ = mean, s$\bar{x}$ = standard error expressed as a percentage of the mean, and n = number of samples. (Based on data given by Martin and Turner.[13])

†R_0 = mr/hr at 3 ft aboveground at H + 24.

When P_0 or S_0, B_t, and A_t are given, the parameter values required to solve Eqs. 4 to 6 are W_p, W_b, T_p, T_b, T_a, f_b, and f_a. Some of these parameter values can be obtained from experimental results reported in the literature, and others can be obtained from the data given in Tables 1 and 2. For our purposes those obtained from the field data may be more accurate.

Various studies[26,27] have indicated that adult jackrabbits consume approximately 100 g of dry plant material per day; therefore W_p = 100 g. Unpublished data collected during this and previous studies[1,2,28] indicate that the average adult jackrabbit in Nevada weighs about 2000 g and has a skeleton weighing 200 g (fresh). Since the ratio of fresh bone weight to bone-ash weight is approximately 4 to 1, W_b = 50 g. The ratio, W_p/W_b = 100/50, indicates a feeding rate of approximately 2.0 g of dry plant material per gram of bone ash per rabbit per day. The feeding

Table 2— AVERAGE CONCENTRATIONS OF ^{131}I IN PLANT SAMPLES AND IN THE STOMACH CONTENTS AND THE THYROIDS OF RABBITS COLLECTED FROM DIFFERENT PARTS OF THE SEDAN FALLOUT FIELD AT VARIOUS TIMES AFTER THE DETONATION*

Study areas	Days after detonation	Plant samples, pc ^{131}I/g (dry)			Rabbit stomach contents, pc ^{131}I/g (dry)			Rabbit thyroids, nc ^{131}I per thyroid		
		$\bar{x}$	$s\bar{x}$	n	$\bar{x}$	$s\bar{x}$	n	$\bar{x}$	$s\bar{x}$	n
Groom Valley	5	11966	±33%	5	5194	±29%	5	467	±34%	5
	10	6671	±39%	5	1283	±32%	4	386	±43%	4
	15	3192	±34%	5	1018	±47%	5	139	±52%	5
	20	1224	±49%	5	424	±28%	5	83	±35%	5
	25	526	±36%	5	161	±50%	5	61	±31%	5
	30	273	±30%	5	149	±32%	5	16	±31%	5
Penoyer Valley	5	1244	±33%	5	1853	±31%	5	257	±34%	5
	10	659	±30%	5	1212	±20%	4	141	±14%	4
	15	412	±36%	5	638	±17%	4	88	±34%	5
	20	227	±46%	5	311	±40%	5	40	±48%	5
	25	192	±64%	5	115	±44%	5	29	±52%	5
	30	81	±41%	5	81	±52%	4	1.5	±70%	5
Railroad Valley	5	713	±11%	5	693	±41%	2	111	±65%	4
	10	376	±10%	5	604	±34%	4	85	±36%	5
	15	211	±11%	5	348	±39%	3	61	±34%	5
	20	119	±17%	5	148	±31%	5	22	±45%	5
	25	96	±14%	5	75	±19%	5	29	±52%	5
	30	48	±25%	5	33	±24%	4	11	±27%	5
Currant Area	5	501	±15%	5	322	±37%	3	26	±27%	5
	10	200	±20%	5	57	±12%	3	7	±23%	5
	15	121	±57%	5	46	±28%	4	6	±50%	5
	20	56	±27%	5	42	±36%	5	6	±30%	5
	25	35	±26%	5	28	±50%	4	1.6	±10%	5
	30	26	±15%	5	7	±43%	5	1.1	±34%	5
All areas	5	3606	±40%	20	2506	±29%	15	221	±28%	19
	10	1977	±44%	20	838	±21%	15	143	±34%	18
	15	984	±40%	20	554	±31%	16	74	±36%	20
	20	406	±43%	20	231	±23%	20	38	±26%	20
	25	212	±32%	20	96	±27%	19	30	±27%	20
	30	113	±27%	20	69	±29%	18	12	±50%	20
Pre-Sedan concentrations		312	±57%	14	207	±51%	17	5.4	±61%	15

*$\bar{x}$ = mean, $s\bar{x}$ = standard error expressed as a percentage of the mean, and n = number of samples. (Based on data given by Turner and Martin.[16])

rate applicable to the accumulation of ^{131}I in the thyroid was taken as 100 g of dry plant material per whole thyroid per rabbit per day.

As shown in Table 1 and Fig. 3, the apparent rate of ^{89}Sr loss from fallout-contaminated plants tended to decrease with increasing time after the detonation, but the average effective half-life, T_p, from D + 5 to D + 30 (5 to 30 days after the detonation) was approximately 18 days. The average concentration of ^{89}Sr in bone ash, B_t, increased rapidly from D + 5 to D + 15 and then more slowly to a maximum (apparent

Table 3—RESULTS OF CORRELATION AND REGRESSION ANALYSES BASED ON ESTIMATES OF INITIAL GAMMA DOSE RATES AT 20 REPRESENTATIVE LOCATIONS IN THE SEDAN FALLOUT FIELD AND ON THE CONCENTRATIONS OF ^{89}Sr AND ^{131}I IN PLANT SAMPLES OR IN THE STOMACH CONTENTS, BONE ASH, OR *THYROIDS* OF RABBITS COLLECTED AT THE SAME LOCATIONS

Variables* [x(y)]	Correlation coefficients	Regression coefficients	Regression formulas [$x = \bar{x} + b_{xy}(y - \bar{y})$]
^{89}Sr			
$P_0(R_0)$	0.755†	83.75 ± 16.65†	$P_0 = 83.75\ R_0 + 335$
$B_{30}(P_0)$	0.698†	0.742 ± 0.250†	$B_{30} = 0.742\ P_0 + 761$
^{131}I			
$P_0(R_0)$	0.738†	0.405 ± 0.187†	$P_0 = 0.405\ R_0 + 0.147$
$S_0(R_0)$	0.835†	0.184 ± 0.029†	$S_0 = 0.184\ R_0 + 0.817$
$A_5(P_0)$	0.626†	12.76 ± 3.72†	$A_5 = 12.76\ P_0 + 122$
$A_5(S_0)$	0.769†	38.82 ± 7.59†	$A_5 = 38.82\ S_0 + 57$

*R_0 = mr/hr at 3 ft aboveground at H + 24; $P_0(^{89}Sr) = 1.26\ P_5$ (pc/g on plants at t = 0); $P_0(^{131}I) = 2.00\ P_5$ (nc/g on plants at t = 0); $S_0(^{131}I) = 2.00\ S_5$ (nc/g in stomachs at t = 0); $B_{30}(^{89}Sr)$ = observed values (pc/g in bone ash at t = 30 days); and $A_5(^{131}I)$ = observed values [nc(total) in thyroids at t = 5 days].

†Statistically significant at the 1% level of probability.

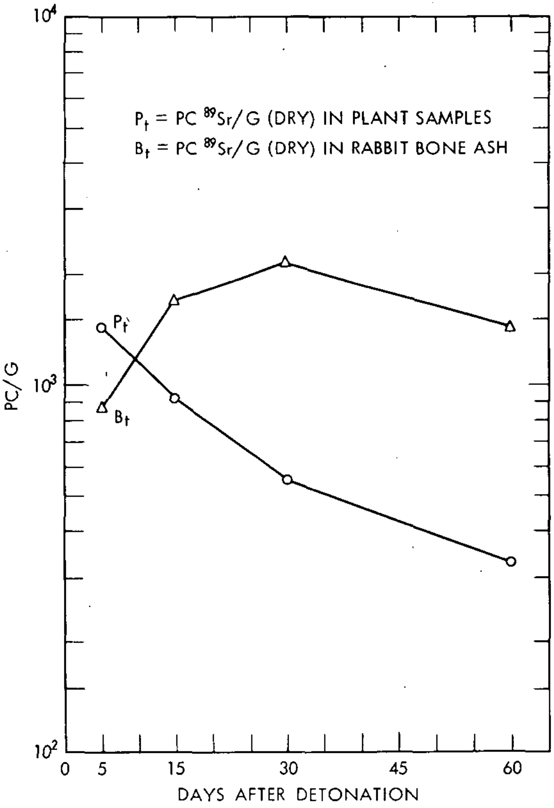

Fig. 3—Average concentrations of ^{89}Sr in plant samples, P_t, and in the bone ash of rabbits, B_t, collected from representative locations (see Fig. 2) in the Sedan fallout field at various times after the detonation.

equilibrium) about D + 30. The rate of decline from D + 30 to D + 60 approximated the radioactive half-life of ^{89}Sr. Estimates of the effective half-life of ^{89}Sr in rabbit bone (T_b = 20 days) were based on the average rates of loss from plants and the average rates of accumulation in bone ash. After estimates of the other required parameter values were obtained, these and the observed values for B_t were used to solve Eq. 5 for f_b. The average value thus obtained was $f_b = 0.0575$.

As shown in Table 2, the average concentrations of ^{131}I in plant samples (sagebrush) from Groom Valley and the Currant Area were higher than the average concentrations in the stomach contents of rabbits from the same locations. In the Penoyer and Railroad valleys, ^{131}I concentrations in the stomach contents of rabbits were somewhat higher than those in plant samples (mostly shadscale) from the same locations. Apparently the rabbits in these areas were feeding on plants other than sagebrush and shadscale.

This supposition is supported by the estimates of f_p given in Table 4. The average f_p values based on the plant samples from all locations are approximately the same for ^{89}Sr and ^{131}I. However, the average f_p value for ^{131}I based on concentrations in plant samples is higher than the average based on concentrations in the stomach contents of rabbits. For both ^{89}Sr and ^{131}I, the f_p values for sagebrush are higher than those for shadscale. The differences between f_p values for ^{89}Sr and ^{131}I in the different study areas are probably due to disparities between actual and theoretical, a_s, deposition rates, i.e., to fractionation or to errors in the estimation of average gamma dose rates. In general, these results indicate that the plants (probably grasses and broad-leaved herbs) representing the average rabbit's diet were less efficient than sagebrush but somewhat more efficient than shadscale in regard to the interception of fallout particles.

As shown in Table 2 and Fig. 4, the average concentrations of ^{131}I in plant samples from all stations were higher than the average ^{131}I concentrations in the stomach contents of rabbits from the same areas;

Table 4 — ESTIMATES OF f_p BASED ON EQS. 1 AND 2 AND OF INITIAL CONCENTRATIONS OF ^{89}Sr AND ^{131}I IN PLANT SAMPLES, P_0, AND OF ^{131}I IN THE STOMACH CONTENTS OF RABBITS, S_0*

Study areas†	Plant species	^{89}Sr	P_0	^{131}I	P_0	^{131}I	S_0
Groom Valley	Sagebrush	4.86	$\times 10^{-3}$	5.61	$\times 10^{-3}$	2.42	$\times 10^{-3}$
Penoyer Valley	Shadscale‡	3.03	$\times 10^{-3}$	1.56	$\times 10^{-3}$	2.32	$\times 10^{-3}$
Railroad Valley	Shadscale	3.14	$\times 10^{-3}$	2.21	$\times 10^{-3}$	2.24	$\times 10^{-3}$
Currant Area	Sagebrush	11.9	$\times 10^{-3}$	7.02	$\times 10^{-3}$	4.51	$\times 10^{-3}$
Average for all locations		4.40	$\times 10^{-3}$	4.34	$\times 10^{-3}$	3.02	$\times 10^{-3}$

*$P_0(^{89}\mathrm{Sr}) = 1.26\ P_5$, $P_0(^{131}\mathrm{I}) = 2.00\ P_5$, and $S_0(^{131}\mathrm{I}) = 2.00\ S_5$.

†Locations of study areas are shown in Fig. 2.

‡Some of the plant samples from this area were *Grayia spinosa*.

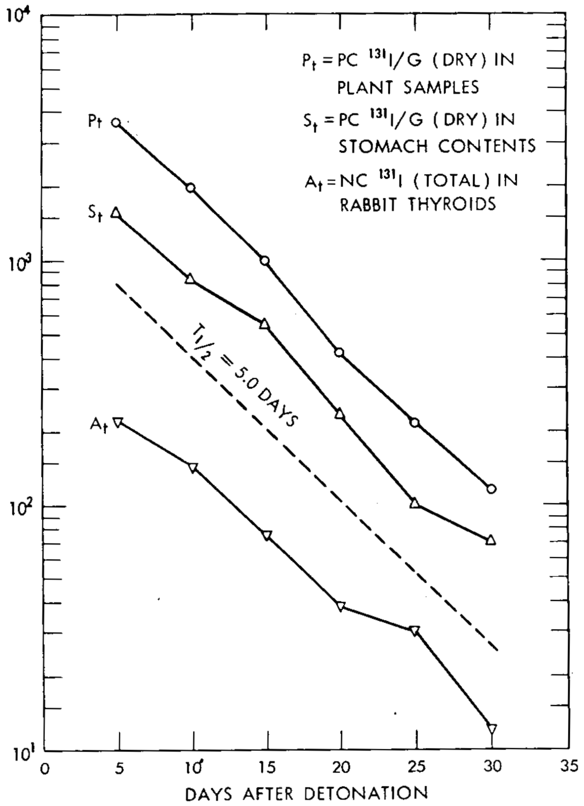

Fig. 4—Average concentrations of ^{131}I in plant samples, P_t, in the stomach contents, S_t, and in thyroids, A_t, of rabbits collected from representative locations (see Fig. 2) in the Sedan fallout field at various times after the detonation.

but the apparent rates of loss, indicating an effective half-life, T_p, of 5.0 to 5.5 days, were about the same. The average concentrations of ^{131}I in rabbit thyroids attained a maximum by or before D + 5 and declined at a half-time rate of 5 to 6 days.

French[27] and French and Van Middlesworth[29] did some experimental work with jackrabbits near the National Reactor Testing Station in Idaho. Their reports give estimates of T_a ranging from 1.5 to 2.5 days and of f_a ranging from 0.29 ± 0.09 to 0.158 ± 0.086. A more recent report by McBride[30] gives estimates of T_a = 2.0 days and f_a = 0.29. By trial and error we have found that estimates of T_p = 5.0 days and T_a = 2.0 days are reasonable approximations in relation to the data given in Table 2 and Fig. 4. With the use of these parameter values and the observed average values of A_t, Eq. 6 was solved for f_a. The results based on plant data, $\bar{P}_0$, indicate f_a = 0.18, and the results based on stomach-contents data, $\bar{S}_0$, indicate $f_a = 0.26$. (N.B. If stomach-contents data were available for ^{89}Sr, one might expect to find a similar difference in estimates of f_b required to fit the observed data points.)

Figures 5 and 6 show the relatively close agreement between observed average concentrations of ^{89}Sr in rabbit bone ash and of ^{131}I in rabbit thyroids and the hypothetical values obtained through solution of Eqs. 5 and 6. Because of variations within and between the different study areas (Groom, Penoyer, Railroad, and Currant), the parameter values that apply to the Sedan fallout field as a whole may or may not apply with equal accuracy to different areas within the fallout field. For example, if they were based on initial ^{131}I concentrations in plant samples, estimates of ^{131}I concentrations in thyroids, A_t, would be higher than those observed in the Groom and Currant study areas but lower than those observed in the Penoyer and Railroad valleys. However, the disparities between hypothetical and observed ^{89}Sr concentrations in the bone ash of rabbits from different parts of the Sedan fallout field, based on R_0 rather than physiography, are generally less than the standard errors of the observed means.[13]

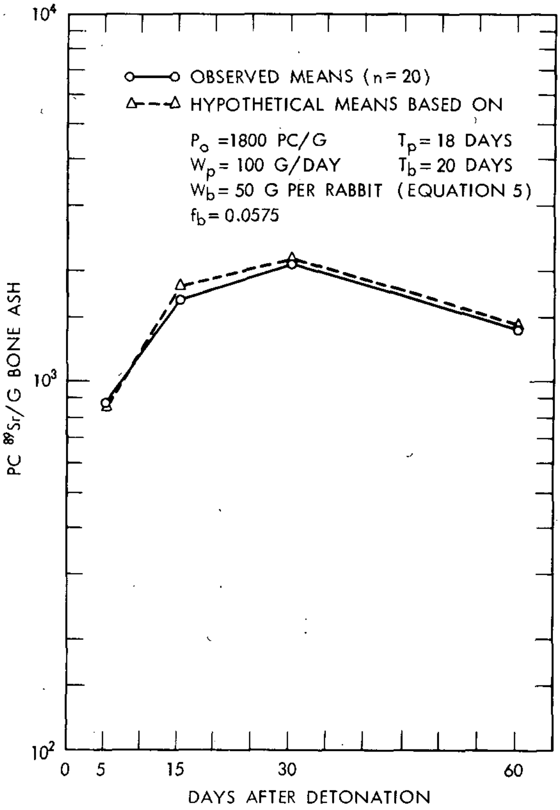

Fig. 5—Observed and hypothetical average concentrations of ^{89}Sr in the bone ash of rabbits collected from representative locations (see Fig. 2) in the Sedan fallout field at various times after the detonation.

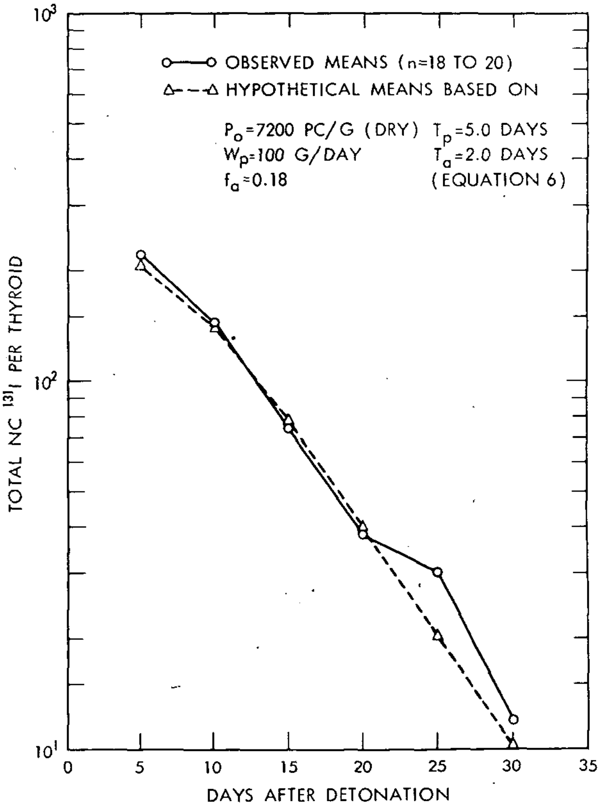

Fig. 6—Observed and hypothetical average concentrations of ^{131}I in the thyroids of rabbits collected from representative locations (see Fig. 2) in the Sedan fallout field at various times after the detonation.

DISCUSSION

These results seem to indicate that Eqs. 4 to 6 function satisfactorily, with estimated parameter values based on observed means, in explaining the early food-chain kinetics of ^{89}Sr and ^{131}I on plants and in the skeletons or thyroids of rabbits collected from 20 representative locations in the Sedan fallout field at between 5 and 60 days after the detonation. The input parameters for Eqs. 4 to 6 (W_p, W_b, f_b, f_a, T_p, T_b, and T_a) are known to vary; but the means of these values can be used, with fair success, as though they were constants. This deterministic approach to the problem permits us to describe and explain certain aspects of food-chain kinetics in relatively simple mathematical terms. It may also permit us to make errors in estimating parameter values; these errors are difficult to detect because the several parameters are interdependent. The variations within and between different study areas and the twofold difference between estimates of f_a based on ^{131}I concentrations in plant samples and in the stomach contents of rabbits are good examples of the kinds of disparities to be anticipated.

Although it is quite tempting to use such models to predict the biological consequences of close-in fallout, there are many good reasons for proceeding with caution. Some of the uncertainties, possible sources of error, and other obstacles to the achievement of this goal are described and discussed below.

From our analyses, the relation between initial gamma dose rates, R_0, and initial concentrations of radionuclides on fallout-contaminated plants, P_0, appears to take the form of a linear regression formula. There are several reasons for viewing this apparently simple relation with suspicion. For example, Guillou[22] has noted that the probable accuracy of R_0 estimates based on aerial-survey data is no greater than ±50%. Consequently the regression coefficients given in Table 3 could be in error by ±50%, and errors associated with extrapolations beyond the standard regression formula limits could be even greater.

Because of nuclide fractionation and downwind variations in the particle-size composition of fallout, one might not expect to find significant correlations between gross gamma dose rates and concentrations of specific radionuclides on plants or soils in fallout fields resulting from surface or low-altitude nuclear detonations. Previous studies[1,7,28] along the hot lines of fallout from balloon- and tower-supported detonations have shown correlations between plant and animal contamination and the distribution of fallout particles $< 44\ \mu$ in diameter.* In several cases, the highest percentages of fallout $< 44\ \mu$ in diameter and the highest levels of plant and animal contamination were found at intermediate distances from ground zero and hence at intermediate levels of gross gamma dose rate. Under these conditions, it would not be possible to predict plant contamination levels by means of linear regression formulas involving R_0 as the independent variable.

As shown in Table 4, it is also necessary to consider those factors which influence a plant's ability to intercept and retain the fallout particles deposited on it. Other things being equal, it may be assumed that plants with dense foliage composed of oily, resinous, or pubescent leaves should have higher f_p values than plants with sparse foliage composed of smooth or waxy leaves; but more data are needed to determine f_p values for a variety of wild and cultivated plant species in relation to specific morphological features, the particle-size composition of fallout, and various deposition rates.

---

*Autoradiographs and microscopic examinations have shown that virtually all the radioactive particles on plant foliage in the Sedan fallout field were $<50\ \mu$ in diameter and that about half of those measured were $< 20\ \mu$ in diameter.

Also needed are data to indicate the effects on f_p of plant density (e.g., g/sq ft) and other phytosociological characteristics of vegetation such as species composition, community structure, and phenology. In desert-shrub communities, for example, shrubs are widely spaced, and it is probably safe to assume that the f_p value for plants in a given area is independent of plant density. In pasture or forest, where plants are more crowded and where some may grow in the shade of others, f_p may decrease as density increases. Some evidence of this relation in regard to ^{131}I has been cited recently by Straub and Fooks.[31]

Many of these factors (fractionation, particle-size composition and distribution, and retention factors, $a_L = f_p$) are considered in the fallout model proposed by Miller.[32] If suitable plant data were available for a given situation, Miller's model would surely provide a theoretically sounder basis than unqualified linear regression formulas for the prediction of the initial concentrations of radionuclides on plants at different locations in a close-in fallout field. If one wanted to use the food-chain model described earlier (Eqs. 3 to 6) to make predictions of P_0, P_t, B_t, and A_t, a fallout model such as Miller's should be substituted for Eq. 3.

After the deposition of fallout, the concentration of a given radionuclide on fallout-contaminated plants can be expected to decline at a rate significantly faster than would be predicted on the basis of its radioactive half-life. Our estimates of effective half-lives on plants in the Sedan fallout field, 18 days for ^{89}Sr and 5.0 to 5.5 days for ^{131}I, indicate environmental half-lives (i.e., half-time rates of loss due to all causes other than radioactive decay) of approximately 28 days for ^{89}Sr and 15 days for ^{131}I. Since there was little or no rain in the area of the Sedan fallout field during the period of this study, the environmental half-life of ^{89}Sr on plants can be attributed primarily to wind action that removed particles from foliage or foliage from plants. The shorter environmental half-life of ^{131}I on plants may reflect the combined effects of wind action and sublimation.[11,12]

Other studies have indicated that our estimates of environmental and effective half-lives may not be applicable to other situations. For example, Bartlett et al.[10] sprayed solutions of different fission products on grass that was then exposed to both wind and rain for periods up to 60 days. Their results indicated an average environmental half-life of about 14 days for each of the radionuclides used. The difference between their results and ours is probably due to the effects of rain in removing soluble materials, but rain should have similar effects on particulate materials.

Considering the large number of variables involved (e.g., plant species, local weather conditions, the particle-size composition of material deposited on plants, the developmental stage of foliage, etc.), one should expect to find a wide range of apparent effective half-lives of different radionuclides on fallout-contaminated plants. In the absence of pertinent measurements, it is reasonable to assume an environmental half-life of 14 days or less for ^{131}I and for other radionuclides on fallout-contaminated plants in humid regions. Except for ^{131}I, an environmental half-life of 28 days should be more accurate for arid regions. In general, the effective half-life of a given radionuclide on plants, T_p, could be estimated, where T_e is the environmental half-life and T_r is the radioactive half-life, by

$$T_p = \frac{T_r \times T_e}{T_r + T_e} \tag{7}$$

Our method[13] of estimating the effective half-life of ^{89}Sr in rabbit bone (T_b = 20 days) was made necessary by the absence of pertinent experimental data, and our only confidence in the accuracy of our estimate is based on the results obtained (Fig. 5) when we used it to solve Eq. 5. Our estimate of the effective half-life of ^{131}I in rabbit thyroids (T_a = 2.0 to 2.5 days) was well within the range of experimental results reported by French[27] (T_a = 1.5 to 2.5 days). Whenever possible, the effective half-lives of radionuclides in animal tissues or organs should be determined by experimental as well as by empirical methods. One can then judge which of several possible values should be applied to a given set of circumstances.

Animal retention factors, e.g., f_b and f_a, are especially difficult to evaluate; and, as shown in Eqs. 5 and 6, errors in the estimation of these parameter values would result in proportional errors in the prediction of tissue burdens. Our estimates of retention factors for ^{89}Sr (f_b = 5.75%) and for ^{131}I (f_a = 18% if based on P_0 or f_a = 26% if based on S_0) represent mathematically arbitrary numbers calculated to obtain reasonably good fits between hypothetical and observed average tissue burdens. Because of the methods used in the estimation of these values, their physiological significance is doubtful; but these values may be just as useful as those obtained from feeding experiments. For example, French's experimental results indicated f_a values ranging from < 10 to >30% for jackrabbits, whereas the averages obtained for Dutch rabbits under laboratory conditions were only half as high. We collected samples of sagebrush and shadscale from the Sedan fallout field and fed them to Dutch rabbits in the laboratory. The results reported by Turner[14] indicated f_a values ranging from 2.0 ± 0.6% (based on samples from the Currant Area) to 12.0 ± 8.0% (based on samples from Groom Valley). Because of the difference in animal species (Dutch rabbits vs. jackrabbits) and because our field data indicate that jackrabbits in the Sedan fallout field were feeding on plants other than sagebrush and shadscale, these results are of dubious value in relation to the food-chain model.

DETERMINISTIC MODELS FOR HUMAN-FOOD-CHAIN KINETICS

The data summarized and discussed in the preceding pages have served to illustrate the usefulness of deterministic exponential models in providing at least a partial explanation of the early food-chain kinetics of radionuclides following a single fallout event. Although the results of these studies are not conclusive, they are promising and provide a basis for the supposition that similar models should be useful in the study of radionuclide transfers in food chains leading to man.

For example, suppose that an ordinary pasture is contaminated by fallout from a single nuclear detonation or from a reactor accident and that the milk produced by dairy cattle grazing in the contaminated pasture is consumed by people living on the farm or in a nearby village. If an estimate of the initial concentration of a given radionuclide, N_i, on pasture plants, P_0, can be obtained from direct measurement or predicted by a suitable fallout model, the subsequent concentration of N_i on pasture plants, P_t, in cow milk, M_t, and in the human tissue or organ of reference, H_t, can be estimated, with the assumptions that $P = P_0$, $M = 0$, and $H = 0$ at $t = 0$, by Eqs. 8 to 10:

$$P_t = P_0 e^{-\lambda_p t} \tag{8}$$

$$M_t = P_0 K_m f_m \left(\frac{e^{-\lambda_p t}}{\lambda_m - \lambda_p} + \frac{e^{-\lambda_m t}}{\lambda_p - \lambda_m} \right) \tag{9}$$

$$H_t = P_0 K_m f_m K_h f_h \left[\frac{e^{-\lambda_p t}}{(\lambda_m - \lambda_p)(\lambda_h - \lambda_p)} + \frac{e^{-\lambda_m t}}{(\lambda_p - \lambda_m)(\lambda_h - \lambda_m)} + \frac{e^{-\lambda_h t}}{(\lambda_p - \lambda_h)(\lambda_m - \lambda_h)} \right] \tag{10}$$

where t = days after fallout

N_i = a given radionuclide (e.g., ^{89}Sr or ^{131}I)

P_0 = pc N_i/g (dry) on pasture plants at $t = 0$

P_t = pc N_i/g (dry) on pasture plants at $t > 0$

M_t = pc N_i/ml (fresh) in milk produced at $t > 0$

H_t = pc N_i/g (fresh) in the human tissue or organ of reference at $t > 0$

K_m = dry weight (g) of plants consumed/volume (ml) of milk produced per day

K_h = volume (ml) of milk consumed per day/weight (g) of human organ or tissue

f_m = fraction of ingested N_i secreted in cow milk

f_h = fraction of ingested N_i deposited in human tissue or organ of reference

$\lambda = 0.693/T$

T_p = effective half-life of N_i on pasture plants

T_m = effective half-life of N_i in cow milk production

T_h = effective half-life of N_i in human tissue or organ of reference

To illustrate the potential value of the model formulated above, we have adopted the parameter values listed in Table 5. Most of these values are based on experimental data reported in the literature; but, when two or more estimates of a given parameter value were found, we usually selected the one resulting in higher concentrations in milk or human tissues. The results of calculations based on Eqs. 8 to 10 and the parameter values listed in Table 5 are shown in Figs. 7 and 8. Obviously, for different values of P_0, the corresponding values of M_t and H_t would be proportionally larger or smaller than shown in Figs. 7 and 8. Using the same effective half-lives but different estimates of K_m, f_m, K_h, or f_h would also result in proportionally higher or lower estimates of M_t and H_t.

Table 5—PARAMETER VALUES USED WITH EQS. 8 TO 10 TO CALCULATE HYPOTHETICAL CONCENTRATIONS OF ^{89}Sr AND ^{131}I ON PASTURE PLANTS, IN COW MILK, AND IN HUMAN TISSUES FOLLOWING A SINGLE FALLOUT EVENT*

Parameter†	^{89}Sr	^{131}I	References
P_0	100 pc/g	400 pc/g	Arbitrary values
K_m	1.4 g/ml/day	1.4 g/ml/day	33
f_m	0.02	0.06	34, 35
K_h (adult)	1/7 ml/day/g	50 ml/day/g	20
K_h (infant)	10/7 ml/day/g	500 ml/day/g	20
f_h	0.21	0.30	20
K_r‡	1.43×10^{-4}	1.17×10^{-5}	20
T_p	18.0 days	5.5 days	13, 16
T_m	2.5 days	2.0 days	34
T_h	50.4 days	7.5 days	20

*Results are shown in Figs. 7 and 8.
†Parameters are defined in the text.
‡Used with Eq. 11 to calculate tissue doses.

The total dose, D_t, delivered by N_i to the human tissue or organ of reference is given, for t = 0 to t = ∞, by

$$D_t = P_0 K_m f_m K_h f_h K_r \left[\frac{1 - e^{-\lambda_p t}}{\lambda_p(\lambda_m - \lambda_p)(\lambda_h - \lambda_p)} + \frac{1 - e^{-\lambda_m t}}{\lambda_m(\lambda_p - \lambda_m)(\lambda_h - \lambda_m)} + \frac{1 - e^{-\lambda_h t}}{\lambda_h(\lambda_p - \lambda_h)(\lambda_m - \lambda_h)} \right] \tag{11}$$

where D_t = total dose (rem) delivered by N_i, from t = 0 to t > 0, to the human organ or tissue of reference

$K_r = [(3.20 \times 10^3 \text{ dis/pc/day})(E)/(6.24 \times 10^7 \text{ Mev/100 ergs/g})]$

E = effective absorbed energy (Mev) per disintegration of N_i [Mev absorbed/disintegrations of N_i × relative biological effectiveness (RBE)]

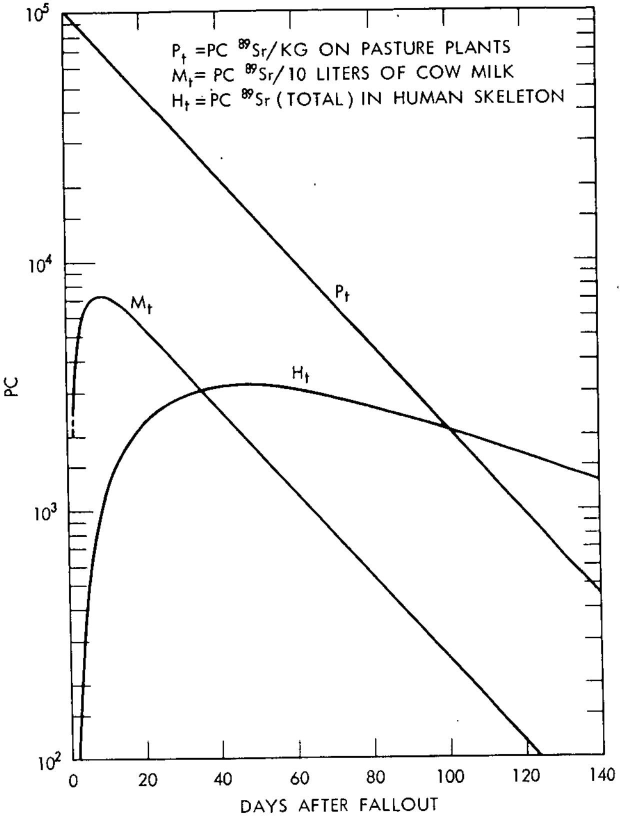

Fig. 7—Hypothetical concentrations of ^{89}Sr on pasture plants, in cow milk, and in human skeletons following environmental contamination by a single fallout event.

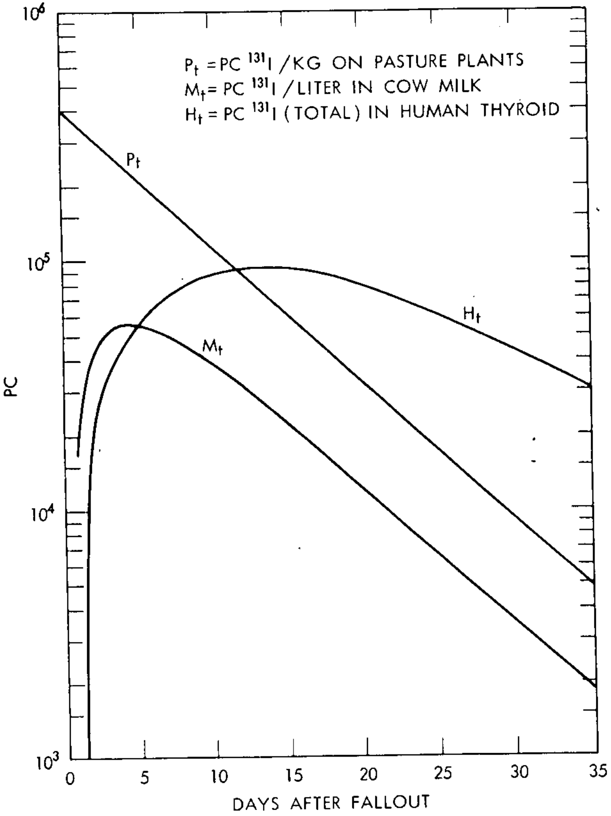

Fig. 8—Hypothetical concentrations of ^{131}I on pasture plants, in cow milk, and in human thyroids following environmental contamination by a single fallout event.

If the concentration of N_i on pasture plants is not known, estimates of doses to human tissue can be based on concentrations in milk (M_t = pc N_i/ml). If the time of fallout is known and M_t is given for a specified time of milking, Eq. 9 can be simplified, as shown in Eq. 12, to obtain an integration constant, I_0, that can then be substituted for the expression $P_0K_mf_m$ in Eqs. 10 and 11 to obtain estimates of concentrations in, H_t, and doses to, D_t, the human tissue or organ of reference:

$$M_t = I_0 \frac{e^{\lambda_p t} - e^{\lambda_m t}}{\lambda_m - \lambda_p} \tag{12}$$

James[36] recently used a similar method to estimate human thyroid doses resulting from a single fallout event, but many of his parameter values (i.e., $f_h = 0.25$, $K_r = 1.0 \times 10^{-5}$, $T_p = 5.0$ days, and $T_m = 1.9$ days) were not as pessimistic as those given in Table 5. James concluded from his investigation that a maximum concentration of 2800 pc of ^{131}I per liter of milk resulting from a single fallout event would, if a milk consumption of 1 liter/day were assumed, result in a total dose of 0.5 rad to a 2.0-g thyroid. Our results (Table 6) indicate that a maximum concentration of only 1850 pc of ^{131}I per liter of milk would be required for a potential dose of 0.5 rem to a 2.0-g human thyroid. (N.B. In this case 1 rem = 1 rad × RBE, and RBE = 1.0; therefore 1 rem = 1 rad.)

Pendelton et al.[37] based their estimates of thyroid doses on estimates of total ^{131}I intake, I_t, by people consuming 1 liter of milk per day in various parts of Utah during the summer of 1962. According to our hypothesis, the value of I_t would be given by

$$I_t = I_0 V_h \left[\frac{1 - e^{-\lambda_p t}}{\lambda_p(\lambda_m - \lambda_p)} + \frac{1 - e^{-\lambda_m t}}{\lambda_m(\lambda_p - \lambda_m)}\right] \tag{13}$$

where I_0 is an integration constant obtained from Eq. 12 and V_h is the volume of milk in milliliters consumed per person per day.

With the use of I_t from Eq. 13, the total thyroid dose would be given, where W_h is the thyroid weight (fresh) in grams, by

$$D_t = \frac{I_t K_r f_h}{\lambda_h W_h} \tag{14}$$

The Radiation Protection Guides (RPG's) recommended by the Federal Radiation Council (FRC)[38] are said to represent "... a reasonable balance between biological risk and benefit to be derived from useful applications of radiation and atomic energy." The RPG's for human bone and thyroid are based on average rates of radiostrontium and radioiodine intakes which, in the opinion of the FRC, should result in doses no greater than 1.5 rem/year to "... individuals in the gen-

Table 6—SUMMARY OF HYPOTHETICAL VALUES THAT, IF INDICATED BY MEASUREMENTS MADE AFTER ENVIRONMENTAL CONTAMINATION BY A SINGLE FALLOUT EVENT, WOULD IMPLY TOTAL DOSES OF 0.5 REM TO THE SKELETONS OR THYROIDS OF INFANTS CONSUMING 1 LITER OF MILK PER DAY

Hypothetical values*	^{89}Sr	^{131}I
Initial concentrations on pasture plants, P_0	61.0 pc/g	13.7 pc/g
Maximum concentrations in milk, M_t	4500 pc/liter	1850 pc/liter
Time after fallout, t_{max}	8 days	4 days
Total intake (to $t = \infty$)	1.60×10^5 pc	2.63×10^4 pc
Maximum concentration in human tissue, H_t	27 pc/g†	1580 pc/g†
Time after fallout, t_{max}	50 days	15 days
Total dose (at $t = \infty$)	0.5 rem†	0.5 rem†

*Calculations were based on Eqs. 8 to 14 and the parameter values listed in Table 5.

†Based on a 700-g skeleton or a 2.0-g thyroid.

eral population. . ." or an average of 0.5 rem/year ". . . to be applied to suitable samples of an exposed population group." Average annual intakes of >2000 pc ^{89}Sr/day or >100 pc ^{131}I/day ". . . would be presumed to result in exposures exceeding the RPG. . . ."

With the assumptions of a skeleton weight of 700 g and a thyroid weight of 2.0 g, Eq. 14 and the parameter values listed in Table 5 indicate that total annual intakes of 160,000 pc of ^{89}Sr or of 26,300 pc of ^{131}I could result in doses of 0.5 rem/year to the bones and the thyroids of infants. These values are lower than those indicated by the FRC (i.e., 720,000 pc ^{89}Sr/year and 36,500 pc ^{131}I/year) because the parameter values in Table 5 are more pessimistic than those adopted by the FRC.

For further comparison with the FRC's recommendations, we have estimated the hypothetical values of various measurements which, if obtained following a single fallout event, could result in doses of 0.5 rem to the bones and thyroids of infants. These hypothetical values are given in Table 6.

Tables 1 and 2 show that initial concentrations of ^{131}I on plants in various parts of the Sedan fallout field were about four times higher than the initial concentrations of ^{89}Sr. The estimates given in Table 6 indicate that initial concentrations of ^{89}Sr about 4.5 times higher than those of ^{131}I are required to deliver comparable doses to human tissues. We might therefore suppose that ^{131}I is considerably more hazardous than ^{89}Sr in an area contaminated by close-in fallout.

The data given in Table 2 indicate that the initial concentration of ^{131}I on plants in the vicinity of Currant, Nev., was approximately 1000 ± 150 pc/g. Similar plant samples collected in a hot spot (centered near Fruitland, Utah), which was discovered after the Small Boy detonation on July 14, 1962, indicated an initial ^{131}I concentration (on July 15) of approximately 800 ± 200 pc ($n = 6$). If we assume an f_p value of about 3.0×10^{-3} for pasture plants compared to approximately 7.5×10^{-3} for desert shrubs, the initial concentrations of ^{131}I on pasture plants in the vicinity of Currant, Nev., and Fruitland, Utah, could have been 400 and 320 pc/g, respectively.

If our hypothetical pastures, dairy herds, and human populations had been located in these areas, the total ^{131}I intakes by people drinking 1 liter of milk per day could have ranged from 670,000 to 825,000 pc, and the doses to the thyroids of children could have been 11.4 to 14.6 rem. With the use of the more optimistic parameters adopted by the FRC, the estimated doses based on these intakes would be 9.2 and 11.3 rem. (N.B. These estimates are comparable to the highest estimates reported by Pendelton et al.[37] for stations located in other parts of Utah).

Actually, there are very few milk cattle in the area of the Sedan fallout field, and, since we collected no milk samples, our treatment of the problem is strictly hypothetical. However, one sample collected near Ely, Nev., and analyzed by the U. S. Public Health Service[39] contained 2800 pc ^{131}I/liter on July 24, 18 days after the detonation. If this value represents the concentration at the time of milking, it could indicate a possible thyroid dose of 2.6 rems.

Solutions to Eq. 13 indicate that ^{131}I intakes during periods of 7, 14, or 21 days following environmental contamination by a single fallout event should account for 42, 85, or 97%, respectively, of the total potential intakes from $t = 0$ to $t = \infty$. Therefore the simplest countermeasures to avoid 85% or more of the potential biological hazard related to ^{131}I would be (1) to feed cattle on stored feed for a period of two or more weeks after a detonation or (2) to use the milk produced during that period for making cheese or other dairy products that would not be consumed for a period of three or more weeks after milk production.

REFERENCES

1. R. L. Lindberg, E. M. Romney, J. H. Olafson, and K. H. Larson, Factors Influencing the Biological Fate and Persistence of Fallout, Operation Teapot, Report WT-1177, University of California at Los Angeles, January 1959.
2. K. H. Larson, H. A. Hawthorne, and J. H. Olafson, Nevada Test Site Fallout: Some Characteristics, Its Apparent Environmental Equilibrium and Biological Availability, in Radioactive Fallout from Nuclear Weapons Tests, A. W. Klement, Jr. (Ed.), USAEC Report TID-7632, pp. 4-24, February 1962.
3. R. S. Russell, Deposition of Sr^{90} and Its Content in Vegetation and in Human Diet in the United Kingdom, *Nature, 182:* 834-839 (1958).
4. National Academy of Sciences, the Behavior of Radioactive Fallout in Soils and Plants, *Natl. Acad. Sci.—Natl. Res. Council Publ. No. 1092,* 37 pp., 1963.

5. H. Nishita, E. M. Romney, and K. H. Larson, Uptake of Radioactive Fission Products by Crop Plants, *Agri. Food Chem., 9:* 101-106 (1961).
6. N. R. French and K. H. Larson, Environmental Pathways of Radioactive Iodine from Nuclear Tests in Arid Regions, USAEC Report UCLA-499, University of California at Los Angeles, December 1961.
7. E. M. Romney, R. G. Lindberg, H. A. Hawthorne, B. G. Bostrom, and K. H. Larson, Contamination of Plant Foliage with Radioactive Fallout, *Ecology, 44:* 343-349 (1963).
8. L. J. Middleton, Absorption and Translocation of Strontium and Cesium by Plants from Foliar Sprays, *Nature, 181:* 1300-1303 (1958).
9. A. A. Selders and F. P. Hungate, the Foliar Sorption of Iodine by Plants, USAEC Report HW-44890, Hanford Atomic Products Operation, Sept. 1, 1956.
10. B. O. Bartlett, L. J. Middleton, G. M. Milbourn, and H. M. Squire, the Removal of Fission Products from Grass by Rain, United Kingdom Agricultural Research Council Report ARCRL-5, pp. 52-54, 1961.
11. W. E. Martin, Losses of Sr^{90}, Sr^{89}, and I^{131} from Fallout Contaminated Plants, *Radiation Botany,* in press.
12. W. E. Martin, Loss of I^{131} from Fallout-contaminated Vegetation, *Health Phys., 9:* 1141-1148 (1963).
13. W. E. Martin and F. B. Turner, Food-chain Relationships of Radiostrontium in the Sedan Fallout Field, USAEC Report PNE-237F, University of California at Los Angeles, March 1965.
14. F. B. Turner, Quantitative Relationships Between Fallout Radioiodine on Native Vegetation and in the Thyroids of Herbivores, *Health Phys., 9:* 1241-1247 (1963).
15. F. B. Turner, the Uptake of Fallout Radioisotopes by Mammals and a Stochastic Simulation of the Process, this volume.
16. F. B. Turner and W. E. Martin, Food-chain Relationships of Radioiodine Following Two Nuclear Tests in Nevada, USAEC Report PNE-236P, University of California at Los Angeles, May 10, 1963.
17. F. B. Turner and W. E. Martin, Food-chain Relationships of I^{131} in Nevada Following the Sedan Test of July 1962, USAEC Report PNE-236F, University of California at Los Angeles, July 24, 1964.
18. G. Friedlander and J. W. Kennedy, *Nuclear and Radiochemistry,* Chap. 5, pp. 127-144, John Wiley & Sons, Inc., New York, 1955.
19. W. E. Siri, *Isotopic Tracers and Nuclear Radiation,* Chap. 15, pp. 388-402, McGraw-Hill Book Company, Inc., New York, 1949.
20. International Committee on Radiation Protection, Report of Committee II on Permissible Dose for Internal Radiation, *Health Phys., 3:* 1 (1960).
21. Health and Safety Laboratory, Manual of Standard Procedures, USAEC Report NYO-4700(Rev.), August 1962.
22. R. B. Guillou, Part II, Aerial Radiometric Survey, Project Sedan, USAEC Report PNE-225P, pp. 36-64, University of California at Los Angeles, August 1962.
23. S. Glasstone (Ed.), *The Effects of Nuclear Weapons,* U. S. Government Printing Office, Washington, D. C., 1962.
24. S. Katcoff, Fission-product Yields from Neutron-induced Fission, *Nucleonics, 18*(11): 201-208 (1960).
25. G. Higgins, Calculation of Radiation Fields from Fallout, USAEC Report UCID-4539, University of California Lawrence Radiation Laboratory, Jan. 25, 1963.
26. A. D. Arnold, Forage Consumption and Preferences of Experimentally Fed Arizona and Antelope Jack Rabbits, *Univ. Ariz. Agri. Expt. Sta. Tech. Bull., 95:* 51-86 (1961).
27. N. R. French, Iodine Metabolism in Wild Jack Rabbits, in Oklahoma Conference — Radioisotopes in Agriculture, Held April 2 and 3 at Oklahoma State University, Stillwater, Oklahoma, USAEC Report TID-7578, pp. 113-121,

Associated Midwest Universities and Argonne National Laboratory, Apr. 13, 1960.

28. K. H. Larson and J. W. Neel, Summary Statement of Findings Related to the Distribution, Characteristics, and Biological Availability of Fallout Debris Originating from Testing Programs at the Nevada Test Site, USAEC Report UCLA-438, University of California at Los Angeles, Sept. 14, 1960.
29. N. R. French and L. Van Middlesworth, Biological Monitoring of Recent Air-borne Fission Products, in *Proceedings of the Second International Conference on the Peaceful Uses of Atomic Energy, Geneva, 1958,* Vol. 18, pp. 516-518, United Nations, New York, 1958.
30. R. McBride, Radioiodine Uptake at the NRTS and Environs, *Health Phys., 9:* 1127-1230 (1963).
31. C. P. Straub and J. H. Fooks, Cooperative Field Studies on Environmental Factors Influencing I^{131} Levels in Milk, *Health Phys., 9:* 1195-1204 (1963).
32. C. F. Miller, *Fallout and Radiological Countermeasures* (2 volumes), Stanford Research Institute, Menlo Park, Calif., 1963.
33. A. C. Chamberlain, J. F. Loutit, R. P. Martin, and R. S. Russell, The Behaviour of I^{131}, Sr^{89}, and Sr^{90} in Certain Agricultural Food Chains, in *Proceedings of the International Conference on the Peaceful Uses of Atomic Energy, Geneva, 1955,* Vol. 13, pp. 360-363, United Nations, New York, 1956.
34. C. L. Comar and R. H. Wasserman, Radioisotopes in the Study of Mineral Metabolism, in *Progress in Nuclear Energy, Biological Sciences,* Series IV, Vol. 1, pp. 153-196, Pergamon Press, Inc., New York, 1956.
35. F. W. Lengemann and E. W. Swanson, Secretion of Iodine in Milk of Dairy Cows Using Oral Doses of I^{131}, *J. Dairy Sci., 40:* 216-224 (1957).
36. R. A. James, Calculation of Radioactive Iodine Concentrations in Milk and Human Thyroid as a Result of Nuclear Explosions, USAEC Report UCRL-7716, University of California Lawrence Radiation Laboratory, Feb. 14, 1964.
37. R. C. Pendelton, C. W. Mays, R. D. Lloyd, and A. L. Brooks, Differential Accumulation of I^{131} from Local Fallout in People and Milk, *Health Phys., 9:* 1261-1270 (1963).
38. Federal Radiation Council, Background Material for the Development of Radiation Protection Standards, Report No. 2, U. S. Government Printing Office, Washington, D. C., 1961.
39. U. S. Atomic Energy Commission, Off-site Environmental Contamination from Nuclear Explosives at the Nevada Test Site, September 15, 1961–September 15, 1962, USAEC Report TID-18892.